ENERGY MIGRATION PROCESSES IN RARE EARTH PENTAPHOSPHATES

By

JACEK KAZIMIERZ TYMINSKI

Magister Inzynier

Politechnika Gdanska

Gdansk, Poland

1978

Submitted to the Faculty of the Graduate College of the
Oklahoma State University in partial fulfillment
of the requirements for the degree of
DOCTOR OF PHILOSOPHY
July, 1983

ENERGY MIGRATION PROCESSES IN RARE

EARTH PENTAPHOSPHATES

Thesis Approved:

Richard C. Powell
Thesis Adviser

Lawrence F. Fleischer

James R. Clarke

Norman N. Durham
Dean of the Graduate College

ACKNOWLEDGMENTS

The author wishes to express his gratitude to his thesis adviser, Dr. Richard Powell for his help, guidance and continuous support throughout this work. Special thanks and appreciation are also extended to the other Graduate Committee members, Dr. J.R. Choike, Dr. L.I. Fleishmen and Dr. G.P. Summers for their kind cooperation. The financial support from the Department of Physics, Oklahoma State University and the U.S. Army Research Office is appreciated. Finally, the author wishes to express his gratitude to Norma Earp, Diana Pettyjohn, Greg Quarles, Robert Schweitzer, and Debbie Shields for their help during writing this thesis.

TABLE OF CONTENTS

LIST OF TABLES

LIST OF FIGURES

Figure Page

Figure Page

CHAPTER I

INTRODUCTION

A. Statement of the Problem

In the recent past there has been dynamic progress made in the field of the spectroscopy. The application of laser techniques made it possible to develop new research methods giving an insight into the new theoretical and practical aspects of spectroscopy. In particular, the application of laser has proved to be beneficial in the investigation of the energy migration in solids. These studies are important from both a basic and a technological viewpoint because obtaining information about the solids basic properties gives the opportunity to test their technological applicability.

B. Summary of Thesis

The second chapter of this thesis will review the progress made in the theorectical efforts to describe energy migration in solids. First, the Master Equation approach and its accomplishments in development of the theory of Generalized Diffusion Coefficient are discussed. The limits of the theory are also discussed. Then, different approaches to compute the survival function are presented. Both phenomenological and first principle description models are presented and the limits of their applicability are discussed. All the theoretical concepts presented in the second chapter address the

question of discrete site distribution. Another worthwhile question would be what is the role of randomness in energy migration processes? As it is shown, none of the theories presented seem to be capable of addressing this problem explicitly.

The third chapter of this thesis describes the technique of Time-resolved site-selection spectroscopy. This technique allows study of the energy migration process through analysis of time evolution of spectra. The interpretation of the experimental data and its correspondence to the theory is discussed through the analysis of the survival function. Results obtained in case of $Eu_xY_{1-x}P_5O_{14}$ are presented and analyzed.

The fourth chapter presents the optical phase conjugation technique of Four-wave mixing. The mechanism of wave mixing is discussed in terms of the Maxwell equation. The interpretation of the mixing process in terms of the excited state holograms and its validity to investigate the energy migration are presented. The results obtained in the case of $Nd_xLa_{1-x}P_5O_{14}$ crystals are analyzed.

In the fifth and final chapter, a summary of results and suggestions for future work are presented.

CHAPTER II

THEORY

A. The Master Equation

The transport properties of the population of states can be described by the Generalized Master Equation (GME) (1) of the form:

$$\frac{\partial P_I(t)}{\partial t} = \int_o^t ds \sum_{J\neq I} [H_{J,I}(t-s)P_J(s) - H_{I,J}(t-s)P_I(s)] \tag{1}$$

where, $P_I(t)$ is the probability of occupying a state enumerated by the vector variable I designating all the possible quantum numbers, and $H_{I,J}(t)$ is the transfer rate from the I-th state to the J-th state.

In the case where the $M_{I,J}(t)$'s are of $\delta(t)$ (Dirac's delta) type equation (1) simplifies to the Pauli Master Equation (PME) of the form

$$\frac{\partial P_I}{\partial t} = \sum_{J\neq I} [F_{J,I}P(t) - F_{I,J}P_I(t)] \tag{2}$$

in which $F_{I,J}$'s are time independent.

In general, the population of states designated by index I in equations (1) and (2) can be influenced by the randomness of the states distribution. Therefore, the degree of symmetry occurring in equations (1) and (2) will be dependent on the physical nature of the system involved.

The interpretation of the Pauli Master Equation suggests that the Generalized Master Equation can be obtained from equation (1) whenever the transport process is of the Markoffian type (i.e., in which there is no correlation between the past and the future of the system).

In studies of the transport properties of materials often the position of the excited states is of exclusive interest. Therefore, equations (1) and (2) need to be subjected to an averaging procedure to extract their forms involving only the space dependence (2). Also, the structural disorder can prove to be troublesome. It is tempting to approximate the energy migration occurring in the disordered structure of the medium by simplification occurring in some sort of "averaged" medium. Klafter and Silbey, in reference 3, showed that the averaging of a structurally disordered system, on which the Markoffian process described by equation (2) was assumed, leads to the Generalized Master Equation describing the evolution of the averaged probabilities of the energy occupying different crystal sites. The procedure of Klafter and Silbey (3) can be generalized on other quantum mechanical degrees of freedom and the conclusion can be drawn, that the Pauli Master Equation describing the dynamics of a disordered system (Markoffian process) leads to the Generalized Master Equation describing the process of the averaged system (non-Markoffian process). The equation describing the dynamics in such an averaged system is

$$\frac{\left\langle dP_i(t)\right\rangle}{dt} = \sum_{j\neq i} \int_0^t d\tau \left[W_{i,j}(t-\tau)\left\langle P_j(\tau)\right\rangle - W_{j,i}(t-\tau)\left\langle P_i(\tau)\right\rangle\right] \qquad (3)$$

where, $P_j(t)$ is the averaged probability, that the j-th site is occupied by the excited state. The relationship between the $W_{i,j}$'s of Equation (2) and the $F_{I,J}$'s of Equation (3) is established through the following procedure.

First, **F** operator is found such that its I,J-th element in matrix representation has the form

$$[\mathbf{F}]_{I,J} = (1-\delta_{I,J})F_{I,J} - \delta_{I,J} \sum_{I \neq J} F_{I,J} \tag{4}$$

($\delta_{I,J}$ is the Kronecker's delta while $F_{I,J}$ are the same as in equation (2)). Summation in the above equation, as in equation (2), reflects the structural disorder of the medium. Having obtained **F** operator, a new **M**(s), self-energy operator, can be defined by equation

$$\left\langle (s\mathbf{1} - \mathbf{F})^{-1} \right\rangle = (s\mathbf{1} - \mathbf{M}(s))^{-1} \tag{5}$$

where s designates the variable in the frequency domain and angle bracket designates ensemble averaging. Obtained from this equation matrix elements $[\mathbf{M}(s)]_{I,J}$ are shown to be equal to the Laplace transformed parameters $W_{I,J}(s)$ of the Laplace transformed equation (3) (for details see reference 3).

It is obvious, that this technique can be bothersome because of computational and interpretational difficulties. Further work needs to be done to explain the structure of the self-energy operator. In particular, the practical ways of **M** operator evaluation need to be discovered. In case of the process of the energy migration between strongly interacting states it is possible to neglect discontinuity of the migration medium. The continuity limit of the Pauli Master

Equation leads to a diffusion like equation involving a nonhomogeneous term and/or a space/time dependent diffusion coefficient. This case was discussed in references 2, 5, and 6.

B. The Theory of the Generalized Diffusion Coefficient

In this section, review of efforts to describe the migration of energy in solids through analysis of the Pauli Master Equation is given. An appropriate description of an energy migration medium is obtained through the choice of geometrical relations between sites contributing to the energy migration, and rates of transfer between sites, related to the particular interaction, responsible for the migration.

The Pauli Master Equation approach was demonstrated by Haan and Zwanzing (6). The equation applied has the form

$$\frac{d}{dt}\tilde{P}_j = \frac{\tilde{P}_j}{\tau} + \sum_{k\neq j} W_{k,j}\tilde{P}_k - \tilde{P}_j \sum_{k\neq j} W_{j,k} \qquad (6)$$

where $\tilde{P}_j$ is the probability that the excitation occupies j-th site, τ is the introatomic lifetime of excitation, and $W_{j,k}$ is the time independent rate of energy transfer between the j-th and k-th sites. Two remarks need to be made at this point. First, the possibility of introatomic excitation decay is built into equation (2) which describes the dynamics of population of states. This is due to the fact that the averaging procedure extracts from equation (2) the dynamics of space distribution of excited states. This leads to the presence in the averaged equation term $\frac{P_j}{\tau}$ expressing the fact that the lifetime of the excited state is finite.

Second, the approximation of the energy migration process by its form averaged over non-spatial degree of freedom can also lead to Generalized Master Equation (3) a fact which is ignored by Equation (6). In this sense Equation (6) provides only an approximate description of the process which should be described by equation (3).

Selection of a set of sites involved in the energy migration (which can be done either through selection of the indexes included in the summations and/or the proper choice of the vectors coupling the transferring sites) expresses the geometrical properties of the transferring medium. Therefore, the summation in equation (6) does not, in general, run through a set of long range ordered sites.

If the new variable $\tilde{P}_j(t)$ is defined through formula

$$\tilde{P}_j(t) = P_j(t)\exp(\frac{-t}{\tau}) \tag{7}$$

then equation (6) can be rewritten in the matrix form

$$\dot{\overline{P}}(t) = \mathbf{W}\,\overline{P}(t) \tag{8}$$

where elements of matrix $\mathbf{W}$ are defined as

$$[\mathbf{W}]_{i,j} = (1-\delta_{i,j})W_{i,j} - \delta_{i,j}\sum_{k\neq j} W_{j,k} \tag{9}$$

and the j-th coordinate of $\overline{P}(t)$ vector is equal $P_j(t)$.

Clearly, the number of sites involved in the migration process in a realistic-medium makes the solution of equation (8) a formiable task. Also, the correspondence between $\overline{P}(t)$ and the fluorescent response of the medium is yet to be established.

The authors of reference 7 addressed the question of the energy diffusion through the medium and this topic will be discussed in this chapter.

The proposed way of investigation of the generalized diffusion process described by equation (8) analyzes the properties of Greens function, which allows expression of the density of excitons inside the volume Ω of the sample, containing discrete set of N active sites, at the moment t of time as

$$P(N,\Omega,\bar{r},t) = \int_{\Omega} d^3r' G(N,\Omega,\bar{r},\bar{r}',t) P(N,\Omega,\bar{r}',0) \tag{10}$$

where $G(N,\Omega,r,t)$ is the Greens function of the form

$$G(N,\Omega,\bar{r},\bar{r}',t) = \frac{\Omega}{N} \sum_{j}^{N} \sum_{i}^{N} \left\langle \delta(\bar{r}_j - \bar{r}) [e^{t\mathbf{W}}]_{j,i} \delta(r_i - r) \right\rangle \tag{11}$$

where N is the number of transferring sites, and $P(N,\Omega,r,0)$ is the initial density of excitons. The angle bracket in formula (11) symbolizes averaging carried out accordingly to the formula

$$\left\langle A(R) \right\rangle = \frac{1}{\Omega^N} \int d\bar{r}_1 \ldots \int d\bar{r}_N A(R) \tag{12}$$

while $[e^{t\mathbf{W}}]_{j,k}$ is the j,k-th element of the matrix $[e^{t\mathbf{W}}]_{NxN}$, which is a function of $\mathbf{W}$.

Few words of explanation should be devoted to the interpretation of the $\mathbf{W}$ matrix. First, the diagonal terms of $\mathbf{W}$ have the form

$$[\mathbf{W}]_{j,j} = - \sum_{k \neq j} W_{j,k} \tag{13}$$

and they describe the overall rate of the transfer from j-th site to any of the available in the neighborhood sites. The off-diagonal terms have the form

$$[\mathbf{W}]_{k,j} = -W_{k,j} \quad ; \quad k \neq j \tag{14}$$

and they define the rate of energy transfer from the site k to the site j. Equation (11) involves double summation over the two index ranges of the matrix $(e^{t\mathbf{W}})$. This matrix function can be represented as a matrix power series

$$(e^{t\mathbf{W}}) = \sum_{n=0}^{\infty} \frac{t^n}{n!} (\mathbf{W}^n) \tag{15}$$

The n-th element of the above sum will contribute to the i,j-th element of the matrix $(e^{t\mathbf{W}})$ with the component $(\mathbf{W}^n)_{i,j}$ which can be written as

$$[e^{t\mathbf{W}}]_{i,j} = \sum_{n=0}^{\infty} \frac{t^n}{n!} [\mathbf{W}^n]_{i,j} \tag{16}$$

Given the fact, that the matrix $\mathbf{W}$ is NxN dimensional the $[\mathbf{W}^n]_{i,j}$ can be expressed as the sum of N^n expressions of the form

$$(\mathbf{W}^n)^{(k)}_{i,j} = (W_{i,I}\, W_{I,J}\, W_{J,K} \cdot \cdot \cdot W_{L,M} \cdot \cdot \cdot W_{O,P}\, W_{P,j})(-1)^{m(k)} \tag{17}$$

where k designates a particular sequence (I,J,...,L,M,...,O,P) of numbers not bigger than N, and $W_{I,J}$ ($I \neq J$) is the I,J-th element of the $\mathbf{W}$ matrix. Given the fact that the distinction between different terms (17) is made by the sequence (i,I,J,K,...,L,M,...,O,P,j), the generation of different terms (17) running over different sequences of (I,J, ...,L, M,...,O, P) does not bury the differences between terms (16) due to the presence of two indices i and j.

If the distribution of sites contributing to the energy migration can be assumed to be symmetric in the sense, that the geometrical distribution of sites surrounding any of the sites is identical and the

energy of interaction between different sites is only distance dependent, then there is going to be a certain number of terms of the type (16) such that their components will satisfy

$$[\mathbf{W}^n]_{i,j} = [\mathbf{W}^n]_{i',j'} \; ; \; i \neq i', \; j \neq j' \tag{18}$$

The two dimensional illustration of the above statement made in reference to formula (17) is shown on the figure 1A. This figure also shows, that the relation (18) will hold only in the case of specially chosen symmetric $i \neq i'$ and $j \neq j'$. However, there also is a number of different sites which, when coupled by different terms (17) will show exactly the opposite

$$[\mathbf{W}^n]_{i,j} \neq [\mathbf{W}^n]_{i',j'} \; ; \; i \neq i', \; j \neq j' \tag{19}$$

Clearly, the procedure of constructing terms of form (17) obeying either condition (18) or (19), will be dependent on assumed symmetry and the particular procedure developed to enumerate the N sites contributing to the energy migration.

The analysis of the Greens function (11), because of the summations involved, still remains difficult. The authors (7) simplified equation (11) assuming the validity of the following approximation

$$G(N,\Omega,\bar{r},\bar{r}',t) = \delta(\bar{r}-\bar{r}')\left\langle [e^{t\mathbf{W}}]_{1,1} \right\rangle + (N-1)\left\langle \delta(\bar{r}_{1,2}-\bar{r}+\bar{r}')[e^{t\mathbf{W}}]_{1,2} \right\rangle$$

(where $\bar{r}_{1,2} = \bar{r}_1 - \bar{r}_2$). (20)

To obtain the above approximation of formula (11) the following conditions have to be satisfied

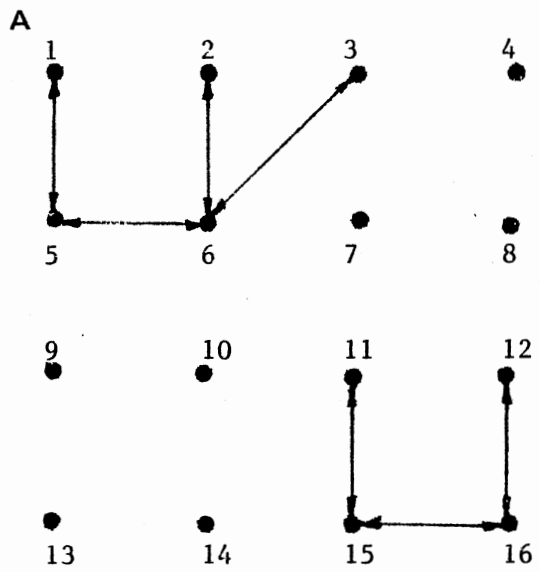

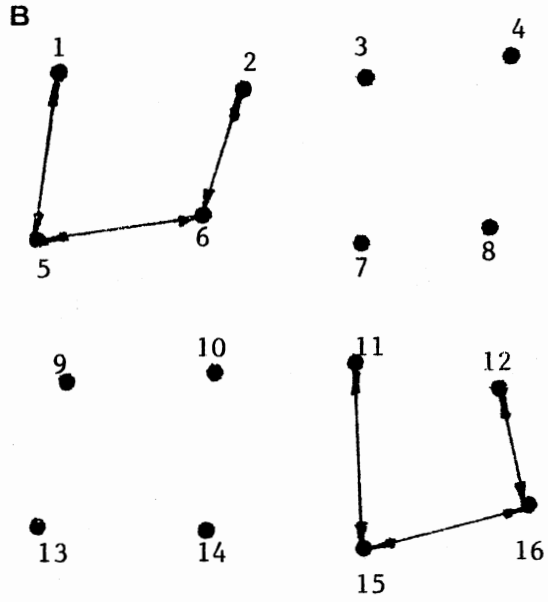

$W_{1,5}W_{5,6}W_{6,2} = W_{11,15}W_{15,16}W_{16,12}$

$W_{1,5}W_{5,6}W_{6,2} \neq W_{1,5}W_{5,6}W_{6,3}$

$W_{1,5}W_{5,6}W_{6,2} \neq W_{11,15}\ W_{15,16}W_{16,12}$

Figure 1. Geometrical representation of different terms contributing to the power expansion of the e^{tW} matrix in perfectly ordered (A) and disordered (B) systems.

$$\left\langle \delta(\bar{r}_i-\bar{r})[e^{tW}]_{i,i}\right\rangle = \left\langle \delta(\bar{r}_1-\bar{r})[e^{tW}]_{1,1}\right\rangle ; \; i = 1,2, \ldots N \qquad (21)$$

$$\sum_{i}^{N}\sum_{j\neq i}^{N}\left\langle \delta(\bar{r}_j-\bar{r})[e^{tW}]_{i,j}\delta(\bar{r}_i-\bar{r})\right\rangle = N(N-1)\left\langle \delta(\bar{r}_{1,2}-\bar{r}+\bar{r}')[e^{tW}]_{1,2}\right\rangle \qquad (22)$$

In the light of the discussion of the properties of the power expansion (16), condition (21) requires neglecting of the randomness of the site distribution. Condition (22) however, is even more restrictive; it requires that $W_{i,j}$ are distance independent (e.g. on the Figure 1A $W_{6,2}$ would have to be equal to $W_{6,3}$). This requirement is obviously physically more restrictive than any limitation due to low symmetry of site distribution or its randomness.

Motivated by equation (20) Haan and Zwanzing (7) defined $D(\bar{k},s)$ as a Generalized Diffusion Coefficient (GDC), by the formula

$$G(\bar{k},s) = [s+k^2D(\bar{k},s)]^{-1} \qquad (23)$$

where $G(\bar{k},s)$ is the Laplace-Fourier transform of the migration equation, Greens function, and $\bar{k}$ is the vector in the reciprocal space domain. As a consequence the Laplace transform of the mean displacement of excitation, $r^2(t)$ in the small $|\bar{k}|$ limit can be expressed by the generalized Einstein formula (for details see references 7 and 9)

$$\int_0^\infty dt\; e^{-st}\left\langle r^2(t)\right\rangle = (\frac{6}{s^2})D(0,s) \qquad (24)$$

Using a scaling argument the authors (7) concluded, that in the low density, short time limit the mean square displacement is proportional to $\rho t^{5/6}$ (where ρ is the density of sites, and t designates time). A density

expansion of the Greens function in the thermodynamical limit ($N/\Omega < \infty$ while $N, \Omega \longrightarrow \infty$) suggests representing the mean square displacement and consequently, the Generalized Diffusion Coefficient as

$$\left\langle r^2(t) \right\rangle = R_o^2 \left(\frac{t}{\tau}\right)^{1/3} \left[2.97514C\left(\frac{t}{\tau}\right)^{1/2} + 0.3268C^2 \frac{t}{\tau} + \ldots\right] \qquad (25)$$

$$D(0,s) = \frac{R_o^2}{\tau} (s\tau)^{2/3} \left[0.46647 \frac{C}{(s\tau)1/2} + 0.06486 \frac{C^2}{s\tau} + \ldots\right] \qquad (26)$$

where $C = \frac{4\Pi\rho R_o}{3}$ is the dimensionless site density, r is the radius of Förster interaction, and τ is the mean excitation lifetime. To derive equations (25) and (26), dipole-dipole type of energy migration was assumed.

Values of the numerical coefficients in equations (25) and (26) have been estimated considering the mean square excitation displacements in two and three site systems, as the systems corresponding to the second and third powers of the density expansion terms.

Gochanour, Andersen, and Fayer (8) attempted to treat equation (20) in a more formal way. First, they found the Laplace Fourier transform of equation (20) and then expanded the matrix function $(s-\mathbf{W})^{-1}$ as

$$(s-\mathbf{W})^{-1} = s^{-1} + \sum_{n=1}^{\infty} \left(\frac{1}{s^{n+1}}\right)(\mathbf{W}^n) \qquad (27)$$

The above allowed authors to write the Laplace-Fourier transform of the Greens function as

$$G(\bar{k},s) = s^{-1} + \sum_{n=1}^{\infty} \left(\frac{1}{s^{n+1}}\right) \left\langle [\mathbf{W}^n]_{1,1} \right\rangle + (N-1)\left\langle \exp(i\,\bar{u}\,\bar{r}_{1,2})\left[s^{-1} + \sum_{n=1}^{\infty} \left(\frac{1}{s^{n+1}}\right)[\mathbf{W}^n]_{1,2}\right]\right\rangle \qquad (28)$$

Again, the power representation of equation (27) can be expressed by the sum of the terms of form (17) (this time, however i=1, j=2). Of course, this approach inherited all the symmetry limitations discussed in reference to the Haan and Zwanzing (7) work.

In their theory Gochanour, Andersen, and Fayer (8) repeated the requirement that the energy migration is distance independent, and in particular wrote that

$$s^{-2}\left\langle \sum_{i\neq 1} (-W_{i,j}) \right\rangle = s^{-2}(N-1)\left\langle -W_{1,2} \right\rangle \tag{29}$$

$$\sum_{i\neq 1}^{N} s^{-3}\left\langle W_{1,i}W_{i,1} \right\rangle = s^{-3}(N-1)\left\langle W_{1,2}W_{2,1} \right\rangle \tag{30}$$

(which requires $W_{i,j} = W_{i,2}$, $i = 2,3,\ldots,N$).

Given the above, it is possible to express the contribution to the n-th symetric term in the series (28) by the $(N-1)(N-2)\ldots(N-m)$ numerically equivalent terms of the type

$$\frac{1}{s^{n+1}}\left\langle \Pi(-1)\Pi W_{i,j} \right\rangle = \frac{1}{\Omega}\,\frac{1}{s^{n+1}}\int d\bar{r}_1 \ldots \int d\bar{r}_N\, \Pi(-1)\ \Pi\ W_{i,j} \tag{31}$$

where the particular $W_{i,j}$ factor repeats in formula (31) m-times ($m \leq n$). In other words, each symetric term in equation (28) will be equal to the sum of the terms of the type

$$\frac{(N-1)(N-2)\ \ldots\ (N-m)}{\Omega^m\, s^{n+1}} \int d\bar{r}_1 \ldots \int d\bar{r}_N\, \overset{i}{\Pi}\,(-1)\ \overset{m}{\Pi}\, W_{i,j} \tag{32}$$

where i is the number of diagonal terms $[\mathbf{W}]_{L,L}$ contributing to the expression (32).

A pictorial representation of the distinct terms involving (32) has been represented by means of diagrams. Given certain topological properties of the different diagrams the authors (7) could reduce the number of diagrams distinctly contributing to equation (28). They expressed the symmetric part of the Greens function as

$$G^s(s) = \left\langle [s-\mathbf{W}]^{-1}_{1,1} \right\rangle = s^{-1} + \begin{pmatrix}\text{The sum of all distinct diagrams}\\ \text{representing (32) beginning and}\\ \text{ending on the site 1)}\end{pmatrix} \tag{33}$$

In reference to the contribution to equation (28) from the off-diagonal elements of the matrix $\mathbf{W}$, the authors (8) represented $(N-2)(N-3)\ldots(N-m-1)$ equivalent terms by the expression of the type

$$\frac{N-1}{s^{n+1}} \left\langle \exp(i\,\bar{k}\,\bar{r}_{1,2})\ \Pi(-1)\ \overset{m}{\underset{}{\Pi}}\ W_{i,j} \right\rangle$$
$$= \frac{N-1}{s^{n+1}\ \Omega^{m+1}} \int d\bar{r}_{1,2} \cdots \int d\bar{r}_{1,\,m+1}\ \Pi(-1)\ \overset{m}{\underset{}{\Pi}}\ W_{i,j}\ \exp(i\,\bar{k}\,\bar{r}_{1,2}) \tag{34}$$

Each distinct term of the type (34) can also be represented by a diagram.

The remaining, nonsymetric contribution to Greens function $(G^m(\bar{k},s) = N-1)\exp(-i,\bar{k},\bar{r}_{1,2})[(s-\mathbf{W})^{-1}]_{1,2}$ can be expressed as

$$G^m(\bar{k},s) = \begin{pmatrix}\text{The sum of all distinct diagrams such that each}\\ \text{starts at the site 1 and ends at the site 2 and}\\ \text{involves zero or more other sites coupled by}\\ \text{"}W_{i,j}\text{" or "}-W_{i,j}\text{" term.}\end{pmatrix} \tag{35}$$

Topological properties of expression (35) suggest a following expression

$$\sum(k,s) = \frac{1}{\rho\, G^s(s)^2} \cdot \begin{pmatrix}\text{The sum of all diagrams of the type}\\ (35) \text{ with no nodes)}\end{pmatrix} \tag{36}$$

where $\delta = \frac{N}{\Omega} < \infty$ while $N, \Omega \longrightarrow \infty$(a node occurs in the diagram at the site M, coupled by the string $W_{1,j}, W_{j,k}, \ldots, W_{n,M}$ with the site 1 and by the string $W_{M,r}, W_{r,s}, \ldots W_{t,M}, \ldots, W_{0,2}$ with the site 2 such that the site M is again involved).

The fact that the frequency variable s dependence of formula (30) is contained in $G^s(s)$ functions, can be expressed by the notation

$$\sum(k,s) = \widetilde{\sum}(k,G^s(s)) \tag{37}$$

Finally, the following expression was obtained

$$G(\bar{k},s) = G^s(s)\ [1-\rho G^s(s)\widetilde{\sum}(k,G^s(s))] \tag{38}$$

Given the fact, that

$$\lim_{k \to 0} G\ (\bar{k},s) = s^{-1}$$

it is possible to obtain

$$G^s(s) = [s+\rho\widetilde{\sum}(0,G^s(s))]^{-1} \tag{40}$$

From the above and equation (38) the following is obtained

$$G(\bar{k},s) = \{s+\rho[\widetilde{\sum}(0,G^s(s)) - \widetilde{\sum}(k,G^s(s))]\}^{-1} \tag{41}$$

From the definition of Generalized Diffusion Coefficient the following is obtained

$$D(\bar{k},s) = \frac{\rho}{k^2}\ [\widetilde{\sum}(0,G^s(s)) - \widetilde{\sum}(k,G^s(s))] \tag{42}$$

To evaluate expression (37) the authors (8) used a two body approximation. In particular they approximated the terms (32) and (34)

by their contributions involving only combinations of $W_{1,2}$'s (transfer note between site 1 and 2). It should be mentioned, that this approximation will be built out of all the power components contributing to formula (27) under the assumption, that the two sites dominate the energy migration. This seems to be consistent with, but not necessarily equivalent to the assumption that the energy migration rate is distance independent.

Using formula (33) and (40) in the two body approximation the authors (8) obtained

$$G^s(s) = \frac{\{\frac{\Pi^2 C^2}{4}\left[1-\left(1+\frac{32s\tau}{\Pi^2 C^2}\right)^{1/2}\right]+4s\tau\}}{4s\tau} \tag{43}$$

To interpret the preceding steps, requirement that the transfer rate is the distance independent has to be made. In spite of that, dipole-dipole mechanism of sites interaction was assumed (8). This implies the following

$$W_{1,2} = W(r_{1,2}) = \frac{1}{\tau}\left(\frac{R_o}{r_{1,2}}\right)^6 \tag{44}$$

where R_o is the Förster radius of interaction and τ is the excitation lifetime and $C = (\frac{4R_o^3}{3})\rho$ is dimensionless density of the sites.

As a consequence, $D(\bar{k},s)$ was obtained in the continuity limit as

$$D(\bar{k},s) = \frac{CR_o}{6\tau}\int_o^\infty dx \frac{x^{2/3}}{x^2+2G^s(s)/\tau} \tag{45}$$

Integration of the above, together with formula (43) yields

$$D(0,s) = 0.4665\, R_o^2 s^{-1/6} \tau^{5/6} + 0.08635\, C^2 R_o^2 s^{-1/3} \tau^{-4/3} + O(s^{-5/6}) \quad (46)$$

or, in the long time limit ($s \longrightarrow 0$), from formula (43) and (47) D(0,0) is obtained as

$$D(0,0) = 0.483 C^{4/3} R_o^2 \tau^{-1} \quad (47)$$

Estimation of $G^s(s)$ in a three body approximation leads to the evaluation of the long time limit of the diffusion coefficient of the form

$$D(0,0) = 0.428 C^{4/3} R_o^2 \tau^{-1} \quad (48)$$

The similarity of result (46) to result (26) obtained by Haan and Zwanzing (7) is not surprising; the physical limits of both models are the same and have already been discussed. In particular, the first numerical factor in formula (46) agrees very closely with the first numerical factor in formula (26). To obtain formula (26), a model requires that the energy be trapped in between donor site (which conceptually represents the first body) and acceptor continuity (what conceptually represents second body in the so-called "two body approximation" of Haan and Zwanzing (7)).

In the case of the second numerical factor in formula (46) as compared to its equivalent in formula (26) the discrepancy can be explained by the conceptual difficulty of defining a three body approximation in the continuity limit, as it was established by Haan and Zwanzing (7).

Also, a remark should be made about the $k \longrightarrow 0$ limit of both of the discussed concepts. In fact, this limit requires a low concentration

of the energy transferring sites. This requirement seriously limits the applicability of the two-body approximation of the Generalized Diffusion Coefficient. It is expected, that two-body process will dominate the energy migration in the case of a high concentration of sites.

The diffusion constant obtained by Förster (10) for the perfect crystal lattice in the case of the dipole-dipole energy migration has the form

$$D = S\, C^{4/3} R_o^{2} \tau^{-1} \tag{49}$$

where S is the structure dependent constant. In the case of the simple cubic lattice S is equal to 0.409 while in case of the diamond lattice S= 0.447. Formula (49) agrees very well with the long time limit of the Generalized Diffusion Coefficient expressed by formula (48). Resemblance is intuitively justified, given the fact that in the derivation of formula (49), the spatial distribution of the exciton probability was approximated by its lowest term, invariant under the rotation in the Taylor series density expansion. This pretty well matches ones image of the physical limitations built into the Generalized Diffusion Coefficient theory, since Förster's (10) approach clearly will favor transfer of energy to the nearest neighbor.

C. Fluorescent Response of the Solids

The theory of a Generalized Diffusion Coefficient offers an insight into the energy migration process by means of the time dependence of the diffusion coefficient. Formula (24) establishes the relationship between the diffusion coefficient and the mean square

displacement in case of the small site concentration. As shown in reference 9, this formula can be readily generalized in the case of the higher concentrations. The theory showed the time dependence of the diffusion coefficient, and of the mean square displacement, as being the result of the discrete distribution of the sites participating in the energy migration.

An alternative approach to the theoretical problems associated with the energy migration is to develop models offering the results in the form of the fluorescent response of the material. This approach derives its inspiration directly from the experimental work, since the comparison between the theoretical and experimental result is in this case straightforward. It seems to be intuitively justified to start the theoretical investigation of the energy migration from the equation approximating processes expressed by equation (6). However, in different approaches this equation was subjected to the different modifications, depending on which aspects of the energy migration processes were to be emphasized.

An example of this approach was demonstrated decades ago by Förster (11). The author set up an equation describing the dynamics of the probability of the energy occupying sensitizer site surrounded by the population of N activators. The finite lifetime of the sensitizer excitation as well as the dipole-dipole interaction between the sensitizer and the activator was assumed. The possibility of the back activator-to-sensitizer energy migration was excluded. The equation proposed has the form

$$-\frac{d\rho}{dt} = \frac{1}{\tau_o} + \frac{1}{\tau_o}\sum_{k=1}^{N} \left(\frac{R_o}{R_k}\right)^6 \qquad (50)$$

where ρ is the probability that sensitizer site maintains excitation, τ_o is the sensitizer lifetime, R_o is the dipole-dipole interaction radius, R_k and is the distance between the sensitizer and the k-th activator.

The above equation requires no preference to the direction of the energy migration. To compute $\bar{\rho}(t)$, an average probability that the energy of excitation remains at the sensitizer site, two assumptions were made:

1. activators are distributed uniformly throughout the medium.

2. $\left(\frac{R_o}{R_g}\right)^6 \frac{t}{\tau_o} << 1$ for $R_g = \sqrt{\frac{3}{4\pi C}}$

where C designates the concentration of the activators.
Condition 2 can be satisfied by the appropriate selection of the concentration (C) or by setting up the time interval of the possible experiment in a reasonable range (t).

The assumptions 1 and 2 are in fact neither equivalent nor mutually dependent. The applicability of the Förster's model require that conditions 1 and 2 are together but independently satisfied.

As obtained by Förster (11) formula for $\bar{\rho}(t)$, averaged probability that at the time t atom is still excited, takes the form

$$\bar{\rho}(t) = \exp\left(-\frac{t}{\tau_o}\right) \exp\left(-\frac{\sqrt{\pi}\, N R_o^3}{R_g^3} \sqrt{\frac{t}{\tau_o}}\right) \qquad (51)$$

The second exponent in equation (51) involving the $\sqrt{t}$ dependence is called a "survival function."

Since the intensity of the sensitizer luminescence is proportional to the $\overline{\rho}(t)$, the formula (51) describes the fluorescent response of the material in the sensitizer part of its spectrum.

The survival function describes a departure from the pure exponential, insulated sensitizer luminescence. This departure is due to the presence in the sensitizer neighborhood of a low number of perfectly smeared out activators.

The parameter R_o allows distinction between different sensitizer-activator systems, since in fact it expresses spectroscopic properties of the dipole-dipole coupled transferring pairs (10,11).

Later on, Dexter (12) extended the scope of the applicability of the Förster's model. The author (12) developed the technique of computing the sensitizer-activator transfer rates in cases other than dipole-dipole coupling interactions. The derived formula also predicted the possibility of the energy transfer between the sensitizers and the activators coupled by means of the forbidden transitions.

The combined efforts of Förster (10,11) and Dexter (12) resulted in the establishment of theoretical tools to investigate the influence of energy migration on the spectroscopic properties of the materials. However, two assumptions made in Förster's description set the limits of the applicability of his model. To extend these limits several other theoretical treatments were developed addressing different aspects of the energy migration processes.

In the following section a review of some of these theories will be made. The main questions asked during the theoretical investigations are about the geometry of the energy migration medium.

The ultimate goals of these approaches is to discuss the influence of the discreteness of the medium on the dynamics of the fluorescent response.

Siebold and Weber (13) developed a Discrete Shell Model (DSM) of the energy migration. However, their model equations were first set in a continuous domain. To describe the exciton dynamics, the following geometrical configuration was assumed: the activator is surrounded by a population of uniformly distributed sensitizers. The energy migration within the sphere of activators is controlled by the radial part of the diffusion operator, while sensitizer-activator transfer takes place in either spontaneous or stimulated process. Application of the diffusion operator descriging the energy migration in this model, in principle, gives the same degree of approximation of the process as the approximation in Forster's (10) work.

The set of the proposed equations takes the form

$$\frac{\partial s_h(r,t)}{\partial t} = -[\tau_s^{-1} - v(r) + w(r)]s_h(r,t) + w(r)a_h(t) + C_s^{-1}\,\mathrm{div}\, DC_s \,\mathrm{grad}\, s_h(r,t) + {}^{e}\tilde{J}_s(t) \tag{52}$$

$$\frac{\partial a_h(t)}{\partial t} = -\tau_a^{-1} a_h(t) + \int_0^{\infty} \{[v(r)+w(r)]s_h(r,t) - w(r)a_h(t)\} n_s(r)\, d\bar{r} + {}^{e}\tilde{J}_a(t) \tag{53}$$

where ${}^{e}J_{s,a}(t)$ is the sensitizer, activator generation term, $w(r)$ is the probability of the energy transfer between sensitizer and activator over the distance r during the stimulated process, $u(r)$ is the probability of the energy transfer between sensitizer and activator

during the spontaneous process, $\tau_{s,a}$ is the sensitizer, activator lifetime, D is the sensitizer energy diffusion coefficient, $n_s(r)$ is the radial sensitizer distribution function, $s_h(r,t)$ is the probability that the sensitizer positioned at r is excited, $a_h(t)$ is the probability that the activator is excited, C_s is the concentration of sensitizers. Given the fact, that each activator contributing to the luminescence of the material can be surrounded by different spheres of influence, a distinction needs to be made between different radii of the activator influence. This distinction is expressed by the index h.

Assuming the uniform distribution of the activators, the distribution of the radii the activator influence can be found as

$$p(h)dh = C_a\ 4\Pi h^2 \exp\left(\frac{-4C_a h^3}{3}\right)dh \tag{54}$$

where h is the radius of the activator influence, and C_a is the concentration of activators.

Expressing the uniform distribution of the sensitizers in a spherical system of coordinates, and assuming that there are no sensitizers outside the sphere of the activator influence, sensitizer distribution can be expressed as

$$n_s(r,h) = C_s\ 4\Pi r^2 \Theta(r-h) \tag{55}$$

where $\Theta(x)$ is the Heavyside step function.

At this point equation (52) can be multiplied by equation (55) (which extinguishes the energy migration outside the activator sphere of influence) and the product can be averaged over the distribution (54). Also equation (53) can be averaged over the distribution (54) and if the slow h-variation of the probabilities $s_h(r,t)$ and $a_h(t)$ is

assumed, the following set of equations is obtained

$$n_s(r)\frac{\partial s(r,t)}{\partial t} = -[\tau_s^{-1}+v(r)+w(r)]n_s(r)s(r,t) + w(r)n_s(r)a(t)$$
$$+D\frac{\partial}{\partial r}n_s(r)\frac{\partial}{\partial r}s(r,t)+n_s(r)^eJ_s(t) \quad (56)$$

$$\frac{\partial a(t)}{\partial t} = \tau_a^{-1}a(t)+\int_o^\infty\{[v(r)+w(r)]s(r,t)-w(r)a(t)\}n_s(r)dr$$
$$+^eJ_a(t) \quad (57)$$

where

$$s(r,t) = \int_o^\infty a_h(t)p(h)dh \quad (58)$$

$$a(t) = \int_o^\infty s_h(r,t)p(h)dh \quad (59)$$

$$n_s(r) = C_s\,4\Pi r^2\exp\left(\frac{-C_s 4\Pi r^3}{3}\right) \quad (60)$$

An inclusion into the model of the possibility of contributing to the energy transfer through the presence of different vibronic states of sensitizers and activators (details of which can be found in reference 13) leads to the formulae

$$n_s(r)\{Z_s\dot{U}_s(r,t)+\tau_s^{-1}Z_sU_s(r,t)+\upsilon(r,T)Z_s[V_s(r,t)-V_a(r,t)]$$
$$-Z_sD\frac{\partial}{\partial r}U_s(r,t)\} = n_s(r)^eJ_s(t) \quad (61)$$

$$Z_a\dot{U}_a(t)+\tau_a^{-1}Z_aU_a(t)-\int_o^\infty\upsilon(r,T)Z_s[U_s(r,t)-U_a(t)]n_s(r)dr = {}^eJ_a(t) \quad (62)$$

where

$$Z_{s,a} = \sum_{1,k}^{L,K}\exp\left(\frac{-E_{1,k}}{kT}\right)$$

$$\upsilon(r,T) = \sum_{1}^{L} \sum_{k}^{K} u_{L,k}(r) \left| \frac{B_k B_1}{B_k - B_1} \right| \frac{1}{Z_s} \tag{63}$$

where $u_{1,k}(r)$ is the transfer rate over the distance r between the i-th vibronic sensitizer state and the k-th vibronic activator state in the spontaneous process and

$$U_a = \frac{a(t)}{Z_a} \tag{64}$$

$$U_s = \frac{s(r,t)}{Z_s} \tag{65}$$

To solve the set of equations (61)-(65) the method of discretization can be used. As it has been already mentioned, the diffusion equation can be obtained from the Pauli Master Equation when the continuity limit is assumed. Following this, a discretization of equations (62)-(65) was done (13). It can be tempting to interpret the algebraic structure resulting from the discretization of the equations as an expression of the fact that the energy migration medium has the discrete nature. However, interpretation of the discretization can be misleading in light of the fact that the energy migration between discrete sites will show a strong local anisotropy. This fact was lost in the approximation of the master equation by the radial part of the diffusion equation.

Therefore, it seems to be more appropriate to treat the discretization procedure performed on equations (61)-(65) as a computer-age trick, rather than to attach to it a crucial physical significance. In fact, the application of the Discrete Shell Model requires an interaction strong enough to justify neglect of the discontinuity of the transferring medium.

Performing simple algebraization procedures it is possible to obtain from equations (61)-(65) a set of equations which in the matrix representation take the form

$$\mathbf{C}\dot{\bar{U}}(t) + \mathbf{B}\bar{U}(t) = {}^{e}\bar{J}(t) \tag{66}$$

where different matrix elements take the form

$$[\mathbf{C}]_{i,j} = N_i Z_s \delta_{ij} \quad ; \quad i = 1,2, \ldots L$$

where L is the number of discrete shells in the activator sphere of influence, and

$$[\mathbf{C}]_{M,M} = C_a = Z_a \qquad [\mathbf{C}]_{M,i} = 0 \ , \ i \neq M$$

where M=L+1.

The matrix **B** has the form

$$\mathbf{B} = \begin{bmatrix} B_{1,1} & B_{1,2} & & & & & B_{1,M} \\ B_{2,1} & B_{2,2} & B_{2,3} & & 0 & & B_{2,M} \\ & B_{3,2} & B_{3,3} & B_{3,4} & & & B_{3,M} \\ & & \ddots & \ddots & \ddots & & \vdots \\ & 0 & & \ddots & \ddots & & \vdots \\ & & & & \ddots & & \vdots \\ B_{M,1} & B_{M,2} & B_{M,3} & \ldots & \ldots & \ldots & B_{M,M} \end{bmatrix}$$

and

$$B_{M,M} = Z_a \tau_a^{-1} + \sum_{i=1}^{I} N_i Z_s V_i$$

$$B_{i,m} = B_{M,i} = -N_i Z_s V_i$$

$$B_{i,i} = N_i Z_s (\tau_s^{-1} + V_i) + Z_s \cdot D \cdot \left[\frac{N_{i+1} + N_i}{Z_s (r_{i+1} - r_i)^2} + \frac{N_i + N_{i-1}}{Z_s (r_{i+1} - t_i)^2} \right]$$

$$B_{i+1,i} = B_{i+1,i} = -Z_s D \frac{N_{i+1} + N_i}{2(r_{i+1} - r_i)^2}$$

where

$$N_i = n_s(r_i)$$

$$V_i = \upsilon(r_i, T)$$

At the same time the vectors involved in the equation (66) have the form

$$\bar{U}(t) = \begin{pmatrix} U_1 \\ U_2 \\ \cdot \\ \cdot \\ \cdot \\ U_i \\ U_M \end{pmatrix}$$

$$V_i = U_s(r_i, t) \; ; \; i = 1,2, \ldots L$$

$$V_M = U_a(t)$$

$$e\bar{J}(t) = \begin{pmatrix} e_{J_1} \\ e_{J_2} \\ \cdot \\ \cdot \\ \cdot \\ e_{J_i} \\ e_{J_M} \end{pmatrix}$$

$$e_{J_i} = e_{J_s}(r_i, t) \; ; \; i = 1,2, \ldots L$$

$$e_{J_M} = e_{J_a}(t)$$

At this point algebraic methods should be applied to solve equation (66) in the different cases. Different physical conditions can be specified by setting apropriate initial conditions expressed by $\bar{U}^o(t=t_o)$ as well as specifying necessary details of **C**, **B**, and $e\bar{J}(t)$.

For example, in the case of the selective excitation of sensitizers with the light pulse ($^{e}J_i(t) = \delta(t)$; i=1,2,...L) equation (66) can be set as

$$\mathbf{C}\dot{\bar{U}}(t)+\mathbf{B}\bar{U}(t) = 0 \tag{67}$$

In this case, matrix algebra allows one to express the fluorescent response of the activator $I_a(t)$ and the fluorescent response of the population of the sensitizers $I_s(t)$ as

$$I_a(t) = \tau_a^{-1} Z_a^{1/2} \sum_{i=1}^{M} E_i V_{M_i} \exp(-\gamma_j t) \tag{68}$$

$$I_s(t) = \tau_s^{-1} N Z_s \sum_{i=1}^{M} E_i^2 \exp(-\gamma_i t) \tag{69}$$

where γ_j's are computed from the equation:

$$(\mathbf{B} - \gamma_j \mathbf{C})\bar{H}_j = 0$$

where N is the initial probability of exciting sensitizer, while the relations between the vectors $\bar{H}_j$'s and the vectors $\bar{V}_j$'s can be expressed as

$$\bar{V}_j = \mathbf{C}^{1/2}\bar{H}_j$$

and the initial condition vector $\bar{U}^o$ allows the finding of the parameters E_i through the formula

$$E_i = \bar{H}_i \cdot \bar{U}^o$$

This example shows how to treat a particular case of the fluorescent response of the energy migration model in terms of the matrix algebra. Siebold and Heber also illustrated the cases of

switching off a continuous excitation source, selective acceptor excitation with a light pulse, and changing the external parameters during the constant pumping of the sensitizers. Details can be found in reference 13.

An alternative method of computing the survival function has been demonstrated by Dornauf and Weber (14). They have considered the survival function of the sensitizer, surrounded by the set of activators distributed on the set of N spheres, the radii which can be designated by $R_1, R_2, \ldots, R_N$. The rate of transfer to each sphere (of course, dependent on the number of activators populating that sphere) can be designated by $n(R_k)$, $k=1,2,\ldots,N$. Obviously, the population of spheres is dependent on the probability of the crystal site being populated by the activators as well as on the structure of the crystal (which in fact, also determines the numerical values of the R_1, R_2, $\ldots R_N$ radii). The probability of the i-th configuration of the activators can be designated by $W_i(R_1, R_2, \ldots, R_N)$, in this case the survival function of the sensitizers takes the form

$$f_N(t) = \sum_i W_i(R_1, R_2, \ldots, R_N) \exp\left[-t \sum_{k=1}^{N} n(R_k)\right] \tag{70}$$

The radius of the last sphere R_N can be computed from the condition that the transfer of the energy to the continuum outside the last sphere has to be smaller than the relative decay rate of the sensitizer. This can be expressed as

$$\frac{1}{\tau_o} \int_{R_N}^{\infty} V(r) C \; 4\pi r^2 dr \ll \frac{1}{\tau_o} \tag{71}$$

where C_a is the concentration of the activators, and $V(R)$ is the sensitizer-activator transfer rate over the distance R.

However, in the case of low activator concentration radius R_N evaluated from condition (71) can be smaller than the distance to the nearest neighbor. In this case the condition

$$\frac{f_N(t)}{f_{N+1}(t)} \simeq 1 \tag{72}$$

can be applied to find R_N radius of the last sphere.

To avoid oversimplification due to the assumption of the uniform distribution of activators Tyminski, Lawson and Powell (15) proposed a method of computing $W_i(R_1,R_2,\ldots, R_N)$ similar to that demonstrated by Stevels and Does De Bye (16). The probability $W_i(R_1,R_2,\ldots,R_N)$ can be factorized in the form

$$W_i(R_1,R_2, \ldots, R_N) = W_i(R_1)W_i(R_2) \ldots W_i(R_N) \tag{73}$$

where $W_i(R_k)$ is the contribution to the probability of the i-th configuration from the k-th sphere which contains L activators distributed on the M sites.

The $W_i(R_k)$ computed in this case takes the form

$$W_i(R_k,L,M) = P^L(1-P)^{M-L} \frac{M!}{N!(M-L)!} \tag{74}$$

Finally, the transfer rate to the k-th sphere containing L activators can be expressed as

$$n(R_k) = V(R_k)L \tag{75}$$

The numerical generation of different configuration (designated by the index i), followed by procedure (70)-(75), gives an insight into dynamics of the survival function, while verifying the assumptions made in reference to the V(R) function. The comparison of the above model,

where dipole-dipole sensitizer-activator interaction had been assumed (15) to the experimental data obtained for Eu P_5O_{14} gave reasonable agreement between the theory and time resolved experiment (15).

Another theoretical description of the energy migration has been developed by Huber and his coworkers (18,20,21,23,25,26). In their work the technique called Average T-matrix Approximation (ATA)was used. The equation describing the energy migration accompanied by the sensitizer-activator transfer is in fact a modification of equation (6), which can be written as (18)

$$\frac{dP_n(t)}{dt} = -[\beta_R + X_n + \sum_{n''} W_{n,n''}]P_n(t) + \sum_{n'} W_{n,n'} P_{n'}(t) \qquad (76)$$

where $P_n(t)$ is the probability that the n-th sensitizer is excited, β_r is the inverse of the sensitizer excitation lifetime, X_n is the rate of transfer between the n-th sensitizer and any of the available activators, and $W_{n,n'}$ is the rate of energy migration between the n-th and n'-th sensitizers.

The fluorescent response of the material is investigated after turning off the excitation source, which allows one to eliminate the exciton generation term in equation (76).

Of course, the index n designating the particular sensitizer site participating in the energy migration carries all the information about the distribution of sensitizer sites, as well as the information about the activator distribution around the specified sensitizers.

In matrix representation equation (76) can be expressed as

$$\dot{\bar{P}}(t) = -(\mathbf{1}\beta_R + \mathbf{X})\bar{P}(t) + \mathbf{\Gamma}\bar{P}(t) \qquad (77)$$

where

$\mathbf{1}$ is the unit matrix

$$[\mathbf{X}]_{n,n'} = X_n \delta_{n,n'}$$

$$[\boldsymbol{\Gamma}]_{n,n'} = \delta_{n,n'} \sum_{n''} W_{n,n''} - (1-\delta_{n,n'}) W_{n',n}$$

$$\overline{P}(t) = [P_1(t), P_2(t), \ldots, P_{N_s}(t)]$$

and N_s is the number of the sensitizer sites involved in the process.

Averaged over the population of N_s sensitizers, the fluorescent response of the material can be expressed as

$$F(t) = \exp(-\beta_R t) \frac{1}{N} \sum_{n,n'} [\exp(-t(\boldsymbol{\Gamma}+\mathbf{X}))] \tag{78}$$

From the above, accordingly to its definition, the survival function $f(t)$ can be expressed as

$$f(t) = \frac{1}{N} \sum_{n,n'} [\exp(-t(\boldsymbol{\Gamma}+\mathbf{X}))]_{n,n'} \tag{79}$$

The n-n′ mode of the energy migration can be defined as the distinct way to transfer energy to the sensitizer n′ while assuming, that initially the n-th sensitizer was excited. The fluorescent response of the material averaged over all the possible modes of excitation is equal to the fluorescent response of the sample while the 0-n′ mode of excitation is averaged over all the possible configurations of the sensitizers and activators. Such an average is called a "configurational average" and is designated by the symbol $\langle\ \rangle_c$. Obviously formula (79) can be written as

$$f(t) = \sum_{n} \left\langle [\exp(-t(\boldsymbol{\Gamma}+\mathbf{X}))]_{n,o} \right\rangle_c \tag{80}$$

The Laplace transform of formula (80) can be expressed as

$$\hat{f}(s) = \sum_{n} \left\langle G_{n,o}(s) \right\rangle_c \tag{81}$$

where

$$G_{n,o}(s) = [\mathbf{G}(s)]_{n,o} = [(\mathbf{1}s + \mathbf{r} + \mathbf{X})^{-1}]_{n,o} \tag{82}$$

The Fourier transform $G(\bar{k},s)$ defined through the formula

$$\left\langle G_{n,o}(s) \right\rangle_c = \frac{1}{N_s} \sum_{\bar{k}} \exp[-ik(\bar{r}_n - \bar{r}_o)]G(k,s) \tag{83}$$

allows one to express the Laplace transform of the survival function as

$$\hat{f}(s) = \left\langle G(0,s) \right\rangle_c \tag{84}$$

If the approximation, of the sensitizer-sensitizer and the sensitizer-activator interaction by their averaged values, is assumed to provide an adequate description of the process, the ATA results can be used (for details see reference 17). Using ATA results equation (84) is expressed in the form

$$\hat{f}(s) = [s + C_a \sum_{i,i'} \hat{t}_{i,i'}(s)]^{-1} \tag{85}$$

where $C_a = \frac{N_A}{N_S}$ is the ratio of the activator to sensitizer numbers.

The operator $\hat{t}$ in its matrix representation can be obtained through the solution of equation

$$\hat{t}_{i,i'}(s) = X_{o,i}\delta_{i,i'} - \sum_{i''} X_{o,i}\, \hat{g}_{i,i''}(s)\hat{t}_{i'',i'}(s) \tag{86}$$

while the operator $\hat{g}$ represents the Laplace transform of the energy migration operator in the activator free medium and can be expressed as

$$\hat{g}(s) = (\mathbf{1}s + \mathbf{r})^{-1} \tag{87}$$

or in the matrix representation it takes the form

$$\hat{g}_{i,i'} = \frac{1}{N_s} \sum_{k} \exp[i\bar{k}(\bar{r}_{i'}-\bar{r}_i)]\hat{g}(\bar{k},s) \tag{88}$$

for

$$\hat{g}(\bar{k},s) = (s + \sum_{n,n'} W_{n,n'}\{1-\cos[\bar{k}(\bar{r}_n-\bar{r}_{n'})]\})^{-1} \tag{89}$$

The formulae (85)-(89) represent the foundation of the Average T-Matrix Approximation method developed to gain an insight into the energy migration processes and its influence on the spectroscopic properties of the solids. However it should be stressed, that the ATA formalism requires the approximation of sensitizer-sensitizer as well as sensitizer-activator interactions by their averaged values (17).

The short time behavior of the material is determined by the $s \longrightarrow 0$ limiting case (18). In this limit the result

$$\hat{f}(s) = (s + C_A \sum_i X_{o,i})^{-1} \tag{90}$$

can be represented in the time domain as

$$f(t) = \exp(-C_A\, t \sum_i X_{o,i})^{-1} \tag{91}$$

Another limiting case is the weak sensitizer-sensitizer interaction case. It allows the neglect of the off-diagonal elements of the t matrix and leads to the following form of the survival function in the frequency domain

$$f(s) = [s + C_A \sum_i X_{o,i}(1 + X_{o,i}\hat{g}_{o,i}(s))^{-1}]^{-1} \tag{92}$$

The above case physically corresponds to the model considered by Burshtein (19). The formula derived by Burshtein is

$$f(t) = f_o(t)e^{-t/\tau_o} + \frac{1}{\tau_o}\int_o^t dt\ f_o(t-\tau)e^{-(t-\tau)/\tau_o}f(\tau) \qquad (93)$$

where $f_o(t)$ is the survival function in the activator-free medium, τ_o^{-1} is the averaged sensitizer-activator transfer rate, and f(t) is the survival function in the medium in which the sensitizer-sensitizer migration is perturbed by the sensitizer-activator transfer. Formula (93) was derived assuming the Markoffian type of migration process.

It's possible to express (92) by its power of C_A expansion. In the low C_A limit it is justified to truncate all the terms involving higher than first power of C_A contributions. The correspondence between the obtained formula and the Laplace transform of equation (93) requires, that

$$\hat{g}_{i,i}(s) = \frac{1}{s + \tau_o^{-1}} \qquad (94)$$

This is not suprising given the fact that interpretation of Markoffian process is close to the requirement of the lack of correlation between the different sensitizer-sensitizer processes τ_o^{-1} represents operator Γ in the random hopping process.

In the case when the diffusion limit of the energy migration is under investigation, formulae (85)-(89) take the continuous form (18, 20)

$$\hat{f}(s) = [s + C_A \int d\bar{r}\ d\bar{r}'\ \hat{t}(\bar{r},\bar{r}',s)]^{-1} \qquad (95)$$

$$\hat{t}(\bar{r},\bar{r}',s) = \upsilon(\bar{r})\delta(\bar{r}-\bar{r}') - \int d\bar{r}''\ \upsilon(\bar{r})\hat{g}(\bar{r},\bar{r}'',s)\hat{t}(\bar{r}'',\bar{r},s) \qquad (96)$$

As a consequence of interpreting equation (87) as the Laplace-Fourier transform of the Greens function of the diffusion operator in the activator-free medium, equations (88) and (89) give

$$\hat{g}(\bar{k},s) = (s + k^2 D)^{-1} \tag{97}$$

$$g(\bar{r},\bar{r}',s) = \frac{1}{(2\Pi)^3} \int d\bar{k}\, \exp[-i\bar{k}(\bar{r}-\bar{r}')]g(\bar{k},s) \tag{98}$$

In equation (97), D is the energy diffusion coefficient which is dependent on both the structure of the medium, as well as on the type of the interaction responsible for the energy migration.

The computations demonstrated in reference 21 allow one to express the fluorescent response of the material as

$$\hat{f}(s) = [s + 4\Pi C_A \int_o^\infty dr\, r^2 h(\bar{r},s)]^{-1} \tag{99}$$

while $h(r,s)$ obeys an integral equation of the form

$$h(r,s) = \upsilon(r)\{\sqrt{4\Pi} - \frac{1}{2\sqrt{sD}} \int_o^\infty dr'[e^{-\chi|\bar{r}-\bar{r}'|} - e^{-\chi|\bar{r}+\bar{r}'|}](\frac{r'}{r})h(r,s)\} \tag{100}$$

where $\chi = \sqrt{\frac{s}{D}}$

The long time limit of equation (100) gives

$$h(r,s\rightarrow 0) = \upsilon(r)[\sqrt{4\Pi} - \frac{1}{2D} \int_o^\infty dr'(r+r'-|\bar{r}-\bar{r}'|)](\frac{r'}{r})h(r,s\rightarrow 0)] \tag{101}$$

The fluorescent response of the medium can be expressed as

$$f(t) = \exp(-4\Pi C_a D a_s t) \tag{102}$$

where a_s can be identified as Yokota-Tamimoto's (22) scattering length, and according to equations (101) (102) it can be written as

$$a_s = \frac{1}{\sqrt{4\Pi}\, D} \int_o^\infty dr r^2 h(r,s=0) \tag{103}$$

Finally, the theoretical survival function was fitted to the set of experimental data for comparison and the result was presented in reference 21. In the case of $Pr_{1-x}F_e:Nd_x^{+3}$ crystals at the temperature 12.5 K the best fitted diffusion coefficient was D = 14.0×10^{-9} cm^2/s in case of the Ghosh-Hegarty-Huber (20) model, and D = 8.5×10^{-9} cm^2/s in the case of the Yokota-Tanimoto (22) model. Ghosh and coworkers (20) attributed over sixty percent difference between the diffusion coefficients to the fact, that in their model the assumed sensitizer-activator transfer rate took the form

$$\upsilon(r) \sim \begin{cases} \dfrac{1}{r^6} & r \geqslant r_c \\ 0 & r < r_c \end{cases} \tag{104}$$

where r_c was estimated from the condition, that the sum of the transfer rates to all the sites in a discrete lattice is equal to the total transfer rate to the continuum outside of the sphere of the radius r_c. In the Yokota-Tamimoto (22) model the case of

$$\upsilon(r) \sim \frac{1}{r^6} \tag{105}$$

was assumed. As shown by the authors of reference 20, the correction of the Yokota-Tamimoto's diffusion coefficient by assuming a non-zero scattering length in the sensitizer-activator transfer, reduces the diffusion coefficient discrepancy down to about ten percent.

Considering the case of a fast sensitizer-activator process allows neglect of the off-diagonal sensitizer-sensitizer correlation in formula (86) and leads to equation (92). In the case of high concentrations of activators it is justified to make the approximation that (23)

$$C_a \sum_i \frac{X_{o,i}}{1-X_{o,i}R_o(s)} = n_a \int \frac{\bar{dr}\, x(r)}{1+x(r)R_o(s)} \tag{106}$$

where $R_o(s) = \hat{g}_{i,i}(s)$, $x(r)$ is a function describing the r dependence of the sensitizer-activator transfer rate, and n_a is the density of activators. According to equation (87) $R_o(s)$ can be interpreted as the Laplace transform of the survival function of the activator-free medium. Assuming a dipole-dipole type of sensitizer-activator transfer as well as the dipole-dipole type of sensitizer-sensitizer migration it is possible to obtain

$$\hat{f}(s) = \{s + (\tfrac{2}{3}\pi^2) n_a [\frac{\alpha}{\hat{R}_o(s)}]^{1/2}\}^{-1} \tag{107}$$

$$\hat{R}_o(s) = s^{-1}\{1 - \sqrt{\pi}\,[\frac{\Delta_{s,s}}{(2^{3/2}s^{1/2})}] \exp[\frac{\Delta_{s,s}^2}{(8s)}]\ \text{erfc}\ [\frac{\Delta_{s,s}}{(2^{3/2}s^{1/2})}]\} \tag{108}$$

where $\Delta_{s,s} = (\frac{4}{3}\pi^{3/2}) n_s \beta^{1/2}$, erfc(x) is the complementary error function, $\frac{\alpha}{r^6}$ is the sensitizer-activator transfer rate, and $\frac{\beta}{r^6}$ is the sensitizer-sensitizer transfer rate. To make formula (108) applicable, the assumption is made that the concentration of sensitizers is small. In addition, applicability of equation (107) requires, that

$$\frac{n_a}{n_s} << 1 \tag{109}$$

In the case, when condition (109) doesn't hold, the Coherent Potential Approximation (CPA) can be used (23). Applicability of CPA requires a lack of correlation between the different sensitizer-activator processes contributing to the dynamics of the survival function (24). This condition will hold true if no

activator-sensitizer back transfer is taken into consideration. In the Coherent Potential Approximation, the survival function can be expressed as

$$f(s) = [s + X_{CPA}(s)]^{-1} \tag{110}$$

while $X_{CPA}(s)$ has to satisfy the condition

$$\int_0^\infty \frac{dX\ P(X)[X - X_{CPA}(s)]}{1 + [X + X_{CPA}(s)]\hat{R}(s)} = 0 \tag{111}$$

where $P(X)$ is the probability distribution function of the transfer rate X due to the distribution of sensitizers and activators in the material, and $R(s)$ is the Laplace transform of the conditional probability that the sensitizer will maintain its energy given the possibility of sensitizer-activator transfer.

In light of equation (106) equation (111) should be interpreted as a procedure to create a function $X_{CPA}(s)$, such that the difference $X-X_{CPA}(s)$ in the sense of equation (106) is equal to zero.

Assuming applicability of a continuous sensitizer and activator distribution and a dipole-dipole sensitizer-activator interaction the author (23) obtained

$$P(x) = \left(\frac{\Delta_{s,a}^2}{4\Pi X^3}\right)^{1/2} \exp\left[-\left(\frac{\Delta_{s,a}^2}{4X}\right)\right] \tag{112}$$

where

$$\Delta_{s,a} = \left(\frac{4}{3}\Pi^{3/2}\right) n_a \alpha^{1/2}$$

The form of R(t) was assumed as (23)

$$R(t) = f_o(t)R_o(t)$$

where $R_o(t)$ is the survival function in the activator-free medium, and $R_o(s)$ is the Laplace transform of $R_o(t)$. Förster (11) evaluated the low concentration continuity limit of $f_o(t)$ as

$$f_o(t) = \exp(-\Delta_{s,a} t^{1/2}) \tag{113}$$

what leads to

$$\hat{R}(s) = s^{-1}\{1 - \sqrt{\pi}\,[\frac{\Delta_T}{2s^{1/2}}] \cdot \exp[\frac{\Delta_T}{(4s)}] \cdot \operatorname{erfc}\,[\frac{\Delta_T}{(2s^{1/2})}]\} \tag{114}$$

where

$$\Delta_T = \Delta_{s,s} / \sqrt{2} + \Delta_{s,a}$$

Either, the numerical or the approximate solution of the problem (110)-(114) leads to the Coherent Potential Approximation of the energy migration in the slow sensitizer-activator transfer limit.

In the case of $\Delta_{s,a} R(s)^{1/2} \geq 1$, the following result can be obtained (23)

$$X_{CPA}(s) = \frac{\pi^{1/2}\,\Delta_{s,a}}{[2R(s)]^{1/2}} \tag{115}$$

In the case of $\Delta_{s,a} R(s)^{1/2} << 1$, another formula can be obtained, namely (23)

$$X_{CPA}(s) \simeq R(s)^{-1} \tag{116}$$

what complements the result (110)-(114). Finally, the modifications of the Average T-Matrix Approximation method in case of the high concentration of interstital activators was suggested in reference 25.

The formal distinction between the applicability of formula (92), of the rapid sensitizer-activator, as opposed to the formula (95), of the diffusion limit of the Average T-Matrix Approximation result, can be made in reference to R_o, the radius of sensitizer influence, and n the concentration of sensitizers.

Formula (92) is applicable whenever the condition

$$n_s R_o^3 \leqslant 1 \tag{117}$$

is satisfied, while the application of formula (95) requires

$$n_s R_o^3 >> 1 \tag{118}$$

If the multipole-multipole interaction is assumed to be responsible for the energy migration, a straightforward consideration leads to the following conditions limiting the different cases (18). The condition

$$n_s^{1-\upsilon/v} \left(\frac{\alpha}{\beta}\right)^{3/v} \leqslant 1 \tag{119}$$

limits the applicability of formula (92), and the condition

$$n_s^{1-\upsilon/v} \left(\frac{\alpha}{\beta}\right)^{3/v} >> 1 \tag{120}$$

limits the applicability of formula (95), (where $\frac{\alpha}{r^v}$ is the assumed as the sensitizer-sensitizer migration rate, and $\frac{\beta}{r^\upsilon}$ is the sensitizer-activator transfer rate).

Finally, the question of the activator luminescence can be of importance (26). If the possibility of back, activator-sensitizer transfer is excluded, the dynamics of the activator site can be described by the approximated form of the Pauli Master Equation

$$\frac{dP_i(t)}{dt} = -\beta_a P_i(t) + \sum_k x_{k,i} f_k(t) \tag{121}$$

where $P_i(t)$ is the probability that i-th activator is excited, β_A is the activator excitation lifetime, $x_{k,i}$ is the transfer rate between the k-th sensitizer and the i-th activator, $f_k(t)$ is the survival function of the k-th excited sensitizer.

Equation (121) leads to the following configurationally averaged probability of the excitation of the activator

$$\left\langle P(t)\right\rangle_c = C_s e^{-\beta_a t} \sum_{i\neq 0} x(r_{o,j}) \int_o^\infty dt' e^{-\beta_a t'} \left\langle \Phi^{o,j}(t')\right\rangle_c \qquad (122)$$

where C_s is the probability that the site is occupied by the sensitizer, $X(r_{o,j})$ is the transfer rate between the 0-th activator site and j-th sensitizer site, $\left\langle \Phi^{o,j}(t)\right\rangle_c$ is the configurational average of the survival function of the sensitizer, while the sensitizer occupies the j-th site and the activator occupies the 0-th site. The above forumula, in the case of the fast sensitizer-sensitizer migration, leads to

$$\left\langle P(t)\right\rangle_c = C_s f_s x \frac{e^{-(\beta_s + C_a x)t} - e^{-\beta_a t}}{\beta_a - \beta_s - C_a x} \qquad (123)$$

where $x = \sum_{j\neq 0} x(r_{o,j})$, and β_s is the inverse of the sensitizer lifetime, C_a is the probability, that a site is occupied by the activator, f_s is the fraction of the initailly excited sensitizers.

The set of coupled rate equations describing the process analogous to the one described by equation (121) gives a result identical to formula (123) (for details see reference 26).

In case of the negligible sensitizer-sensitizer migration, equation (122) yields

$$\left\langle P(t)\right\rangle_c = C_s f_s \sum_{j\neq 0} x(r_{o,j}) \frac{e^{-[\beta_s + x(r_{o,j})]t} - e^{-\beta_a t}}{\beta_a - \beta_s - x(r_{o,j})} \qquad (124)$$

The above formula, in the case of a very small activator concentration gives

$$\left\langle P(t)\right\rangle_c = C_s f_s x \frac{e^{-\beta_s t} - e^{-\beta_a t}}{\beta_a - \beta_s} \tag{125}$$

The continuity limit of equation (124) together with the assumption that $\beta_a < \beta_s$

and

$$x(r_{o,j}) = \frac{\alpha}{r^v_{o,j}}$$

give the result

$$\left\langle P(t)\right\rangle_c \sim 4\pi C_s f_s v^{-1}(\beta_s^{-1} - \beta_a^{-1})\Gamma(\tfrac{3}{v})\alpha^{3/v}\exp(-\beta_a t) \tag{126}$$

and the result

$$\left\langle P(t)\right\rangle_c \sim 4\pi C_s f_s v^{-1}\beta_a^{-1} n_L \Gamma(1 - \tfrac{3}{v})\ \alpha^{\frac{3}{v}}\exp(-\beta_s t)t^{(\frac{3}{v} - 1)} \tag{127}$$

for $\beta_a > \beta_s$ (n_L is the lattice site density, and $\Gamma(x)$ is the gamma function). In the case of the long time limit, the luminexcence of the activator is controlled by the exponential term involving either the lifetime of the sensitizer or the activator. This depends on the relationships between the activator and sensitizer decay rates.

D. Conclusions

In this chapter the conclusions of the review of the energy migration theories are presented.

Further work is required to scrutinize the degree of simplication caused by the assumption of the Pauli Master Equation validity to

describe the energy migration process in case of the Generalized Diffusion Coefficient theory. If possible, the description of the energy migration process based on the Generalized Master Equation could be fruitful.

As far as Generalized Diffusion Coefficient theory goes, further theoretical efforts are required to remove the restrictions of the theory applicability due to the two body approximation. The creative discussion of the energy migration Greens function is also required.

Sophistication of the Generalized Diffusion Coefficient results removing the assumption about low site concentration, together with the constructive criticism about the two body approximation will be beneficial.

The Average T-Matrix Approximation approach to the energy migration problem also needs to be discussed in terms of the possible influence of the randomness on the dynamics of the process, the question which has been buried in the assumption, that environments of the transferring sensitizers are identical.

Applicability of the ATA method is impressive indeed. However, care should be exercised in comparing the experimental data with the theoretical results. Complexity of the processes involved together with the necessity of mathematical simplication require, that beforehand verification of the consistency between the formal assumptions and the experimental conditions must be undertaken prior to any attempt to discuss every piece of the experimental data in terms of the Average T-Matrix Approximation energy migration model.

It should be mentioned, that two simplifications can set serious limit for the Average T-Matrix Approximation applicability. One of

them is inherent for the method, the assumption that the sensitizer-sensitizer and the sensitizer-activator interaction is averaged over the volume of the sample. This assumption eliminates from the consideration possibility of investigating the role of the structural randomness in the energy migration processes. The second assumption is the result of the frequently used continuity limit of the derived formulae, which can bring about the loss of information on the influence of the discreteness on the migration process.

The trouble to elucidate the correspondence between the Generalized Diffusion Coefficient and the survival function theory needs to be undertaken. It can explain the relationship between spectroscopical properties of solids and the exciton migration dynamics. An attempt in this direction has been made by Blumen, Klafter, and Silbey (27). They attempted to set the correspondence between both theories through the identification of the f(s) survival function and the $G^s(s)$ function defined by formula (33) of the Generalized Diffusion Coefficient theory, (which defines the diagonal part of the Greens function). Clearly such an identification has a very approximate nature because it ignores the back-transfer process. This brings new limitation in addition to the formal simplifications of the Generalized Diffusion Coefficient theory.

Further theoretical work will extend the scope of the energy migration applicability and and will give a detailed picture of the physical factors determining the exciton dynamics in solids.

CHAPTER III

TIME-RESOLVED SITE-SELECTION SPECTROSCOPY

A. Experimental Equipment and Samples

To investigate the energy migration process in $Eu_xY_{1-x}P_5O_{14}$ crystals Time-resolved site-selection Spectroscopy was used. The experimental scheme is demonstrated in Figure 2. (See also the description in references 28,29.)

A high resolution tunable dye laser pumped by a nitrogen gas laser was used to excite the sample. The sample temperature was controlled by a cryogenic refrigerator. The fluorescence signal was sent through a high resolution spectrometer to a photomultiplier tube. The output of the photomultiplier tube was analyzed by a Boxcar Integrator and was recorded by the LSI-11 computer and X-Y recorder. The samples investigated were small single crystals of $Eu_xY_{1-x}P_5O_{14}$ with x=1.0 and 0.01. The "effective" site symmetry for the Eu^{3+} ions is C_{2v} although the actual symmetry is probably even lower (30). For the 100% sample, the concentration of Eu^{3+} is 9.69×10^{-3} cm. The excitation wavelengths used were around 5290 Å for the 100% sample. The dominant fluorescence emission originates from the $^5D_0$ level and the lifetimes of the ions in both sensitizer and activator sites are approximately the same and independent of temperature between 12 and 300 K for both samples. For the 100% sample τ=5 ms and for the 1.0% sample τ=4 ms with no observable rise times.

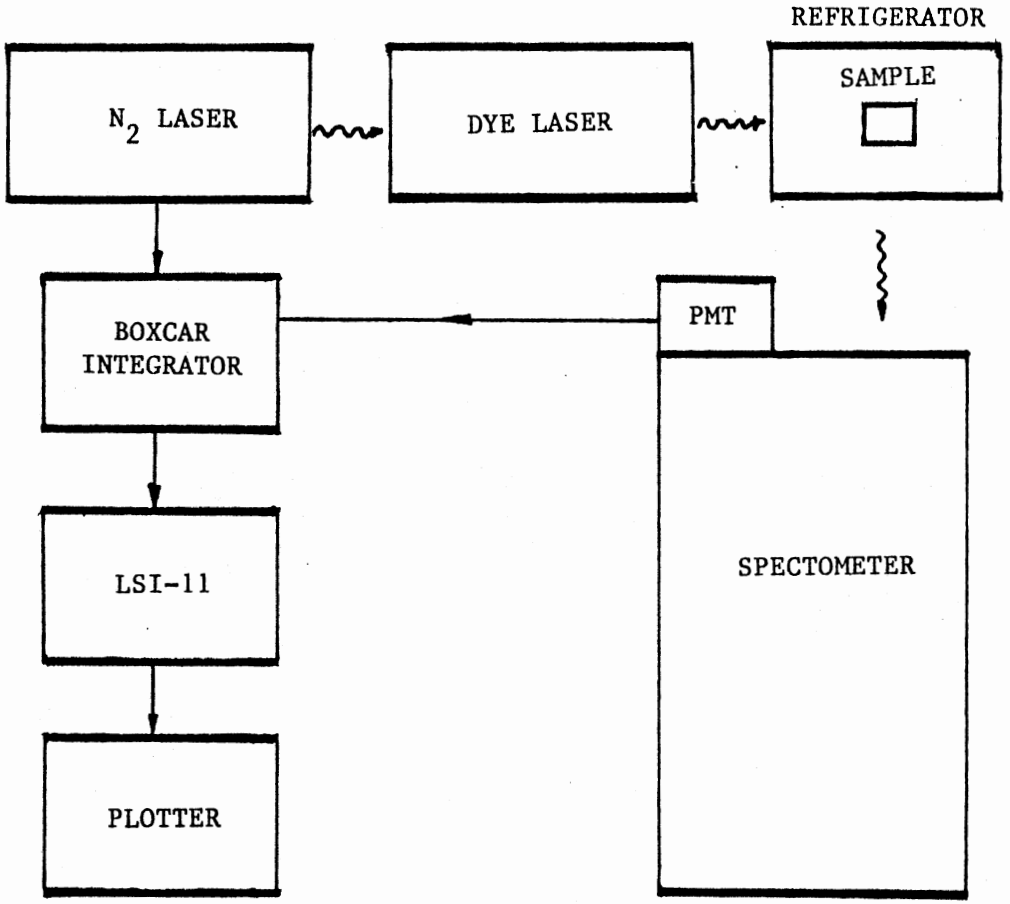

Figure 2. Time-resolved, site-selection experimental apparatus.

The energy level diagram of Eu^{3+} ions is shown in Figure 3. To monitor the energy migration process the $^5D_0 \longrightarrow {}^7F_2$ transition was chosen because of its distinct presence in the fluorescence spectrum and its sensitivity to the local symmetry of sites.

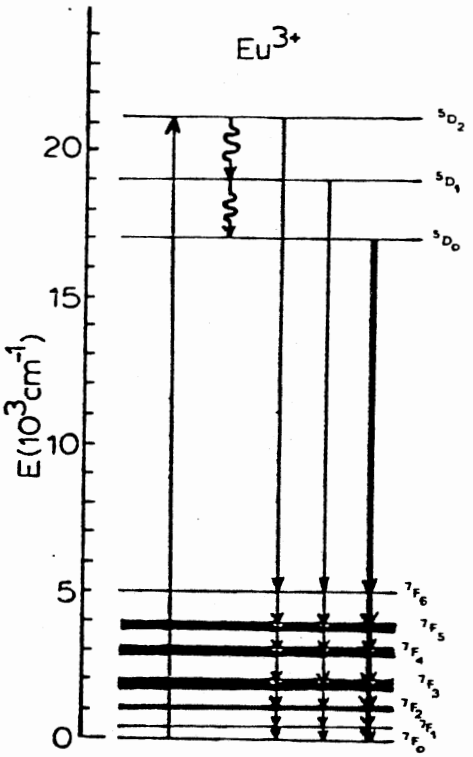

Figure 3. Lowest lying energy levels and transitions for Eu^{3+} ions. The widths of the levels indicate approximate splittings of crystal field states in various hosts.

The fluorescence spectrum of EuP_5O_{14} is shown in Figure 4. The spectrum was recorded at 1 ms after the laser excitation pulse. The wavelength of excitation was λ_{exc} = 5290 Å for the dot line and λ_{exc} = 5691 Å for the dash line. The fluorescence of $Eu_{0.01}Y_{0.99}P_5O_{14}$ is shown in Figure 5. The spectrum was recorded at 1 ms after laser excitation

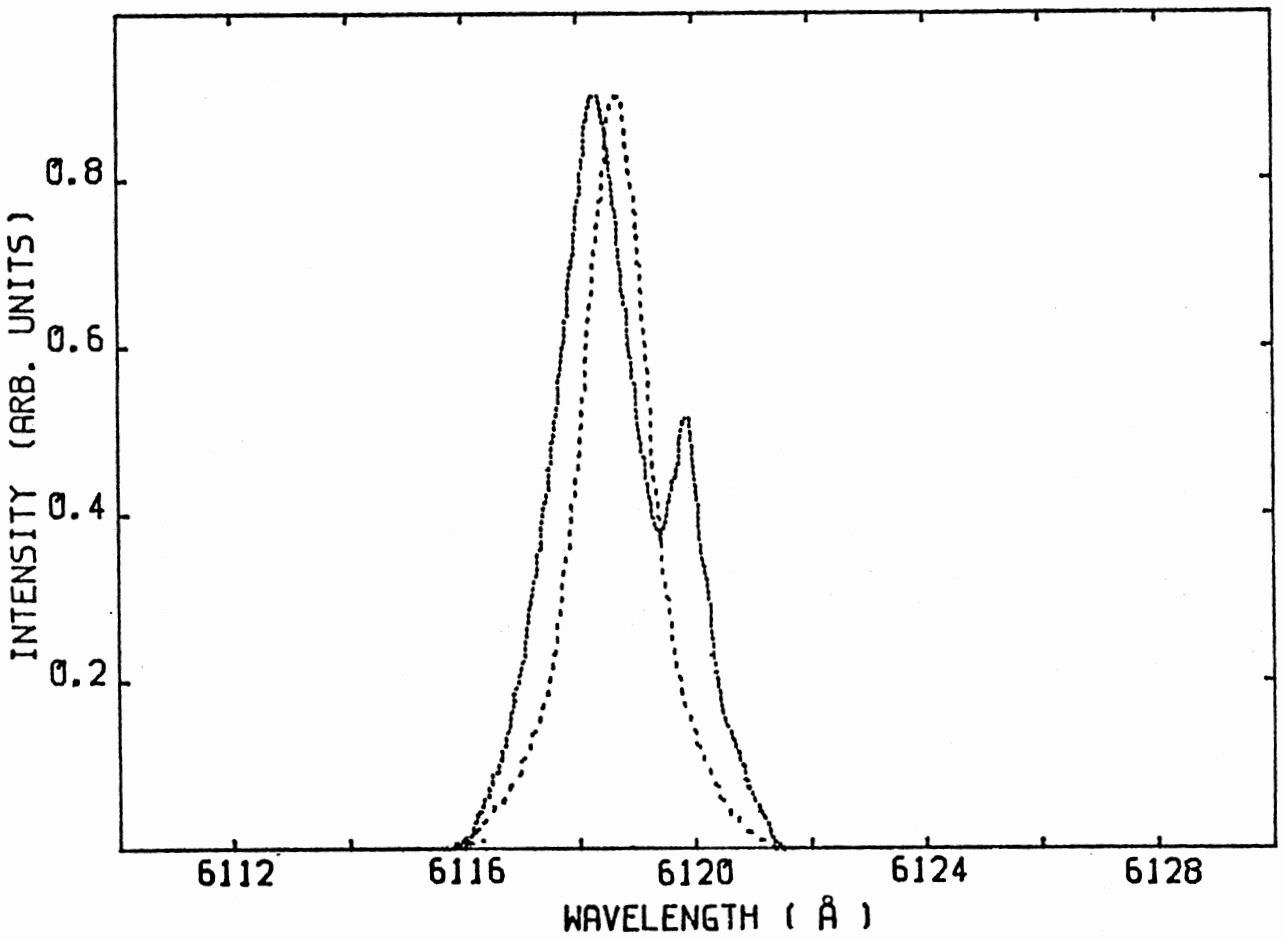

Figure 4. Fluorescence spectra of EuP_5O_{14} at two different excitation wavelengths. Temperature of the sample was 12 K. Spectra were taken at 1.0 ms after excitation. For the dot line excitation wavelength was 5920 Å. For the dash line excitation wavelength was 5291 Å.

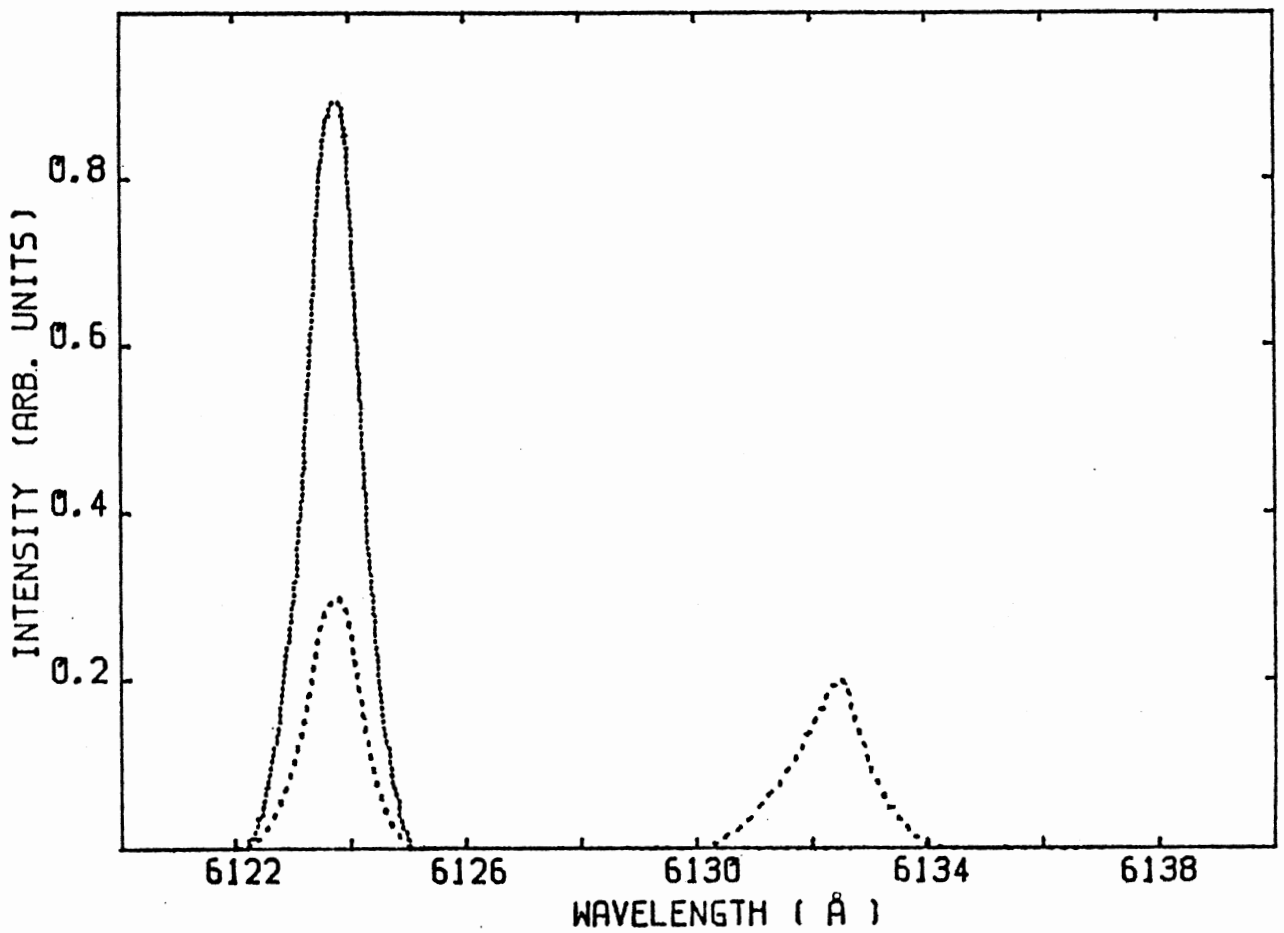

Figure 5. Fluorescence spectra of $Eu_{0.01}Y_{0.99}P_5O_{14}$ at two different wavelengths. Temperature of the sample was 12 K. Spectra were taken at 1.0 ms after excitation. For the dot line excitation wavelength was 5232 A. For the dash line excitation wavelength was 5237 Å.

pulse. The wavelength of excitation was λ_{exc} = 5232 Å for the dot line and λ_{exc} =5237 Å for the dash line. Both samples were kept at the temperature of 12 K.

For this host two different spectral lines appear for this specific transition and their relative intensities vary with laser excitation wavelength. The positions and relative splitting of these lines are significantly different for the 100% and 1.0% samples. In the former sample, the transition energy difference is $\Delta E_{SA} \simeq 5\ cm^{-1}$ and 0.5% of the Eu^{3+} ions are in activator sites, while for the latter sample $\Delta E_{SA} \simeq 25\ cm^{-1}$ and about 36.3% of the Eu^{3+} ions are in activator sites.

In the case of the 100% sample the specific initial excited state distribution created by the laser pulse leads to an energy transfer from ions in the sites giving rise to the lower energy transitions, to ions in the sites associated with the higher energy transitions. In the lightly doped sample the energy transfer goes from the ions giving rise to the higher energy transition to those producing the low energy transition. Figure 6 shows the time evolution of EuP_5O_{14} spectrum, while Figure 7 shows the time evolution of $Eu_{0.01}Y_{0.99}P_5O_{14}$ spectrum.

B. Results and Interpretation

To discuss the experimental data of the Time-resolved spectroscopy experiment in terms of a theoretical model, a two level system description can be applied. Its pictorial representation when possibility of back-transfer is excluded is shown in Figure 8.

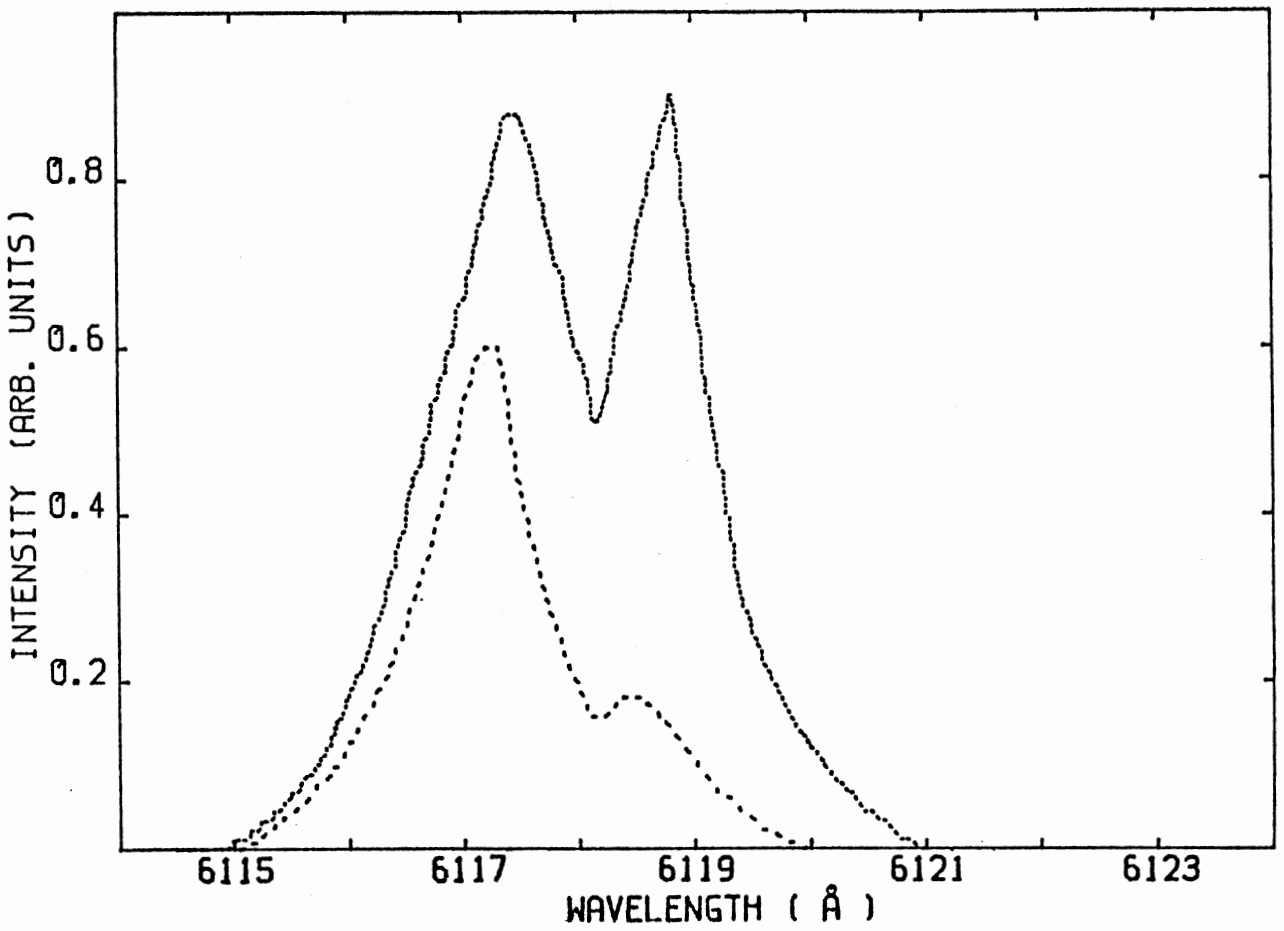

Figure 6. Time evolution of EuP_5O_{14} spectrum. Spectra were taken at 12 K. For the dot line spectrum was taken at 0.05 ms after excitation. For the dash line spectrum was taken at 1.6 ms after excitation. Excitation wavelength was 5291 Å.

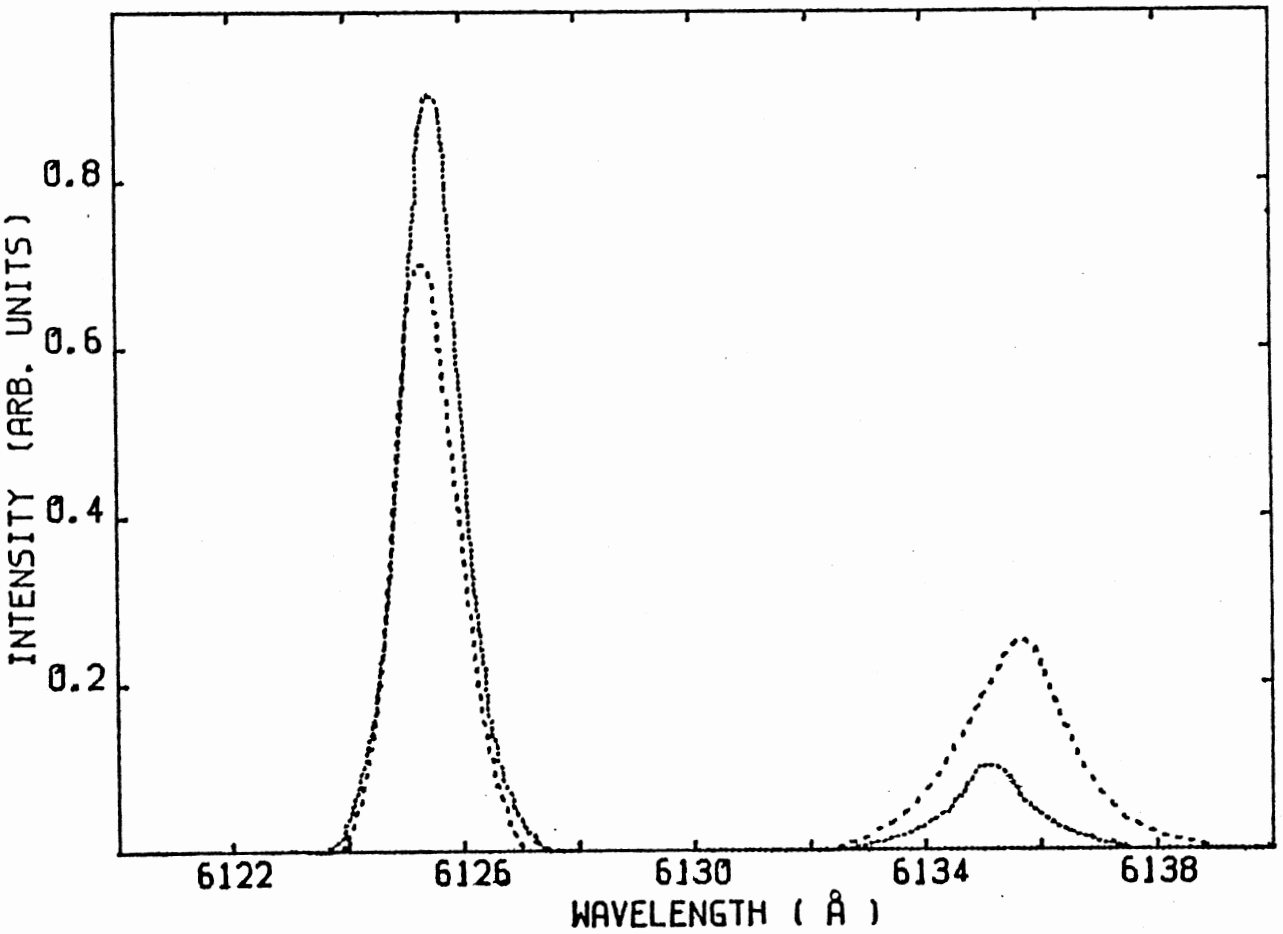

Figure 7. Time evolution of $Eu_{0.01}Y_{0.99}P_5O_{14}$ spectrum. Spectra were taken at 12 K. For the dot line spectrum was taken at 0.05 ms after excitation. For the dash line spectrum was taken at 1.6 ms after excitation. Excitation wavelength was 5236 Å.

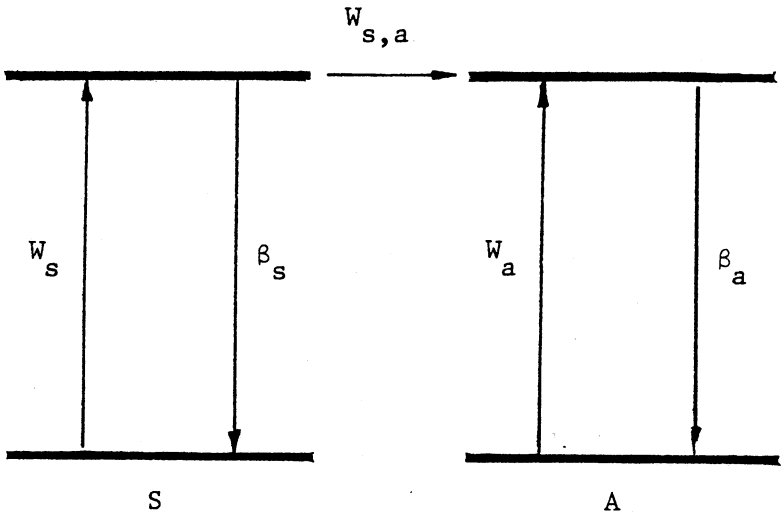

Figure 8. Two level system including the possibility of the sensitizer (S) to activator (A) energy transfer.

In the above figure the meaning of the symbols is the following: W_s is the sensitizer pumping rate, W_a is the activator pumping rate, $\beta_{s,a}$ is the inverse of the sensitizer, activator lifetime, and $W_{s,a}(t)$ is the sensitizer-activator transfer rate.

The survival function of the sensitizer state in the two level system, representing the averaged populations of the sensitizers and activators in the real crystal, can be written as

$$f(t) = \exp[-W_{s,a}(t)\ t] \tag{128}$$

From the above formula, the $W_{s,a}(t)$ transfer rate can be found as a solution of

$$W_{s,a}(t) - \dot{W}_{s,a}(t)\ t = -\frac{f(t)}{\dot{f}(t)} \tag{129}$$

The set of the differential equations describing the evolution of the number of the excited sensitizers, and the activators in the above two level system is

$$\dot{n}_a = -\beta_a n_a + W_{s,a}(t) n_s + W_a \tag{130}$$

$$\dot{n}_s = -\beta_s n_s - W_{s,a}(t) n_s + W_s \tag{131}$$

where n_a and n_s are the number of activators and sensitizers, and remaining symbols are the same as in Figure 8.

Assuming delta function type of excitation term ($W_s(t) \sim \delta(t)$ and $W_a(t) \sim \delta(t)$) the following result is obtained

$$\frac{n_a(t)}{n_s(t)} = \frac{n_a(0)}{n_s(0)} \frac{\exp(-\beta_a t)\left[1 + \frac{n_s(0)}{n_a(0)}\,\Phi(t)\right]}{\exp(\beta_s t)\exp\left(-\int_o^t W_{s,a}(t')dt'\right)} \tag{132}$$

for

$$\Phi(t) = \int_o^t W_{s,a}(t')\exp[(\beta_a - \beta_s)t']\exp\left[-\int_o^{t'} W_{s,a}(t'')dt''\right]dt' \tag{133}$$

where $n_s(0)$ and $n_a(0)$ are the initial numbers of excited sensitizers and activators.

The luminescence intensities of sensitizers and activators can be written as

$$I_{s,a}(t) \sim \beta_{s,a}\, n_{s,a}(t)$$

In the case of a Förster's dipole-dipole type of migration process, the $W_{s,a}(t)$ can be obtained in the form (11)

$$W_{s,a}(t) = \frac{4}{3}\pi^{3/2} R_o^{\,3} C_a \beta_s^{\,1/2} t^{1/2} \tag{134}$$

where C_a is the concentration of activators, and R_o is the dipole-dipole energy interaction radius.

The formulae (132)-(134) yield

$$\frac{I_a(t)}{I_s(t)} = \left(\frac{I_a(0)}{I_s(0)} + 1\right)\exp(-2\gamma t^{-1/2}) - 1 \tag{135}$$

where

$$\gamma = \frac{3}{4}\pi^{3/2} R_o^3 C_a \beta_s^{1/2} \tag{136}$$

The two level system, when the possibility of a back transfer is assumed, is shown in Figure 9.

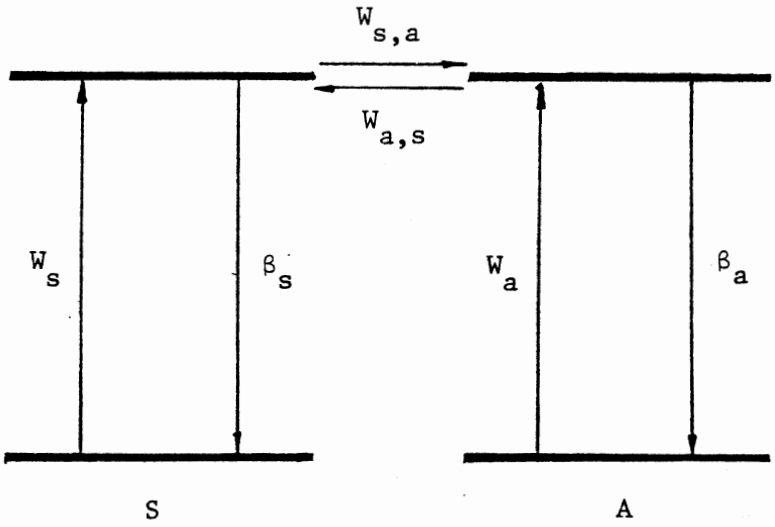

Figure 9. Two level system including the possibility of the sensitizer (S) to activator (A) and back, activator-to-sensitizer energy transfer.

The meaning of the symbols on the figure is the same as in figure 8. Additionally, $W_{a,s}$ designates the rate of the back transfer process.

The set of equations describing the evolution of the above system is

$$\dot{n}_s = -(\beta_s + W_{s,a})n_s + W_{a,s}n_a + W_s \tag{137}$$

$$\dot{n}_a = -(\beta_s + W_{a,s})n_a + W_{a,s}n_s + W_a \tag{138}$$

Assuming a delta function type of excitation ($W_s(t) \sim \delta(t)$ and $W_a(t) \sim \delta(t)$), the time independence of $W_{s,a}$ and $W_{a,s}$ and equality of sensitizer, activator lifetimes, it is obtained

$$\frac{I_a(t)}{I_s(t)} = \frac{(\frac{W_{s,a}}{W_{a,s}})[1 + \frac{I_a(0)}{I_s(0)}] - [\frac{W_{s,a}}{W_{a,s}} - \frac{I_a(0)}{I_s(0)}]\exp[-(W_{s,a} + W_{s,a})t]}{[1 + \frac{I_a(0)}{I_s(0)}] + [\frac{W_{s,a}}{W_{a,s}} - \frac{I_a(0)}{I_s(0)}] \exp[-(W_{s,a} + W_{a,s})t]} \quad (135)$$

Having the measured time evolution of spectra it is possible to integrate the areas under the spectral lines to obtain the time variation of the sensitizer and activator intensity ratios. It is possible then to perform a fitting procedure in an attempt to match energy transfer models with the experimentally obtained data. The results obtained in case of $Eu_xY_{1-x}P_5O_{14}$ crystals are contained in Table 1. These results are shown in Figures 10,11.

Very different models are required to give good fits to the data for the two samples, which is not surprising considering the significant concentration and spectral differences. For the 100% sample, the model giving the best fit to the data assumes negligible back transfer, equal values for the sensitizer and activator decay times, and $t^{1/2}$ dependence of the energy transfer rate. Formulae (132) and (133) were used to fit the data.

To fit the data obtained case of x=0.01 a constant parameter with back transfer model was used. Formula (139) was used to fit the data. Interpretation of this model requires the assumption of the energy migration between equally spaced pairs of sensitizer and activator.

Table 2 summarizes the result of experiments made in the case of EuP_5O_{14} and $Eu_{0.01}Y_{0.99}P_5O$ crystals.

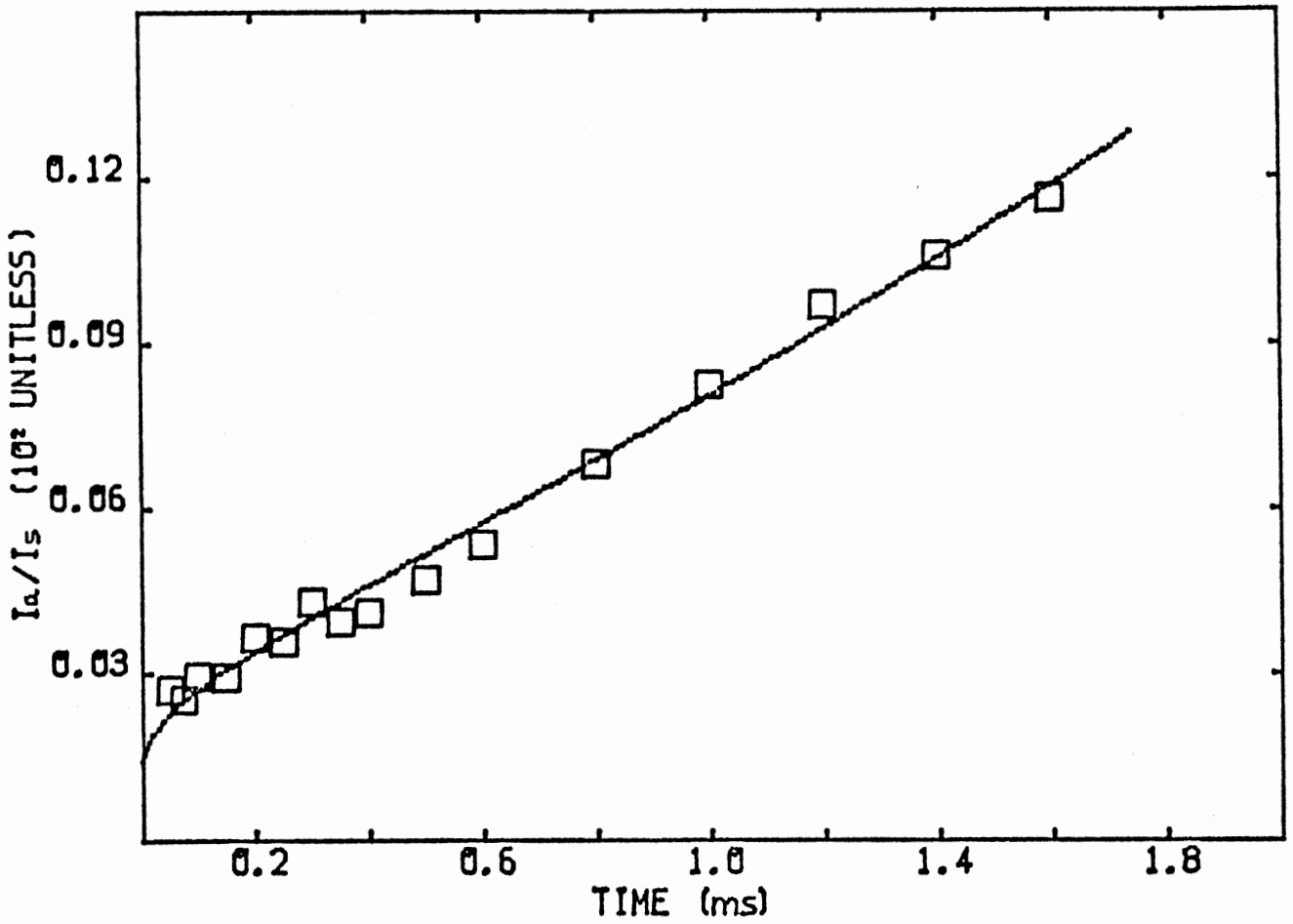

Figure 10. Time evolution of ratio of fluorescence intensities of sensitizer and activator transitions for $Eu_{0.01}Y_{0.99}P_5O_{14}$ crystals. Temperature of the sample was 12 K. Wavelength of excitation was 5232 Å.

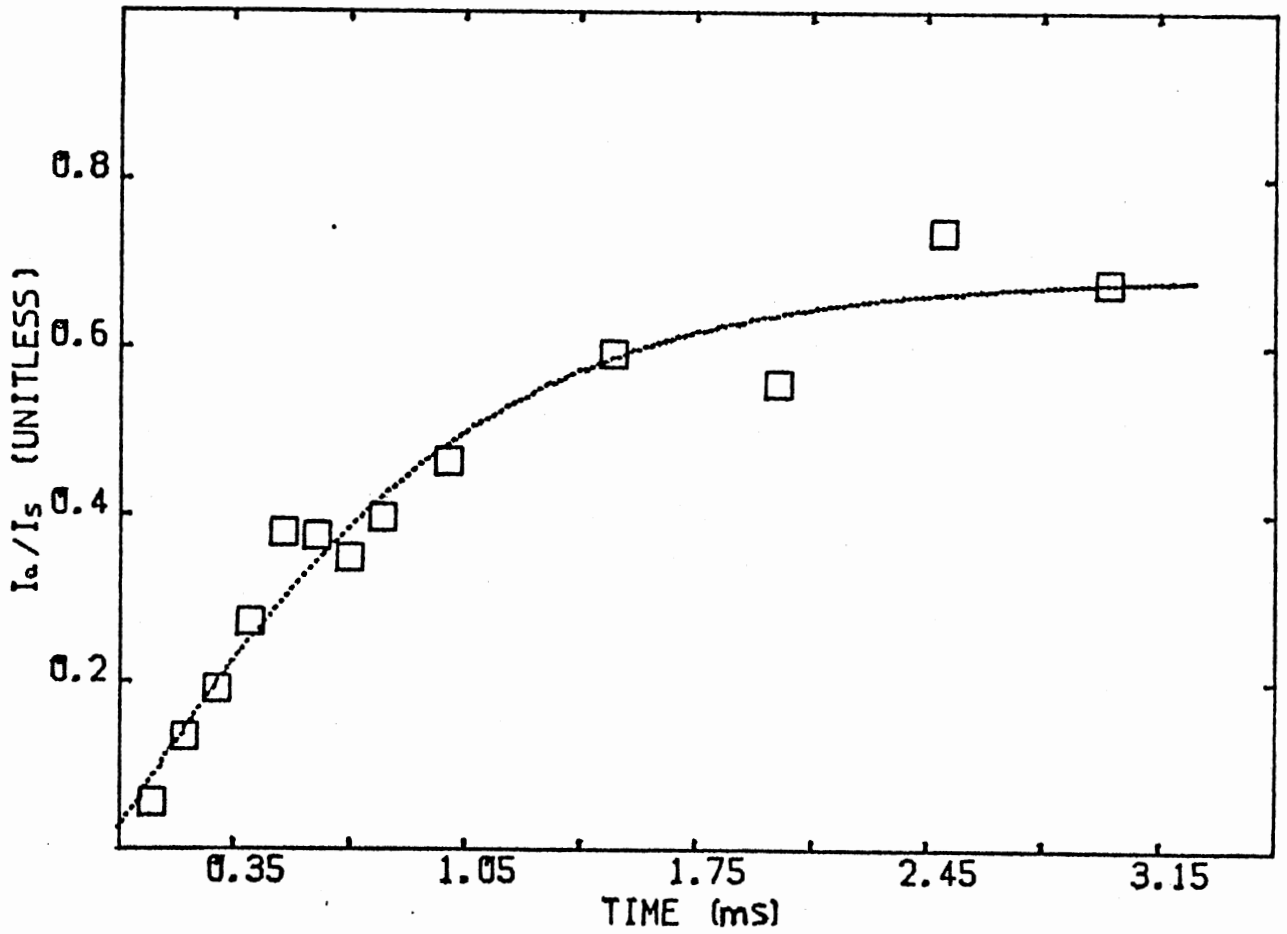

Figure 11. Time evolution of ratio of fluorescence intensities of donor and acceptor transitions for EuP_5O_{14} crystals. Temperature of the sample was 12 K. Wavelength of excitation was 5290 Å.

TABLE 1

RATIO OF ACTIVATOR INTENSITY TO SENSETIZER INTENSITY AT DIFFERENT TIMES AFTER THE EXCITATION PULSE IN $Eu_xY_{1-x}P_5O_{14}$

x = 1.0 T = 12K, λ_{ex} = 5290Å		x = 0.01 T = 43K, λ_{ex} = 5232Å	
t[μs]	$\frac{Ia}{Is}$	t[μs]	$\frac{Ia}{Is}$
50	2.73	100	0.055
75	2.55	200	0.133
100	3.97	300	0.191
150	2.95	400	0.273
200	3.67	500	0.379
250	3.50	600	0.375
300	4.32	700	0.349
350	3.96	800	0.397
400	4.12	1000	0.464
500	4.72	1500	0.592
600	5.36	2000	0.556
800	6.83	2500	0.737
1000	8.28	3000	0.676
1200	9.71		
1400	10.6		
1600	11.6		

C. Discussion

For the systems investigated, the observed characteristics of the time dependence of the transfer of energy between Eu^{3+} ions in nonequivalent crystal field sites are consistent with a resonant, single-step process through electric dipole-dipole interaction and has a relatively weak interaction strength. Two different types of spatial distributions of sensitizer-activator pairs were observed: a uniform distribution with a fixed value for the sensitizer-activator separation distance which results in a time independent energy transfer rate, and a random distribution with variable sensitizer-activator separations which results in an energy transfer rate with a $t^{1/2}$ time dependence. These general characteristics and the interaction strengths are consistent with the results obtained on Eu^{3+} in other host crystals (31). In glass hosts, the energy transfer has been found to be phonon assisted (32) and in some cases a multistep process (33).

The variations of fluorescence lifetimes, number of different sites, site separations and values for R_o from host to host indicate the sensitivity of the Eu^{3+} ions to its local surroundings. There does not appear to be a consistent trend of these parameters with any specific host crystal property. The origin of the different nonequivalent sites was not investigated here. Several obvious possibilities are local chemical or structural imperfections, substitution for different types of host ions, and local host distortions surrounding the Eu^{3+} impurity ion.

A theoretical estimate for R_o can be obtained from the expression (12)

$$R_o = \left(\frac{3e^4 f_s f_a \Omega \tau_s}{8\pi^2 m^2 c^3 \bar{\nu}_{s,a}^2} \right)^{1/6} \qquad (136)$$

where f_s and f_a are the oscillator strengths of the sensitizer and activator transitions, Ω is the overlap integral of the absorption spectrum of the activator and the emission spectrum of the sensitizer ions, and $\bar{\nu}_{s,a}$ is the average wave number in the region of spectral overlap. Since the $^5D_0 \longrightarrow {}^7F_2$ transitions involved in the energy transfer are extremely weak, it is difficult to resolve lines coming from ions in different sites and thus determine the spectral overlap. As a good approximation, the spectral overlap integral can be determined from the transitions shown in Figures 4 and 5. This is valid if the line positions and shapes are determined primarily by the $^5D_0$ level. The oscillator strengths are taken to be 2.62×10^{-1} (33).

The theoretically predicated value for the critical interaction distance for these four samples is found to be about R_o = 2.8 Å. Although the estimates of some of the parameters in equation (140) are fairly rough, these are all taken to the 1/6th power and thus the resulting value for R_o should be accurate.

In the case of x=1.0 sample, the best fit was obtained for $W_{s,a} \sim t^{1/2}$ and no back-transfer model. There is a difference of 30 percent between the theoretical and the fitted value of R_o in this case. This discrepancy is probably due to the simplified nature of the models used to describe the energy transfer characteristics in these systems. One modification which can be made to these models to make them more accurately reflect the physical situation is to account for the discrete nature of the crystal lattice.

An attempt to fit the data using formula (132) and (133) and having the survival function determined by the procedure (70)-(75) and (129) gave R_o of the order of 4 Å. This disagreement is mainly due to the necessity to compromise between physical size of the model involved and the finite speed of the available computer, as well as the finite size of its memory.

In the case of $Eu_{0.01}Y_{0.99}P_5O_{14}$ the leveling off of the intensity ratio (see Figure 11) indicates the presence of the back transfer process. The rapid initial slope of the intensity ratio rules out the possibility of the time dependent back transfer rate unless an unphysically large value of R_o would be allowed. Therefore, a model involving a constant parameter with the possibility of back transfer is appropriate to describe the process in $Eu_{0.01}Y_{0.99}P_5O_{14}$.

Using forumula (139) to perform the fitting procedure a value of $R_o = 8.8$ Å was obtained. As it has been mentioned, the interpretation of this model suggests that sensitizers and activators are distributed in equally spaced pairs. This would imply that Eu^{3+} ions agregate instead of being distributed randomly.

The results of experimental data analysis are summarized in Table 2.

In summary, high-resolution laser time-resolved site-selection spectroscopy techniques coupled with phenomenological rate parameter models have been used to compare the characteristics of energy transfer between Eu^{3+} ions in nonequivalent crystal field sites in two types of crystal hosts. Although the strength and mechanism for the interatction in the two samples were found to be similar, the effects of the spatial distributions of the ions were different. These results demonstrate that as laser techniques probe the characteristics of energy transfer in greater detail, it becomes increasingly important to develop more sophisticated modeling techniques to account for all of the properties of the system.

TABLE 2

ENERGY TRANSFER MODEL PARAMETERS FOR $Eu_xY_{1-x}P_5O_{14}$ CRYSTALS

Parameter	x = 0.01	x = 1.0
$W_{s,a}$ (s^{-1})	1.2×10^3	$6.6 \times 10^2 t^{-1/2}$
$W_{a,s}$ (s^{-1})	1.7×10^3	
τ_s (ms)	4.1	5.7
τ_a (ms)	4.1	5.7
N_a/N_{Eu}	0.36	0.005
ΔE_{s-a}(Å)	g	2
R_o (Å)	8.8	2.2

CHAPTER IV

FOUR-WAVE MIXING TRANSIENT GRATING SPECTROSCOPY

A. Experimental Equipment and Samples

The experimental configuration used to investigate the energy migration process in $Nd_xLa_{1-x}P_5O_{14}$ crystals was similar to the one described earlier (35,36) and it is shown in Figure 12.

An argon ion laser pumped tunable dye laser was used to excite the sample. A variable beam splitter (VBS) split off the weak probe beam (designated as "p" in Figure 12), while the remaining beam was chopped by the chopper (CH) atenuated by a variable, neutral density filter (VND) and split again by the beam splitter (BS) and the mirrors (M) into two pump beams (designated as a and b in Figure 12). A set of mirrors and lenses (S) directed beams a and b such, that they intersected inside the sample while the difference between their optical paths was kept shorter, than the coherence length of the laser beam. Another set of mirrors and a lense aligned the probe beam p to be counterpropagating to the a beam.

The scattered beam (designated as s in the Figure 12), counterpropagated to the pump beam b and the beam splitter (SBS) sent it to the photomultiplier tube (PMT).

The photomultiplier signal was analyzed by a Boxcar Integretor whose output was sent to the input of a signal averager. In this double-averaging configuration it was possible to average out both low

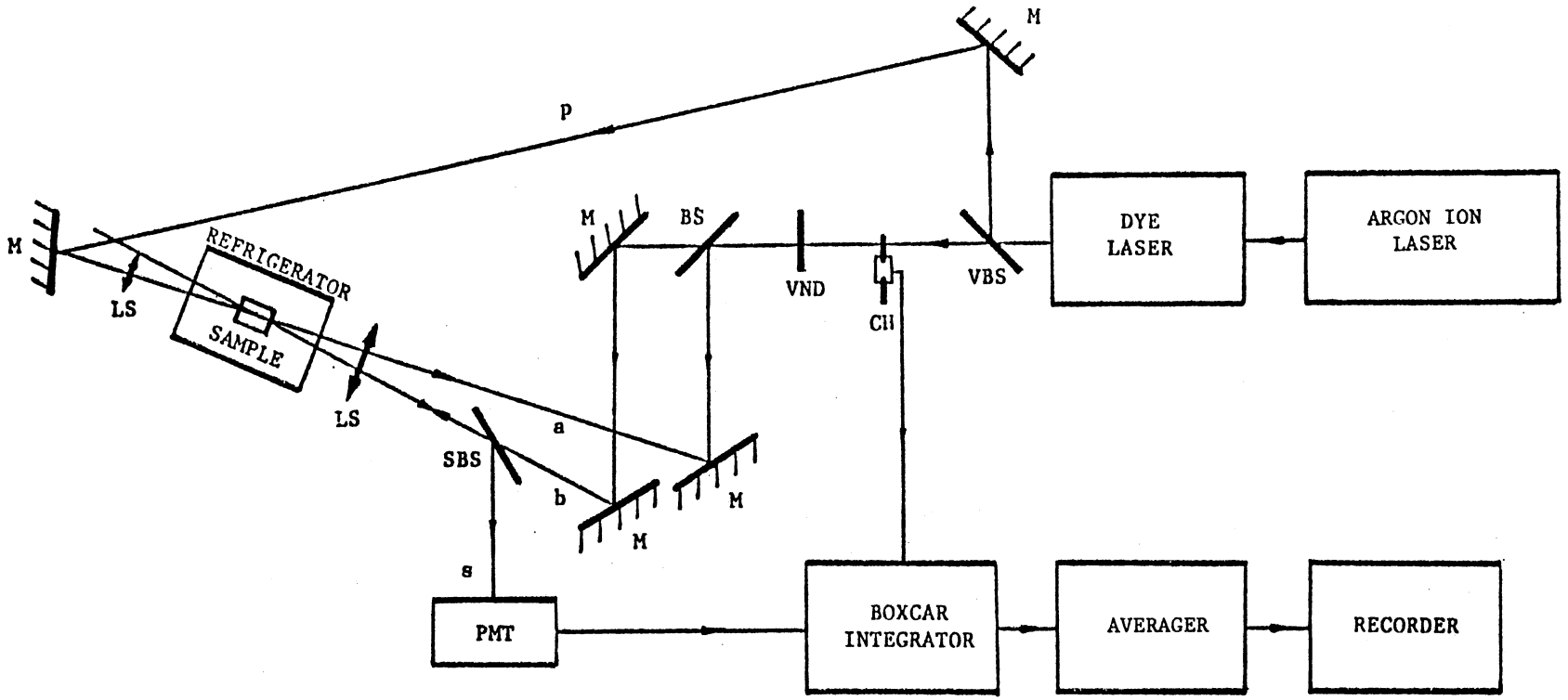

Figure 12. Four-wave mixing experimental configuration.

and high frequency noise. The memory content of the averager was displayed on a scope or output to a recorder. Cryogenic refrigerator or a liquid helium dewar was used to cool down the sample whose temperature was adjusted by the temperature control unit.

High optical quality $Nd_xLa_{1-x}P_5O_{14}$ crystals were grown from hot phosphoric acid (37). The large size of crystals facilitated their fine polishing and orientation. The two samples under study had fractional concentrations of Nd^{3+} ions of x=1.0 nad x=0.2.

The laser beam was pumping the absorption band of Nd^{3+} ions consisting of overlapping $^2G_{7/2}$ and $^4G_{5/2}$ levels. Radiationless relaxation populated the metastable state $^4F_{3/2}$ levels. Radiationless relaxation components of $^4I_{9/2}$ ground state occurred.

B. Theoretical Background

The theory of Four-wave mixing (FWM) experiments describes the response of the material through analysis of the wave equation coupling the electric fields (35,36,38,39,40). The mechanism of field coupling is modeled by the analysis of a two level system responding to the external electric field perturbation (35,41). In reference 40 a suggestion was made to approximate the susceptibility of the three level system by a linear combination of two, two level systems susceptibilities. Such an approach would allow emphasizing the mechanism of wave mixing as the result of atomic process.

The application of the Four-wave mixing technique to investigate the energy migration process require a different interpretation of the cross-beam configuration (35,36,40,42,43,44). A simple consideration involving the concept of Bragg diffraction of light from an index of

refraction grating leads to the experimental technique for investigating the migration of the nonuniformly distributed excited states. In this chapter the theory and the application of Four-wave mixing is presented.

C. Four-Wave Mixing in a Three Level System

If a three level system (see Figure 13) is excited in a stationary case, the ratio of $R = N_1/N_2$ (N_1 is the number of ions in the metastable state, and N_2 is the number of ions in the ground state) is determined as the resultant of different atomic processes competing in the dynamics of the ground, excited and metastable states.

The susceptibility of such a system can be approximated by the linear combination of susceptibility of the ground and excited states system and susceptibility of the metastable and excited states system. In this approximation, the resulting susceptibility takes the form (40)

$$\chi = \frac{R}{R+1}\chi_1 + \frac{1}{R+1}\chi_2 \tag{141}$$

where χ_1 is the susceptibility of the ground state system, χ_2 is the susceptibility of the metastable state system and R is the ratio of number of ions in the ground state to the number of ions in the metastable state.

The electric field interacting with the medium can be expressed as

$$\bar{E} = e^{i\omega t}(\bar{E}_o + \Delta\bar{E}) \tag{142}$$

where $\bar{E}_o$ is the part of the field which pumps the mixture of the ground-metastable state systems while $\Delta\bar{E}$ is the probing part of the field, and ω is the frequency of the electric field

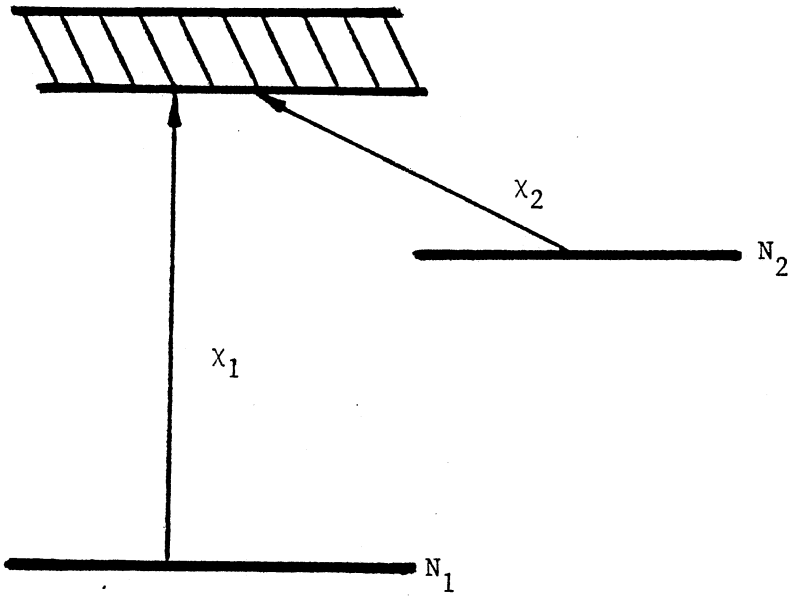

Figure 13. Three level system excited in FWM configuration.

By definition, the polarization of the medium is

$$\overline{P}(\overline{E}) = \varepsilon_o \chi(\overline{E})\overline{E} \tag{143}$$

where ε_o is the dielectric constant of the vacuum, and $\chi(\overline{E})$ is medium dielectric susceptibility.

Approximating $P(E)$, the polarization of isotropic medium, by the linear part of ΔE power expansion (35,36,41) results in

$$P(E_o + \Delta E) = e^{i\omega t}\varepsilon_o \sum_{1,2} R_i \chi_{oi}(E_o)(E_o + \Delta E - \frac{E_o \Delta E + |E_o|^2 \Delta E}{I_{si} + |E_o|^2}) \tag{144}$$

where $R_1 = \frac{R}{R+1}$

$$R_2 = \frac{1}{R+1}$$

$$\chi_{oi}(E_o) = \frac{2\alpha_{oi}}{k} \frac{I_{si}(i + \delta_i)}{I_{si} + |E_o|^2}$$

where α_{oi} is the saturation coefficient of the i-th state, δ_i is detuning parameter between the field frequency and the i-th state absorption, and I_{si} is the i-th state saturation intensity (i=1, designates the ground state and i=2 designates the metastable state).

In Four-wave mixing experiement probe and scattered beams can be kept lower than the pump beams intensity which is expressed as

$$\Delta E = |E_1 + E_3| << E_o = |E_2 + E_4| \tag{145}$$

This justifies formula (144) as the first power of the ΔE approximation of formula (143). The configuration of beams can be schematically represented as in Figure 14 (pump beam a is designated as $\overline{E}_2$, pump beam b is designated as $\overline{E}_4$, probem beam p is designated as $\overline{E}_1$ while scattered beam s is designated as $\overline{E}_3$).

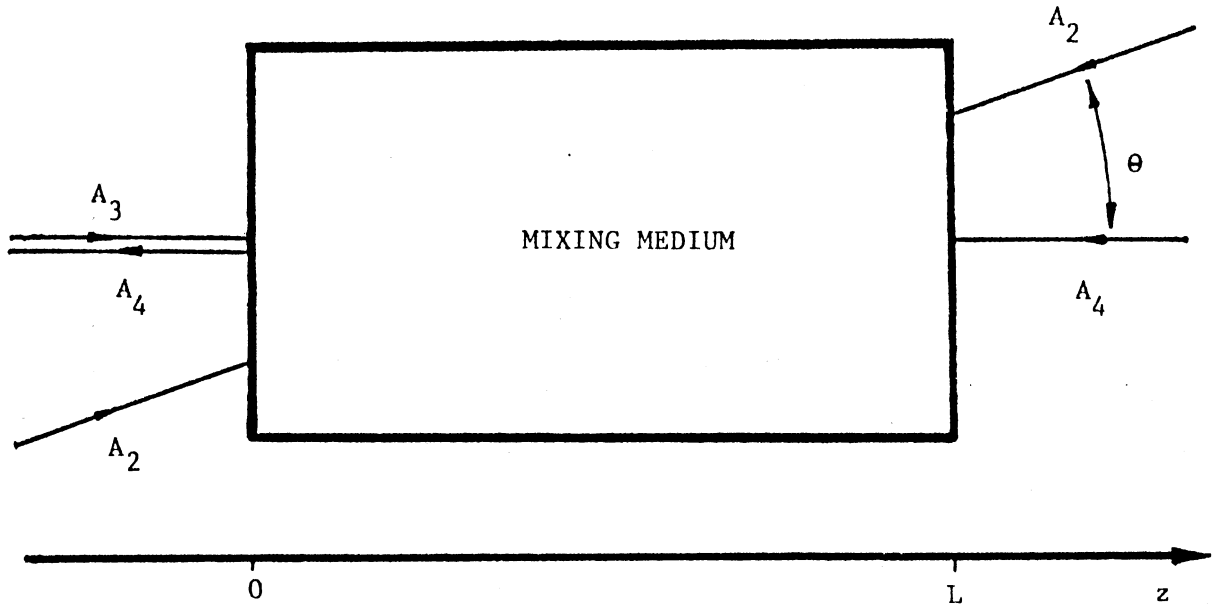

Figure 14. Schematic representation of the mixing fields.

Approximating the cross-beam configuration of the gaussian beams by a configuration of plane waves it is possible to express the mixing beams as

$$E_1 = A_1(z)e^{-\bar{k}_1\bar{r}} = A_1(z)e^{ik(z\cos\Theta + y\sin\Theta)} \tag{146}$$

$$E_2 = A_2(z)e^{-i\bar{k}_2\bar{r}} = A_2(z)e^{-ik(z\cos\Theta + y\sin\Theta)} \tag{147}$$

$$E_3 = A_3(z)e^{-i\bar{k}_3\bar{r}} = A_3(z)e^{ikz} \tag{148}$$

$$E_4 = A_4(z)e^{-i\bar{k}_4\bar{r}} = A_4(z)e^{-ikz} \tag{149}$$

where k_i, $i = 1,2,3,4$, are the wave vectors of the beams, while Θ is the angle of the pump beams crossing. The Maxwell equation describing Four-wave mixing process takes the form

$$\nabla^2 E(\bar{r},t) - \varepsilon_o\mu_o \frac{\partial^2 E(\bar{r},t)}{\partial t^2} = \mu_o \frac{\partial^2 P(\bar{r},t)}{\partial t^2} \tag{150}$$

Computations demonstrated in the Appendix carried out under the assumption of a slow varying envelope of beams, such that

$$|\partial_z^2 A_i| << |k_i \partial_z A_i|; \; i = 1,2,3,4 \tag{151}$$

and the assumption of non-depleting pump beams, such that

$$|\partial_z A_i| << |\partial_z A_j| \quad ; \; i = 2,4 \; ; \; j = 1,3 \tag{152}$$

leads to the set of two equations

$$\partial_z A_1(z) - R(z)A_1(z) = 0 \tag{153}$$

$$\partial_z A_3(z) - P(z)A_3(z) = Q(z) \tag{154}$$

where

$$R(z) = -\sum_{1,2} R_i \frac{\alpha_{oi}|E_{si}|^2(1-i\delta_i)}{\cos\theta} \frac{I_{si} + a\exp(i\beta z + i\Delta)}{[D_{oi} + 2a\cos(\beta z + \Delta)]^2} \quad (155)$$

$$P(z) = -\sum_{1,2} R_i\alpha_{oi}|E_{si}|^2(1 - i\delta_i) \frac{I_{si} + a\exp(-i\beta z - i\Delta)}{[D_{oi} + 2a\cos(\beta z + \Delta)]^2} \quad (156)$$

$$Q(z) = -\sum_{1,2} R_i\alpha_{oi}|E_{si}|^2(1 - i\delta_i) \frac{a\exp(i\Delta)\, A_1(z)}{[D_{oi} + 2a\cos(\beta z + \Delta)]^2} \quad (157)$$

where

$$\beta = k(1-\cos\theta)$$

$$a = |A_2(z)A_4(z)|$$

$$D_{oi} = I_{si} + I_2 + I_4$$

$$I_{si} = |E_{si}|^2/(1 + \delta_i)^2$$

$$\Delta = \text{arctg}\frac{\text{Im}(A_2(z))}{\text{Re}(A_2(z))} - \text{arctg}\frac{\text{Im}(A_4(z))}{\text{Re}(A_4(z))}$$

Equations (153)-(157) have two approximate solutions leading to the expression describing the ratio of the scattered beam intensity to the probing beam intensity while the writing beams are extinguished at the $z = L$ face of the sample. (L is the thickness of the sample.)

This ratio is called "scattering efficiency" and, by definition, can be expressed as

$$\eta = \frac{|A_3(0)|^2}{|A_1(0)|^2}\Bigg|_{E_o = 0} \quad (158)$$

If the pump intensities are well below the saturation of the states absorption, the following expressions are true

$$\frac{a}{I_{si}} << 1 \; ; \; i = 1,2 \quad (159)$$

consequently, after the approximations of equations (154)-(155) by

their first power of ΔE expansions, it is possible to obtain (see Appendix)

$$\eta = S_1 I_2 I_4 \exp(-S_2\sqrt{I_2 I_4}) \tag{160}$$

where

$$S_1 = \frac{L^2}{\cos^2}\left[\left(\sum_{1,2}\frac{R_i\alpha_{oi}\delta_i}{(1+\delta_i)^2}\right)^2 + \left(\sum_{1,2}\frac{R_i\alpha_{oi}}{(1+\delta_i)^2}\right)^2\right]\exp\left(\frac{2L}{\cos\Theta}\sum_{1,2}\frac{R_i\alpha_{oi}}{(1+\delta_i)^2}\right)$$

$$\left\{\left[L\cos^2\frac{\Theta}{2}\sum_{1,2}\frac{R_i\alpha_{oi}}{(1+\delta_i)^2\cos\Theta} - \frac{L^2}{6}\cos\Theta\left(\left(\sum_{1,2}\frac{R_i\alpha_{oi}}{(1+\delta_i)^2\cos\Theta}\right)^2\right.\right.\right.$$

$$\left.\left.\left. + \left(\sum_{1,2}\frac{R_i\delta_{oi}\alpha_{oi}}{(1+\delta_i)^2\cos\Theta}\right)^2 - 1\right]^2\right. \tag{161}$$

$$\left. + \left[\frac{L\cos^2\frac{\Theta}{2}}{\cos\Theta}\sum_{1,2}\frac{R_i\alpha_{oi}\delta_i}{(1+\delta_i)^2} - \frac{L^2}{3}\frac{1}{\cos\Theta}\left(\sum_{I,2}\frac{R_i\alpha_{oi}\delta_i}{(1+\delta_i)^2}\right)\left(\sum_{1,2}\frac{R_i\alpha_{oi}}{(1+\delta_i)^2}\right)\right]^2\right\}$$

$$S_2 = \frac{2}{\sqrt{\beta}}\left(\cos\Delta\sum_{1,2}\frac{R_i\alpha_{oi}\delta_i}{(1+\delta_i)^2 I_{si}} + 3\sin\Delta\sum\frac{R_i\alpha_{oi}}{(1+\delta_i)^2 I_{si}}\right) \tag{162}$$

When the far-below-saturation condition is not satisfied another approximation is possible. For large values of Θ it is possible to approximate equations (155)-(157) by their values averaged over the length of $\lambda_{osc} = \frac{\lambda}{1-\cos\Theta}$, the distance over which changes in $A_1(z)$ and $A_3(z)$ are negligible. Computations demonstrated in greater detail in the Appendix show that the scattering efficiency can be expressed as

$$\eta = \left|\frac{\rho}{\zeta}\right|^2 \frac{\exp(\Psi_{E_o})}{(\cos^{-1}\Theta - 1)^2}\{\exp(-2\zeta_R L) + \exp(-2\zeta_R L\cos^{-1}\Theta)$$

$$- 2\exp[-\zeta_R L(1+\cos^{-1}\Theta)]\cos[\zeta_I L(1-\cos^{-1}\Theta)]\} \tag{163}$$

where

$$\left|\frac{\rho}{\zeta}\right| = \frac{\sum_{j=1,2}\left\{\sum_{i=1,2} F_{j,i}\,\frac{R_i\alpha_{oi}}{(1+\delta_i)^2 I_{si}}\,\frac{\sqrt{I_2 I_4}\,(1+\frac{I_2+I_4}{I_{si}})}{[(1+\frac{I_2+I_4}{I_{si}})^2 - 2\frac{I_2 I_4}{I_{si}^2}]^{3/2}}\right\}^2}{\sum_{j=3,4}\left\{\sum_{i=1,2} F_{j.i}\,\frac{R_i\alpha_{oi}}{(1+\delta_i)^2}\,\frac{(1+\frac{I_2+I_4}{I_{si}})^2 - 2\frac{I_2 I_4}{I_{si}^2}}{[(1+\frac{I_2+I_4}{I_{si}})^2 - 4\frac{I_2 I_4}{I_{si}^2}]^{3/2}}\right\}^2} \tag{164}$$

$$F_{1,i} = \cos\Delta + \delta_i \sin\Delta \; ; \; F_{3,i} = 1 \tag{165}$$

$$F_{2,i} = \sin\Delta - \delta_i \cos\Delta \; ; \; F_{4,i} = \delta_i \tag{166}$$

$$\Psi_{E_o} = \frac{2L}{\cos\Theta} \sum_{1,2} \frac{R_i\,\alpha_{oi}}{(1+\delta_i)^2} \tag{167}$$

The formula (160)-(162) and (163)-(167) allows one to express the mixing process as the result of atomic processes occurring in the sample. However, the detail analysis of the results (160)-(162) and (163)-(167) in terms of the experimental variables may encounter a certain amount of difficulty. Practically speaking, the estimation of the R_i coefficients may be difficult and their dependence on the I_2 and I_4 pump intensities may make the analysis of the scattering efficiency additionally difficult.

D. Transient Grating Behavior

Two strong pump beams interfere inside the mixing medium creating standing wave of electric field with a wave vector parallel to the counterpropagating components of the pump beams wave vectors (see Figure 2 of reference 36).

As the result of the pump beams absorption, a population of excitons is created inside the mixing medium. The profile of the exciton concentration follows the pattern of the pump beams interference. If the absorption spectrum of the excited states differs from the absorption spectrum of the ground state, the imaginary part of the index of refraction of the zones of high excitation concentration is not equal to the imaginary part of index of refraction of the zones of ions in the ground state. As the result of this a transient grating of excited states is generated.

If the chopper cuts off the excitation source, the grating begins to fade as the result of the finite excitation lifetime and the energy migration process, smoothing out the initial nonuniform exciton distribution.

At the same time, if the probe beam is still switched on, the transient grating will scatter it generating a set of scattered beams, the directions of which are defined by the geometry of the diffraction process.

Given the fact that the scattered beam is created as the result of constructive interference of the probe field scattered from the excitons, the scattered field is proportional to the number of scatterers and the intensity of the scattered beam is proportional to the square of the number of scatterers. Consequently, the intensity of the scattered beam is proportional to the square of the depth of the exciton concentration transient grating. This can be expressed by formula

$$I_s(t) \sim (P_{max}(t) - P_{min}(t))^2 \qquad (168)$$

where $I_s(t)$ is the intensity of the scattered beam, $P_{max}(t)$ is the probability of encountering an exciton in the peak of the grating, and $P_{min}(t)$ is the probability of encountering an exciton in the valley of the grating.

As the result of this, the time variation of the scattered beam intensity, after chopping off the pump beams, carries information about both, monoionic decay process and the energy migration process contributing to the change in formula (168). Given the fact that the nonuniformity of exciton distribution is one dimensional, the initial exciton distribution can be approximated by formula

$$P_m(0) \sim [1 + \cos(k_g dm)] \tag{169}$$

where $P_m(0) = P_m(t=0)$ is the probability of encountering an exciton at the site m at the moment t=0 of time, and d is the distance between the sites in the direction of the nonuniform exciton distribution.

In the continuity limit, the initial probability of encountering an exciton at the point x of space can be expressed as

$$p(x,0) \sim [1 + \cos(k_g x)] \tag{170}$$

The parameter k_g in formulae (169) and (170) is the wave vector of the transient grating, and it has the form

$$k_g = \frac{4\Pi \sin(\frac{\Theta}{2})}{\lambda} \tag{171}$$

where Θ is the angle between the pump beams and λ is the excitation beam wavelength.

Wong and Kenkre (45) treated the cases of different energy migration processes contributing to the time variation of (168). In general, the energy migration process is described by formula (1) of the form

$$\frac{dP_m(t)}{dt} = \int_o^t dt' \left[\sum_n V_{m,n}(t-t')P_n(t') - V_{n,m}(t-t')P_m(t') \right] - \frac{P_m(t)}{\tau} \tag{172}$$

where $V_{m,n}(t)$ defines the probability of energy migration from the m-th to the n-th site, and τ is the excitation lifetime.

Function $V_{m,n}(t)$ of formula (172) is called the memory function and it reflects the degree of coherence influencing the energy migration process. Kenkre (43) computed the memory function in case of the exciton interacting with its nearest neighbor submerged in the phonon bath. The ion-ion interaction was defined by the nearest neighbor matrix element j, and the interaction with the phonon bath was defined by the single, randomized parameter α. Assuming one-dimensionality of the energy migration process the following was obtained

$$V_{n,m} = (t) = 2j^2 e^{-\alpha t} \left([J^2_{m-n+1}(2jt) + J^2_{m-n-1}(2jt) + 2J_{m-n+1}(2jt)J_{m-n-1}(2jt)] \right.$$

$$\left. - \{2J^2_{m-n}(2jt) + J_{m-n}(jt)[J_{m-n+2}(2jt) + J_{m-n-2}(2jt)]\} \right) \tag{173}$$

where $J_i(x)$ is the Bessel function of te first kind and i-th order.

The degree of coherence influencing the energy migration process depends on the relation between parameters α and j. In fact, the phonon bath will tend to destroy the coherence of the ion-ion interaction. Therefore, the bigger the $\frac{\alpha}{j}$ ratio, the less coherent the energy migration process will be.

A number of limiting cases were treated, which led to a number of different formulae describing different time variations of the intensity of scattered light in the transient grating experiments. All

these results are limited by the model assumptions e.g. ion-ion interaction taking place between the nearest neighbors and phonon-ion interaction approximated by a single parameter.

1. Purely Incoherent Energy Migration (45,46).

If the conditions $\alpha \longrightarrow \infty$ and $\frac{j}{\alpha}$ = const. are satisfied, equation (175) simplifies to

$$\frac{dP_m(t)}{dt} = F\,[P_{m+1}(t) + P_{m-1}(t) - 2P_m(t)] - \frac{P_m(t)}{\tau} \tag{174}$$

The resulting probability $P_m(t)$ has the form

$$P_m(t) = \frac{1}{2}\, e^{-t/\tau}\, \{1 + \exp\,[-4Ft\sin^2(k_g dm)]\} \tag{175}$$

and the intensity of the scattered light is

$$I_s(t) = I_s(0)\exp\,\{-2t\,[4F\sin^2\,(\frac{k_g d}{2}) + \frac{1}{\tau}\,]\} \tag{176}$$

Whenever the continuity limit of the purely incoherent energy migration is applicable, the energy migration process is of the diffusive type. In this case formula (174) leads to (45)

$$\frac{\partial p(x,t)}{\partial t} = D\,\frac{\partial^2 p(x,t)}{\partial x^2} - \frac{p(x,t)}{\tau} \tag{177}$$

where $D = Fa^2$ (178)

Consequently, $p(x,t)$ and $I_s(t)$ are obtained as (45)

$$p(x,t) = \frac{1}{2}\, e^{-t/\tau}\,[1 + \exp(-k_g^2 Dt)\cos(k_g x)] \tag{179}$$

$$I_s(t) = I_s(0)\exp\{-2t[\frac{1}{\tau} + k_g{}^2 D]\} \tag{180}$$

If the condition $F \longrightarrow \infty$ is satisfied, approximation (174) of equation (172) has to be replaced by the appropriate form of the Pauli Master Equation (PME). Obtained in this case $P_m(t)$ and $I_s(t)$ take the form (45,46)

$$P_m(t) - \frac{1}{2} e^{-t/\tau} \left[1 - \exp(-t\{ [\alpha^2 + 16j^2 \sin^2(\frac{k_g d}{2})]^{1/2} - \alpha\})\right] \quad (181)$$

$$I_s(t) = I_s(0) \exp\ (-2t\{[\alpha^2 + 16j^2 \sin^2(\frac{k_g d}{2})]^{1/2} - \alpha + \frac{1}{\tau}\}) \quad (182)$$

When the ion-ion interaction and ion-phonon interaction satisfy $\frac{F^2}{2\alpha} << \infty$ condition, the scattered beam decays exponentially and the decay rate K has the form

$$K = 2\ [4F\sin^2(\frac{k_g d}{2}) + \frac{1}{\tau}] \quad (183)$$

which in the continuity limit simplifies to

$$K = 2(k_g^2 D + \frac{1}{\tau}) \quad (184)$$

In the case of the strong ion-ion interaction, the scattered beam decay rate has the form

$$K=2\ \{[\alpha^2 + 16j^2 \sin^2(\frac{k_g d}{2})\ ]^{1/2} - \alpha + \frac{1}{\tau}\} \quad (185)$$

2. Purely Coherent Migration (45,46,47).

The case of $\alpha = 0$ requires solving equation (172). The formalism presented in reference 47 gives the result of the form

$$I_s(t) = I_s(0) e^{-2t/\tau} J_o^2\ (4jt\sin(\frac{k_g d}{2})) \quad (186)$$

In this case the time variation of the scattered beam intensity is of a non-exponential, oscillatory type.

3. Partially Coherent Migration (45,46,47).

In the case of $0 \leq \alpha \leq \infty$ and $0 \leq j \leq \infty$ the formalism presented in reference 47 gives the Laplace transform of the scattered beam intensity of the form

$$I_s(t) = I_s(0)e^{-2t/\tau} \left(\int_c ds e^{-st} \{[s^2 + 16j^2 \sin^2(\frac{k_g d}{2})]^{1/2} - \alpha\}^{-1} \right)^2 \tag{187}$$

where integration is on the Bromwich contour.

Formula (187) leads to the following result (45)

$$I_s(t) = I_s(0)e^{-2t/\tau}[1 - e^{-\alpha t} 4j\sin(\frac{k_g d}{2}) \int_o^t du J_1(4ju\sin(\frac{k_g d}{2})) e^{\alpha(t^2-u^2)^{1/2}}] \tag{188}$$

Formula (188) gives the general description of the time variation of the scattered beam intensity. All the previous cases can be derived as a particular simplification of the result (188).

If the excitons migrate in a diffusive way, such that the mean free path is longer than the nearest neighbor distance, the diffusion equation still provides the adequate description of the process. In this case, however, the diffusion coefficient can not be expressed in a simple form of equation (178), since the process of diffusion is controlled by the scattering of the partially coherent excitons rather than the nearest neighbor hopping. This case was investigated by Salcedo, Siegman, Dlott, and Fayer (42). They obtained the result identical to (180) and (184). However, the estimation of the diffusion coefficient require an analysis of a particular process scattering

excitons migrating along mean free paths in a partially coherent fashion.

Finally, one comment needs to be made aboute the excited state interaction with the bath of phonons. In cases when a single parameter of ion-phonon interaction does not suffice to describe the complexity of energy migration, further sophistication of the theory is desirable. This task might follow the work of Kenkre and Knox (48) and will require application of numerical techniques which allow inclusion of more complicated ion-phonon interaction schemes determining the properties of the memory function.

E. Experimental Results

Figure 15 shows the energy level diagram of the Nd^{3+} ion. As it was previously mentioned, during Four-wave mixing (FWM) experiment samples of $Nd_xLa_{1-x}P_5O_{14}$ the laser beam was exciting the absorption band of Nd^{3+} ion consisting of overlapping states $^2G_{7/2}$ and $^4G_{5/2}$. This absorption band is shown in Figure 16. Figure 16 A shows the absorption of $Nd_{0.2}La_{0.8}P_5O_{14}$ at the liquid nitrogen temperature. Figure 16 B shows the absorption of LaP_5O_{14} at the liquid nitrogen temperature.

Radiationless relaxation populates $^4F_{3/2}$ metastable state. Decay of the $^4F_{3/2}$ to one of the $^4I_{9/2}$ states is accompanied with a near infrared fluorescence. Figure 17 shows the fluorescence emission ion spectrum originating from the luminescent decay of the $^4F_{3/2}$ metastable state of the Nd^{3+} under CW excitation. The spectrum was taken at the temperature of 12.5 K and the sample was NdP_5O_{14}. On this figure different transitions from the metastable state to one of the $^4I_{9/2}$ states are identified.

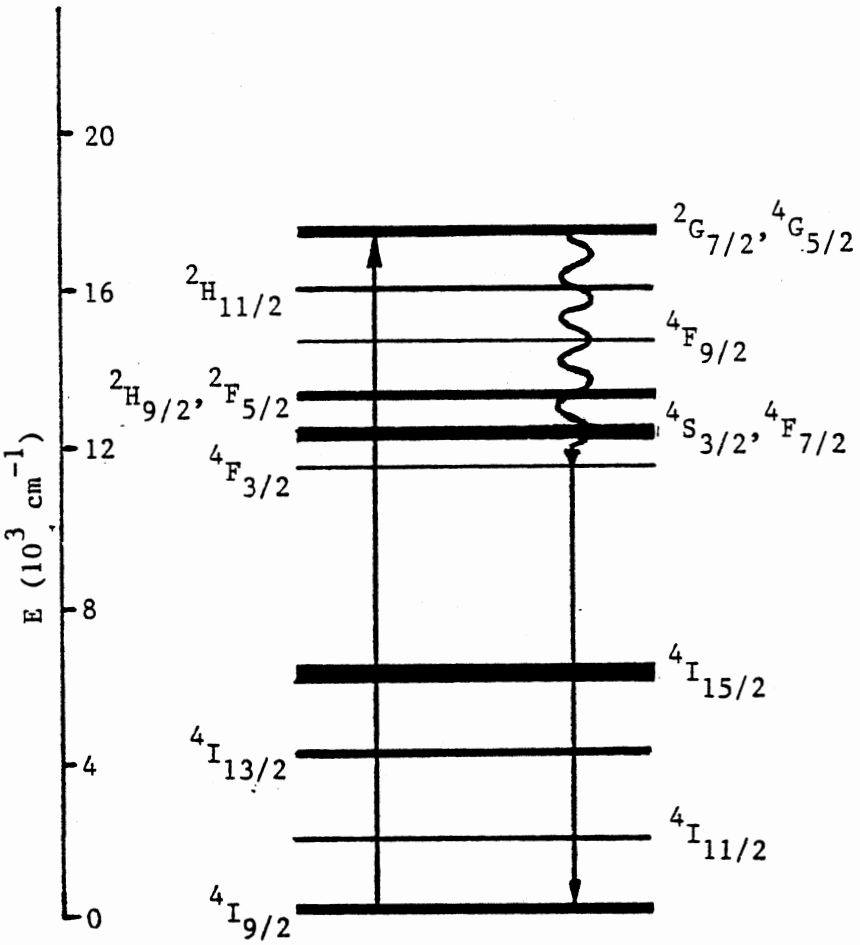

Figure 15. Energy level diagram of the Nd^{3+} ion. On the diagram $^4I_{3/2} \rightarrow {}^2G_{7/2}$ $^4G_{5/2}$ excitation; $^2G_{7/2}$ $^4G_{5/2} \rightarrow {}^4F_{3/2}$ radiationless relaxation, and $^4F_{3/2} \rightarrow {}^4I_{9/2}$ decay are shown.

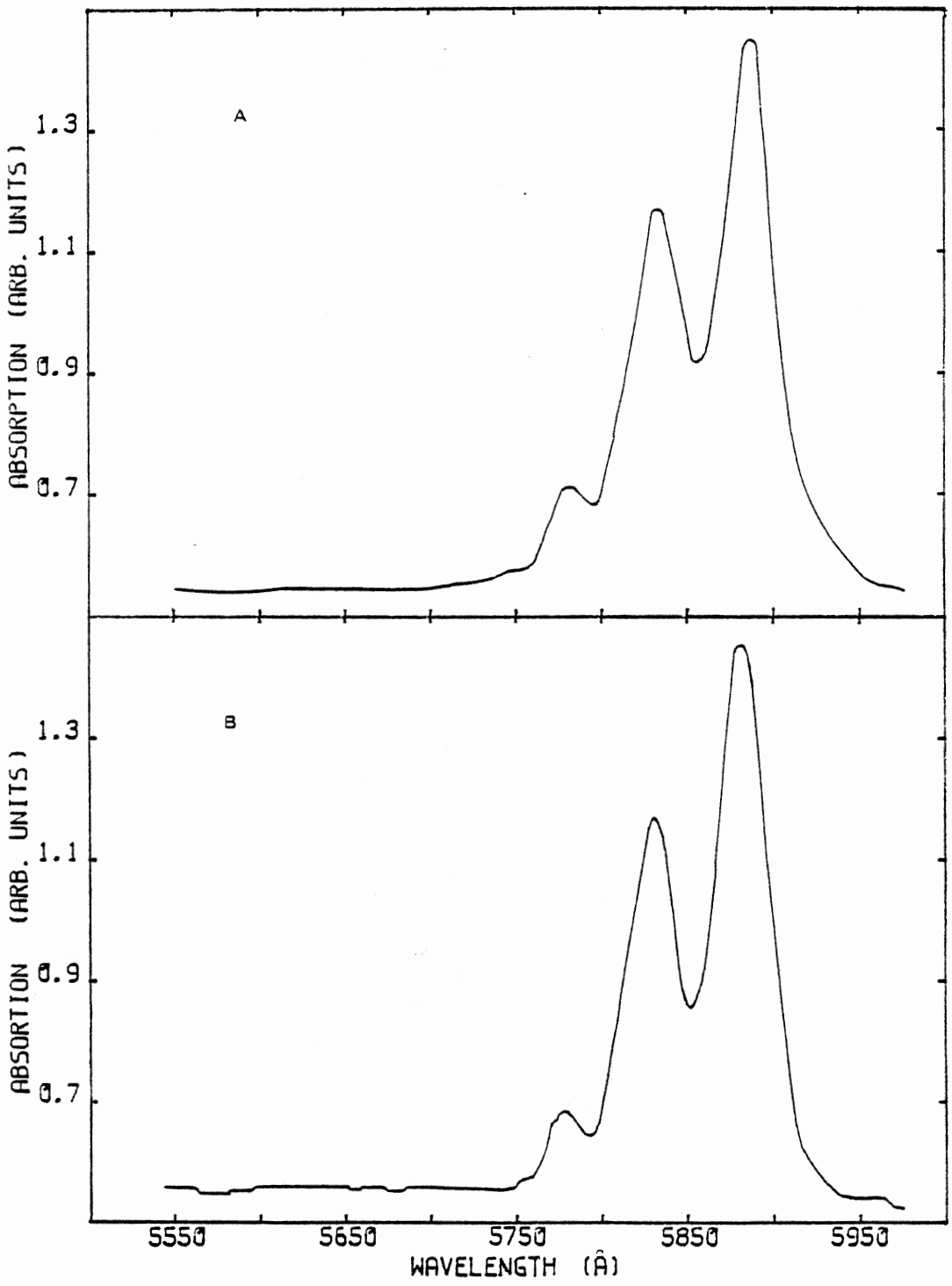

Figure 16. Absorption spectrum of $Nd_xLa_{1-x}P_5O_{14}$ at the temperature of 77 K. For x=2 (A) and x=1 (B).

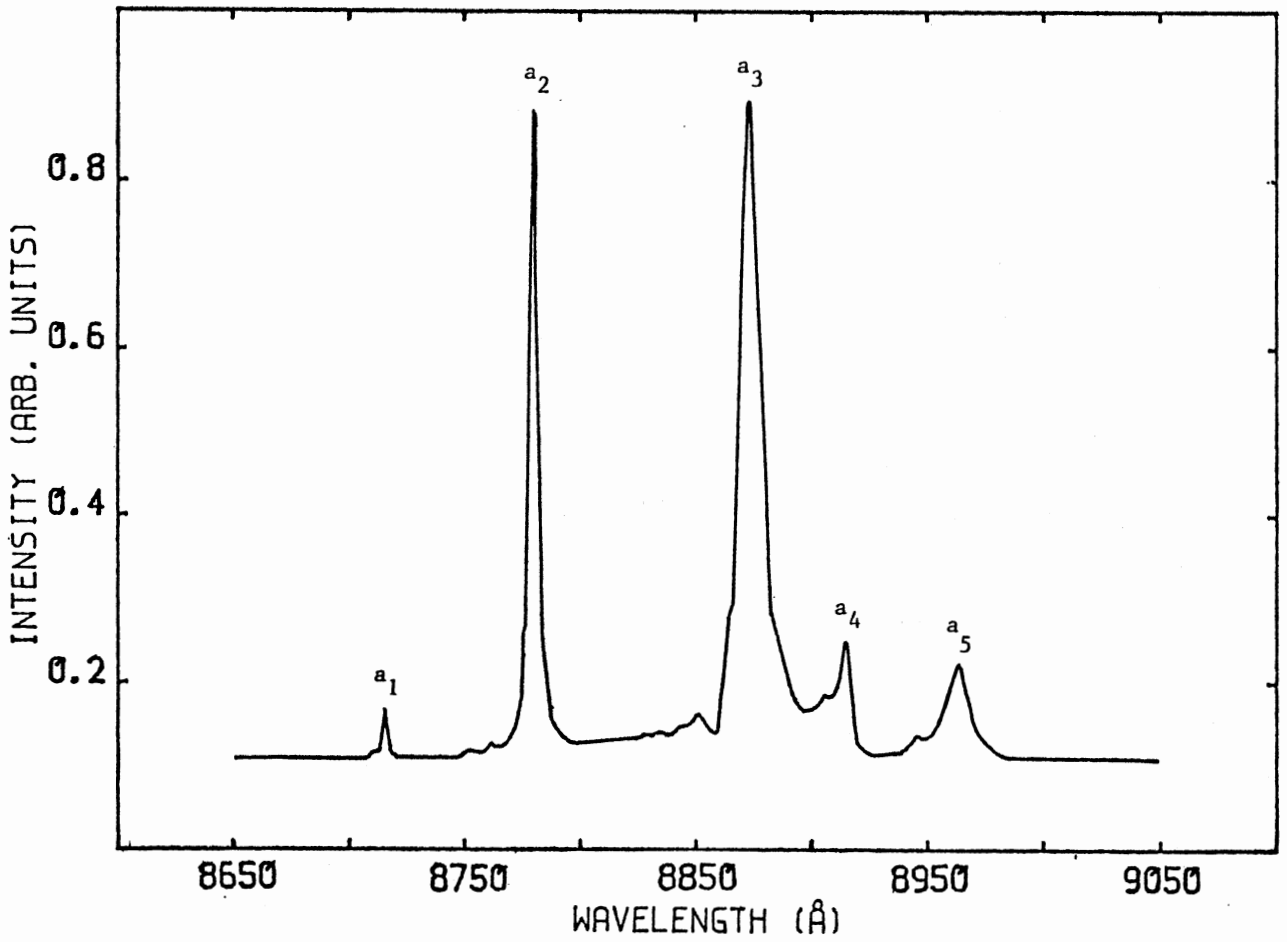

Figure 17. Fluorescence spectrum of the Nd^{3+} ion $^4F_{3/2} \rightarrow {}^4I_{9/2}$ transition in $Nd_{0.2}La_{0.8}P_5O_{14}$ at the temperature of 12.5 K.

Figure 18 and 19 show emission spectra of $Nd_xLa_{1-x}P_5O_{14}$ taken under different conditions. All spectra were taken at the temperature of 12.5 K while exciting with the 0.25 Å broad band dye laser beam. Figure 18 shows the spectra of the x = 0.2 sample. Figures 18 A and B show the spectra taken while exciting Nd^{3+} ions at the wave length of 5720 Å. Figure 18 A shows the spectrum taken while the excitation power was 0.03 W. Figure 18 B shows the spectrum taken while the excitation power was 0.18 W. Figures 18 C and D show the spectra taken while exciting at the wavelength of 5756.5 Å. Figure 18 C shows the spectrum taken while the excitation power was 0.03 W. Figure 18 D shows the spectrum taken while the excitation power was 0.18 W.

Figure 19 shows the spectra of the x = 1.0 sample. Figures 19 A and B show the spectra taken while exciting at the wavelength of 5720 Å. Figure 19 A shows the spectrum taken while exciting with the power of 0.03 W. Figure 19 B shows the spectrum taken while exciting with the power of 0.18 W. Figures 19 C and D show the spectra taken while exciting at the wavelength of 5747 Å. Figure 19 C shows the spectrum taken while exciting with the power of 0.03 W. Figure 19 D shows the spectrum taken while exciting with the power of 0.18 W.

Figures 18 and 19 demonstrate that different excitation conditions create different populations of the metastable state of the Nd^{3+} ion in $Nd_xLa_{1-x}P_5O_{14}$ crystals.

Scattering of the probe beam of the FWM configuration was observed on $Nd_xLa_{1-x}P_5O_{14}$ crystals. The crystals were kept at room temperature. The populations of ground metastable and excited states were mixing the

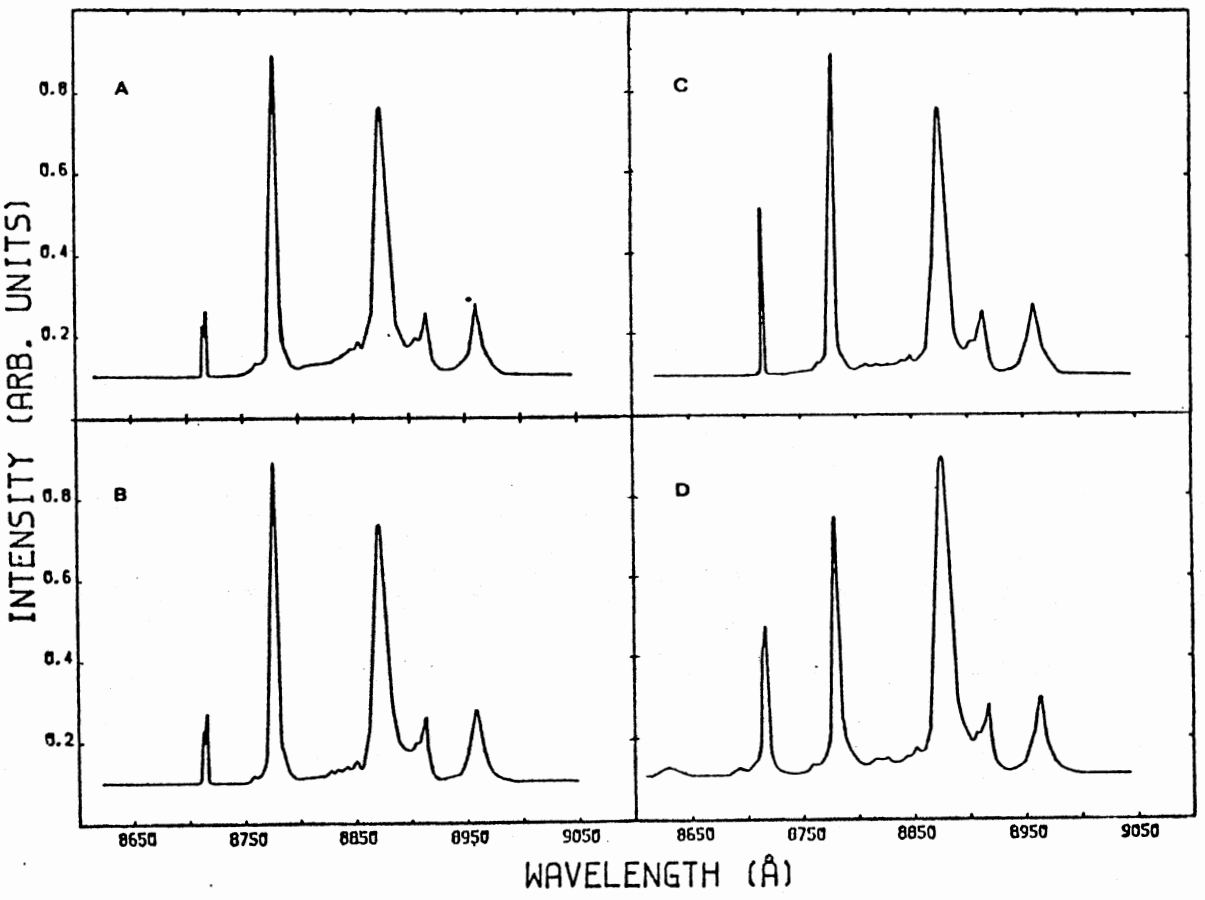

Figure 18. Fluorescence spectra of $Nd_{0.2}La_{0.8}P_5O_{14}$ at the temperature of 12.5 K for: λ_{exc} = 5720 Å, P_{pump} = 0.03 W (A); λ_{exc} = 5720 Å, P_{pump} = 0.18 W (B); λ_{exc} = 5756.5 Å, P_{pump} = 0.03 W (C); λ_{exc} = 5756.5 Å, P_{pump} = 0.03 W.

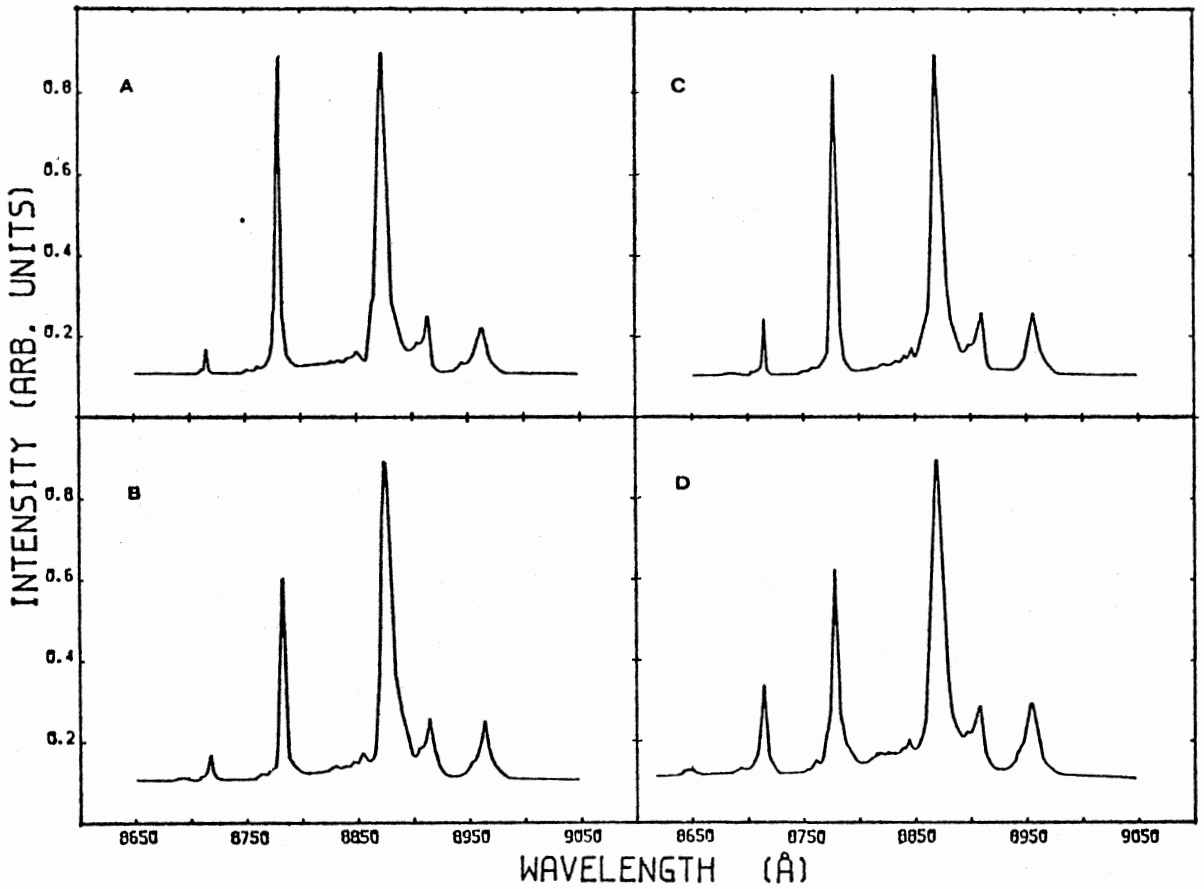

Figure 19. Fluorescence spectra of NdP_5O_{14} at the temperature of 12.5 K for: λ_{exc} = 5720 Å P_{pump} = 0.03 W (A); λ_{exc} = 5720 Å P_{pump} = 0.18 W (B); λ_{exc} = 5747 Å, P_{pump} = 0.03 W (C); λ_{exc} = 5747 Å P_{pump} = 0.18 W (D).

waves. As the result of this, the scattered beam was generated. The intensity of the scattered beam, according to formula (162), was proportional to the scattering efficiency.

The power dependence of the scattering efficiency was measured under the different conditions. Results of this experiment are demonstrated in Figure 20. Figure 20 A shows results obtained for x = 0.2. Figure 20 B shows the results obtained for x = 1.

Using focusing lens of focal length of 30 cm and positioning te sample at different positions in front of the lens, it was possible to obtain different incident-power densities at the surface of the sample. At the same time a variable beam splitter was altering the total pump power allowing one to measure the power dependence of the scattering efficiency. The data shown in Figure 20 A marked by the solid points was obtained while altering the total pump power between 0.195 and 0.013 W while the sample surface power density was changing between approximately 5.6×10^2 and 37.0 W/mm^2. The data in figure 20 A marked by the squares was obtained while altering the total pump power between 0.135 and .013 W while the sample surface power density was changing between approximately 2.2×10^2 and 1.5 W/mm^2.

The data in Figure 20 B marked by the solid points was obtained while altering the total pump power between 0.181 and 0.018 W, while the sample surface power density was changing between approximately 5.3×10^2 and 66 W/mm^2. The data in Figure 20 B was marked by the squares was obtained while altering the total pump power between 0.185 and 0.023 W while the sample surface power density was changing between approximately 2.1×10^2 and 21 W/mm^2.

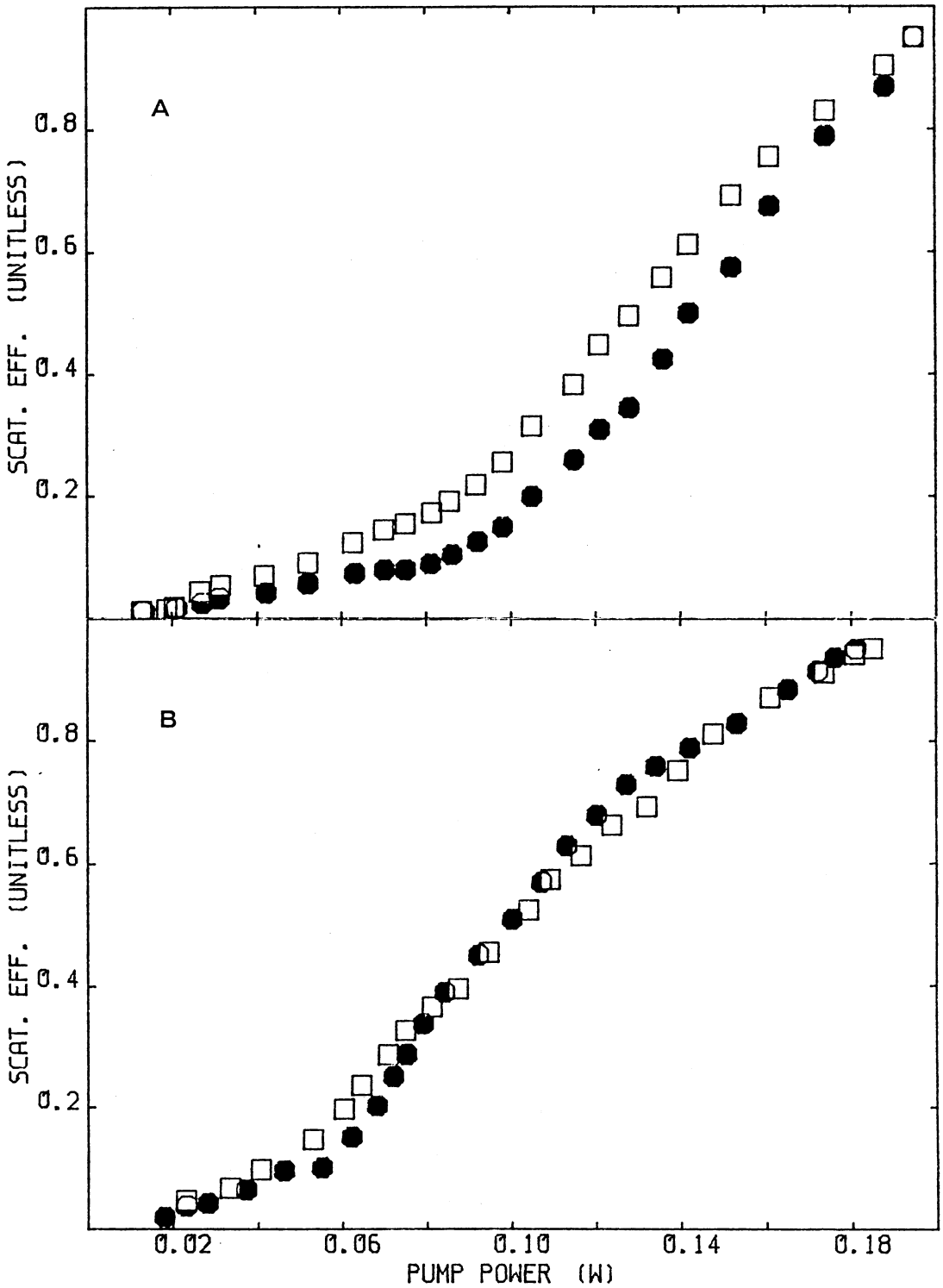

Figure 20. Four Wave Mixing scattering efficiency in $Nd_xLa_{1-x}P_5O_{14}$ for: x = 0.2, surface power density: 5.6×10^2 - 37. W/mm^2 (A, solid points); x = 0.2, surface power density: 2.2×10^2 - 15W/mm^2 (A, squares); x = 1, surface power density: 5.3×10^2 - 66 W/mm^2 (B, solid points); x = 1, surface power density: 2.1×10^2 - 22 W/mm^2 (B, squares).

The results shown in Figure 20 A are summarized in Table 3 while the results shown on Figure 20 B are summarized in Table 4.

Changing the pump part of the FWM configuration excitation in the range of 0.02-0.25 W, the transient grating decay rates of the $^4F_{3/2}$ Nd^{3+} state were measured. In this experiment time variation of the scattered light was observed under different excitation coditions. Temperature of the sample excitation power, as well as excitation wavelength were changed. Examples of the different decay curves are shown in Figure 21.

Figure 21 A shows the result of the x=0.2 sample. Scattered light time-variation was measured while exciting the sample with 0.03 W of the pump power at the excitation wavelength of 5694.5 Å while the crystal was kept at the temperature of 12.5 K.

In the case of x=0.2, while changing the power from 0.2 up to 0.19 W, and changing the wavelength from 5693.8 up to 5767.3 Å, and changing the temperature from 12.5 up to 300 K, the $I_s(t)$ was exponentially time dependent.

Figures 20 B,C, and D show the results of the x=1.0 sample. Figure 21 B shows the results obtained at the temperature of 150 K, the pump power of 0.18 W, and at the wavelength of 5743 Å. The $I_s(t)$ shows exponential behavior.

While changing the wavelength from 5694.5 up to 5732.5 Å, for the temperatures between 12.5 and 300 K and pump power between 0.02 and 0.15 W $I_s(t)$ was changing exponentially.

In the region of the excitation wavelength between 5738 and 5743 Å and the temperature equal to, or higher than 150 K, $I_s(t)$ was changing exponentially in the pump power range between 0.02 and 0.23 W.

TABLE 3

FWM SCATTERINGS EFFICIENCY IN THE $La_{0.2}$ P_5 O_{14} CRYSTAL

Pump Power [W]	Surface Power Density [10^2W/mm^2]	Scattering Efficency [Unitless]	Pump Power [W]	Surface Power Density [10^2W/mm^2]	Scattering Efficiency [Unitless]
0.135	5.59	0.96	0.195	2.23	1.00
0.188	5.39	0.91	0.188	2.15	0.92
0.174	4.98	0.84	0.179	1.99	0.83
0.161	4.61	0.76	0.161	1.84	0.71
0.152	4.35	0.70	0.152	1.74	0.60
0.142	4.07	0.62	0.142	1.63	0.52
0.136	3.90	0.56	0.136	1.56	0.44
0.128	3.67	0.51	0.128	1.47	0.36
0.121	3.47	0.45	0.121	1.39	0.32
0.115	3.29	0.39	0.115	1.32	0.27
0.105	3.01	0.32	0.105	1.20	0.20
0.098	2.81	0.26	0.098	1.12	0.15
0.092	2.63	0.22	0.092	1.05	0.12
0.085	2.44	0.19	0.085	0.97	0.10
0.081	2.33	0.18	0.081	0.93	0.087
0.075	2.15	0.16	0.075	0.86	0.076
0.070	2.00	0.15	0.070	0.80	0.076
0.063	1.79	0.13	0.063	0.72	0.070
0.052	1.49	0.093	0.052	0.60	0.063
0.042	1.19	0.072	0.042	0.48	0.052
0.031	0.90	0.056	0.031	0.36	0.036
0.026	0.75	0.045	0.026	0.30	0.026
0.021	0.59	0.020	0.021	0.24	0.018
0.019	0.54	0.016	0.019	0.22	0.009
0.013	0.37	0.013	0.013	0.15	0.004

TABLE 4

FWM SCATTERING EFFICIENCY IN THE LaP_5O_{14} CRYSTAL

Pump Power [W]	Surface Power Density [10^2W/mm^2]	Scattering Efficiency [Unitless]	Pump Power [W]	Surface Power Density [10^2W/mm^2]	Scattering Efficiency [Unitless]
0.185	5.30	0.98	0.181	2.07	0.95
0.181	5.19	0.97	0.176	2.02	0.94
0.174	4.98	0.94	0.172	1.97	0.92
0.162	4.64	0.90	0.165	1.89	0.88
0.149	4.27	0.84	0.153	1.75	0.83
0.141	4.04	0.78	0.142	1.63	0.79
0.132	3.78	0.72	0.134	1.54	0.76
0.126	3.61	0.69	0.127	1.46	0.73
0.119	3.41	0.64	0.120	1.38	0.68
0.112	3.21	0.60	0.113	1.29	0.63
0.107	3.07	0.55	0.107	1.23	0.57
0.098	2.81	0.48	0.100	1.15	0.51
0.091	2.61	0.42	0.092	1.05	0.45
0.085	2.44	0.39	0.084	0.93	0.39
0.079	2.26	0.35	0.079	0.91	0.34
0.075	2.15	0.31	0.075	0.86	0.29
0.069	1.98	0.26	0.072	0.83	0.25
0.065	1.86	0.22	0.068	0.78	0.20
0.058	1.66	0.17	0.062	0.71	0.15
0.046	1.32	0.12	0.055	0.63	0.10
0.033	1.12	0.09	0.046	0.53	0.097
0.029	0.83	0.07	0.037	0.42	0.066
0.023	0.66	0.05	0.028	0.31	0.044
			0.023	0.26	0.039
			0.018	0.21	0.021

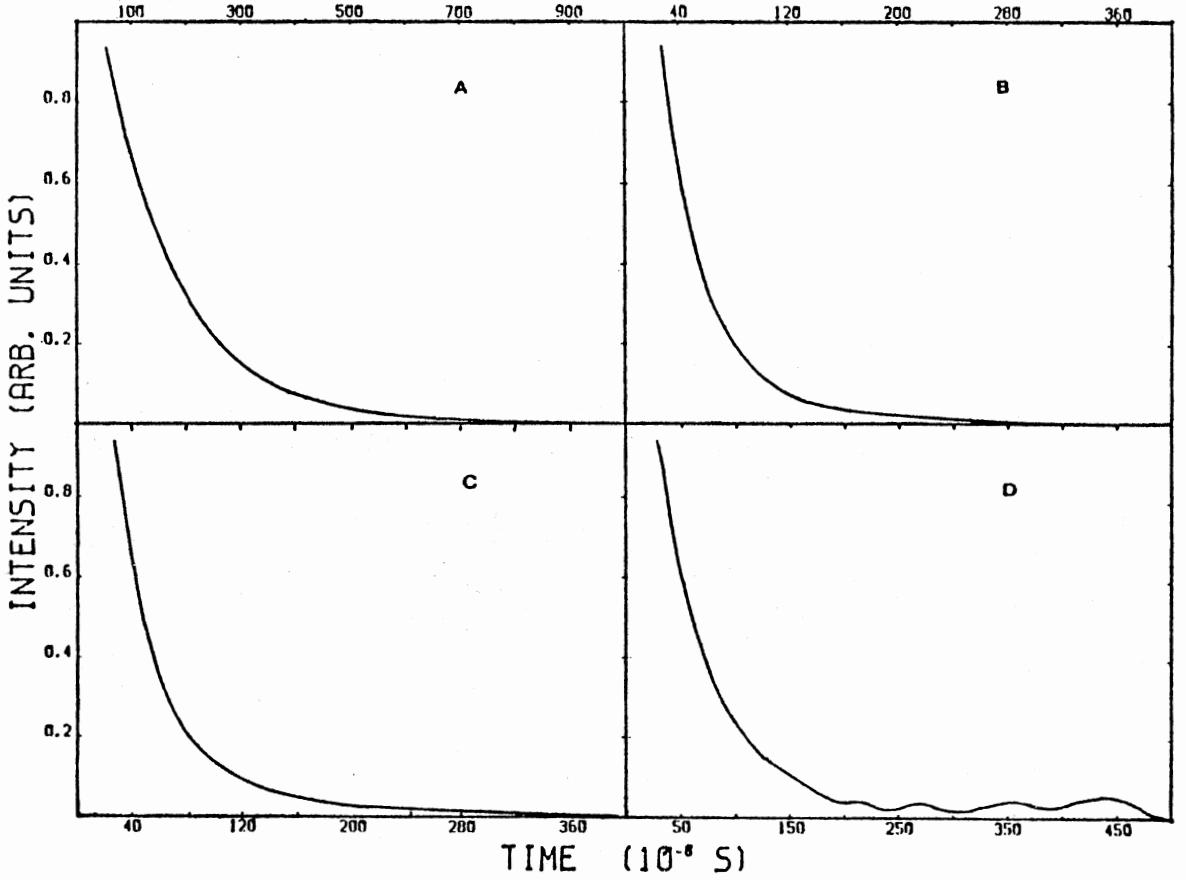

Figure 21. Scattered beam time decay in transient grating experiment on $Nd_xLa_{1-x}P_5O_{14}$ for: x = 0.2, T = 12.5 K, λ_{exc} = 5694.5 Å, P_{pump} = 0.03 W (A); x = 1, T = 12.5 K, λ_{exc} = 5443 Å, P_{pump} = 0.18 W (B); x = 1, T = 12.5 K, λ_{exc} = 5745 A, P_{pump} = 0.18 W (C); x = 1, T = 12.5 K, λ_{exc} = 5745 Å, P_{pump} = 0.03 W (D).

Figure 21 C shows the $I_s(t)$ measured at the temperature of 12.5 K, pump power of 0.18 W and excitation wavelength of 5745 Å. $I_s(t)$ departs from the single exponential shape and shows double exponential time dependence. In the temperature range between 12.5 and 100 K, excitation range between 5738.0 and 5747.6 Å and the power of excitation of about 0.18 W transient grating of the x=1.0 sample shows double exponential time dependence. Figure 21 D shows the $I_s(t)$ measured at the temperature of 12.5 K, at the excitation wavelength of 5743 Å and at the pump power of 0.03 W. $I_s(t)$ shows an oscillatory time dependence. In the range of excitation wavelength between 5738.0, and 5747.6 Å at the temperature between 12.5 and 100 K and for the pump power of about 0.03 W the x=1.0 sample shows oscillatory behavior of the $I_s(t)$ time variation.

Measurements of the angular dependence of the exponential decay rates are shown in Figures 22 and 23. Figure 22 shows the measured values of the grating decay rate plotted versus the squared sine of half the pump beam crossing angle divided by the square of the wavelength of the excitation beam for the x=0.2 at the excitation wavelength of 5749 Å. Figure 22 A shows the data obtained at the temperature of 28 K. Figure 22 B shows the data obtained at room temperature.

Figure 23 shows the measured value of the grating decay rates versus the squared sine of the half the pump beam crossing angle divided by the square of the beam wavelength for the x=1.0 sample at the excitation wavelength of 5699 Å.

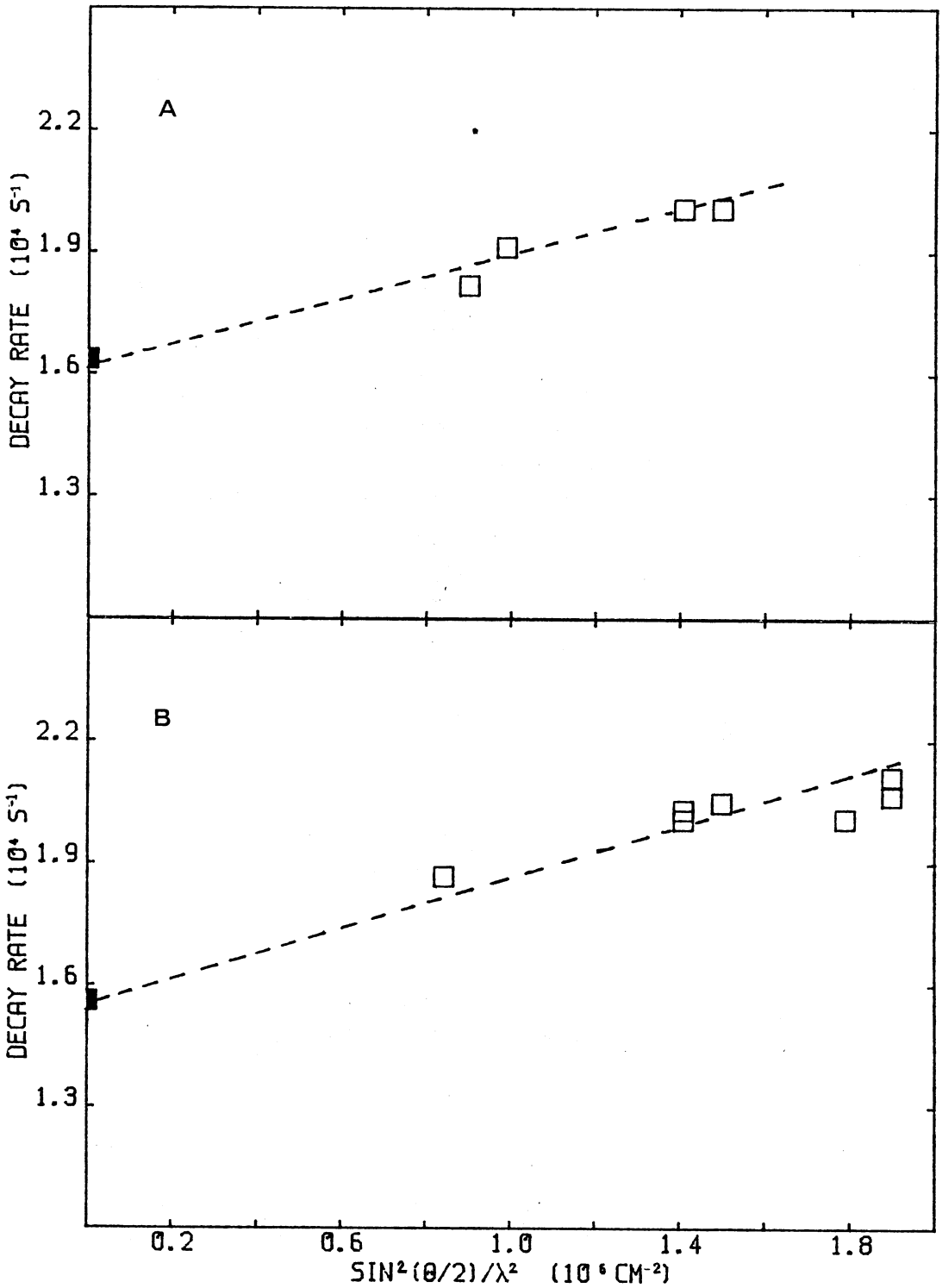

Figure 22. Angular dependence of the grating decay rate in $Nd_{0.2}La_{0.8}P_5O_{14}$ for:
λ_{exc} = 5749 Å and T = 28 K (A);
λ_{exc} = 5749 Å and T = 300 K (B).

Figure 23 A shows the results obtained at 25 K. Figure 23 B shows the data obtained at room temperature. The results of x=0.2 are summarized in Table 5 while the results of x=1.0 are summarized in Table 6.

The solid points represent one half of the fluorescence decay rates obtained by independent measurements. The straight lines are the best fits between the theory and the data using equation (186). The data plotted this way vary linearly and extrapolate to half the decay rates at zero crossing angle. The exciton diffusion coefficients can be obtained from the slopes of the lines.

The type of data fit together with the large value of the obtained diffusion coefficient suggest that the energy migration in the regions of exponential $I_s(t)$ time dependence is partially coherent, and equation (186) provides a proper description of the scattered beam time variation.

The measurements of the angular dependence of $I_s(t)$ in the regions of its exponential behavior allowed estimation of the exciton diffusion coefficient in case of the x=0.2 and x=1.0 samples.

Figure 24 shows the wavelength dependence of the diffusion coefficient of the x=1.0 and x=0.2 sample. The data was obtained at the temperature of 12.5 K and at the pump power of approximately 0.18 W. Figure 24 A shows the data of x=0.2. Figure 24 shows the data of x=1.0. This data is summarized in Table 7.

Figure 25 shows the temperature dependence of the diffusion coefficient in the regions of the strong Nd^{3+}absorption. Figure 25 A shows the data of the x=0.2 sample obtained at the excitation wavelength of 5749 Å. The squares on Figure 25 A mark the data

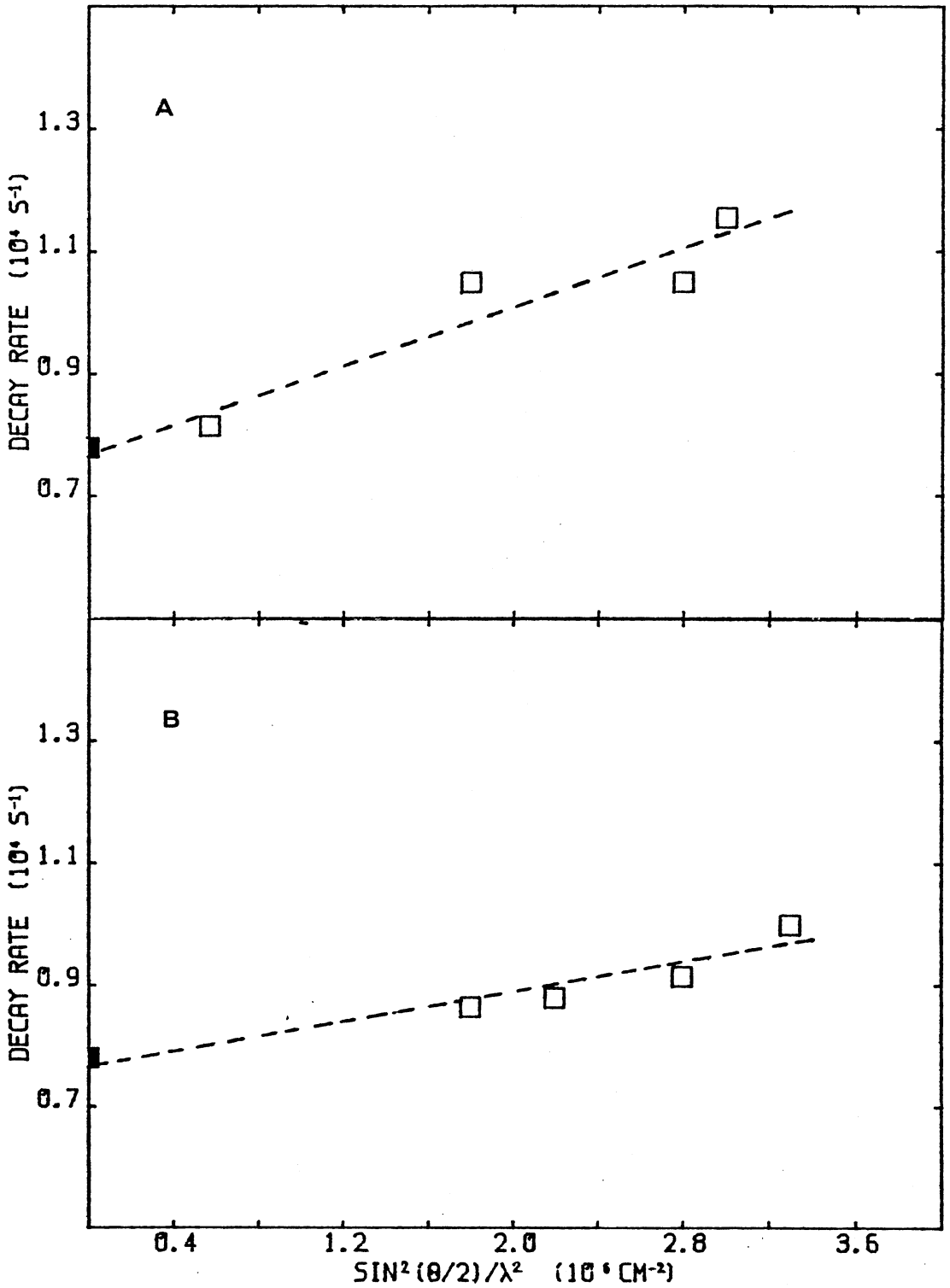

Figure 23. Angular dependence of the grating decay rate in NdP_5O_{14} for λ_{exc} = 5699 Å and T = 23 K (A) λ_{exc} = 5699 Å and T = 300 K (B).

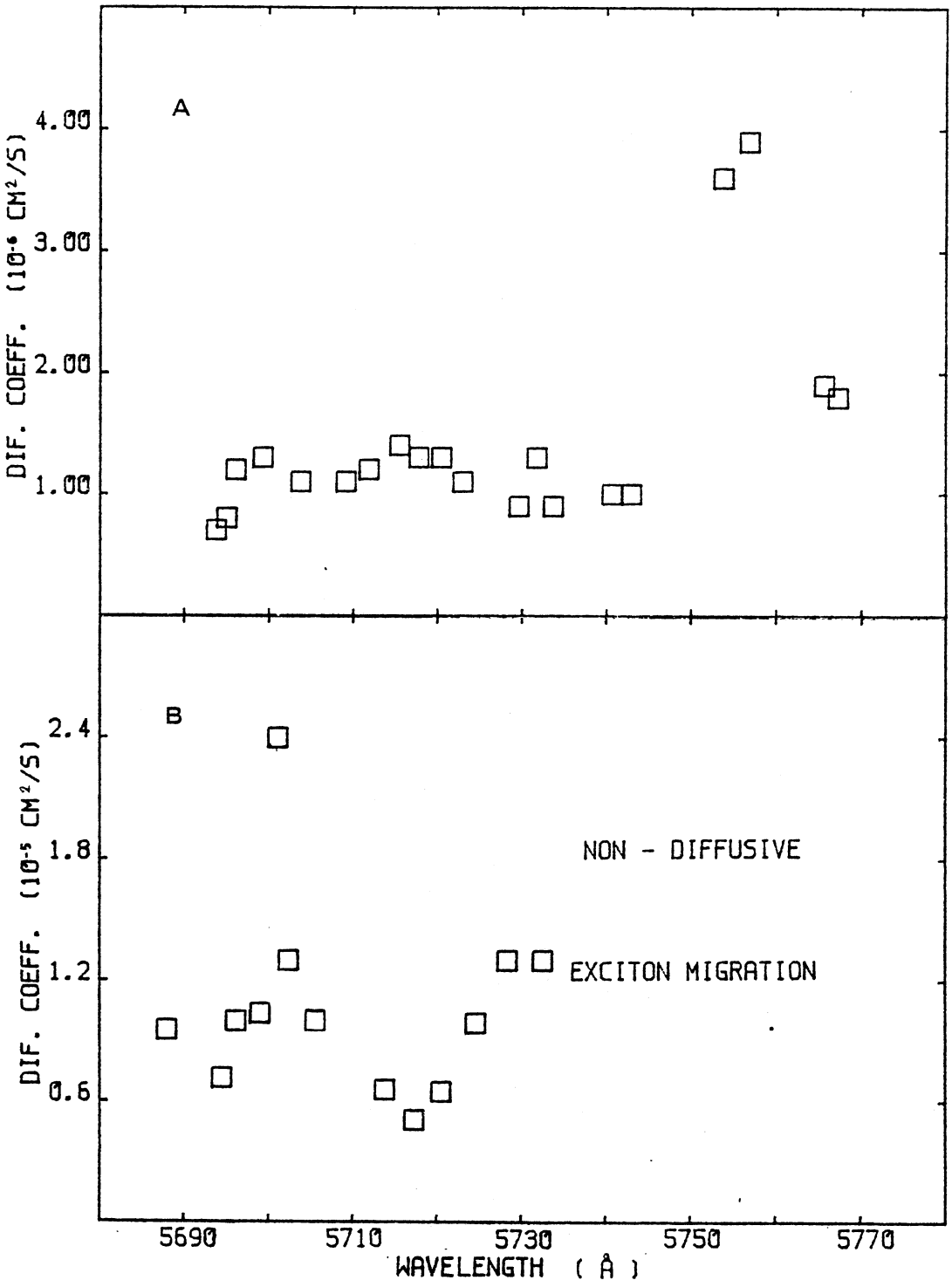

Figure 24. Wavelength dependence of the exciton diffusion coefficient in $Nd_xLa_{1-x}P_5O_{14}$ at T = 12.5 K and P_{pump} = 0.18 W for: x = 0.2 (A) and x = 1 (B).

TABLE 5

THE ANGULAR DEPENDENCE OF THE TRANSIENT GRATING DECAY RATE OF $Nd_{0.2}\ La_{0.8}\ P_5\ O_{14}$

T = 28K, λ_{exc} = 5749 Å		Room Temperature, λ_{exc} = 5749 Å	
$\sin^2(\theta/2)/\lambda^2$ [10^6 cm^{-2}]	Decay Rate [$10^3 s^{-1}$]	$\sin^2(\theta/2)\lambda^2$ [10^6 cm^{-2}]	Decay Rate [10^3 s^{-1}]
0.0	7.8	0.0	7.8
0.6	8.2	1.8	8.6
1.8	10.5	2.2	8.8
2.8	10.5	2.8	9.2
3.0	11.5	3.3	10.0

TABLE 6

ANGULAR DEPENDENCE OF THE TRANSIENT GRATING DECAY RATE IN NdP_5O_{14}

T = 25K, λ_{exc} = 5699Å		Room Temperature , λ_{exc} = 5694Å	
$\sin^2(\theta/2)/\lambda^2$ [10^6 cm^{-2}]	Decay Rate [$10^3 s^{-1}$]	$\sin^2(\theta/2)/\lambda^2$ [$10^6 cm^2$]	Decay Rate [$10^3 s^{-1}$]
0.0	16.4	0.0	15.6
0.9	18.2	0.8	16.7
1.0	19.1	1.4	20.1
1.4	20.1	1.4	20.3
1.5	20.1	1.5	20.5
		1.8	20.1
		1.9	21.1

TABLE 7

THE EXCITATION WAVELENGTH DEPENDENCE OF THE DIFFUSION COEFFICIENT IN $Nd_xLa_{1-x}P_5O_{14}$ AT THE TEMPERATURE OF 12.5K

X = 0.2		X = 1.0	
Wavelength [Å]	Diffusion Coefficient [$10^{-6}cm^2s^{-1}$]	Wavelength [Å]	Diffusion Coefficient [$10^{-6}cm^2s^{-1}$]
5693.8	0.7	5684.5	7.2
5695.0	0.8	5696.2	10.0
5696.1	1.2	5701.1	24.0
5699.3	1.3	5702.4	13.0
5703.8	1.1	5705.6	10.0
5704.1	1.3	5713.8	6.6
5709.2	1.1	5717.3	5.1
5711.9	1.2	5720.5	6.5
5715.5	1.4	5724.6	9.3
5717.8	1.3	5728.3	13.0
5720.5	1.3	5732.5	13.0
5723.0	1.1		
5729.7	0.9		
5731.8	1.3		
5733.8	0.9		
5740.7	1.0		
5743.0	1.0		
5753.8	3.6		
5756.9	3.9		
5765.7	1.9		
5767.3	1.8		

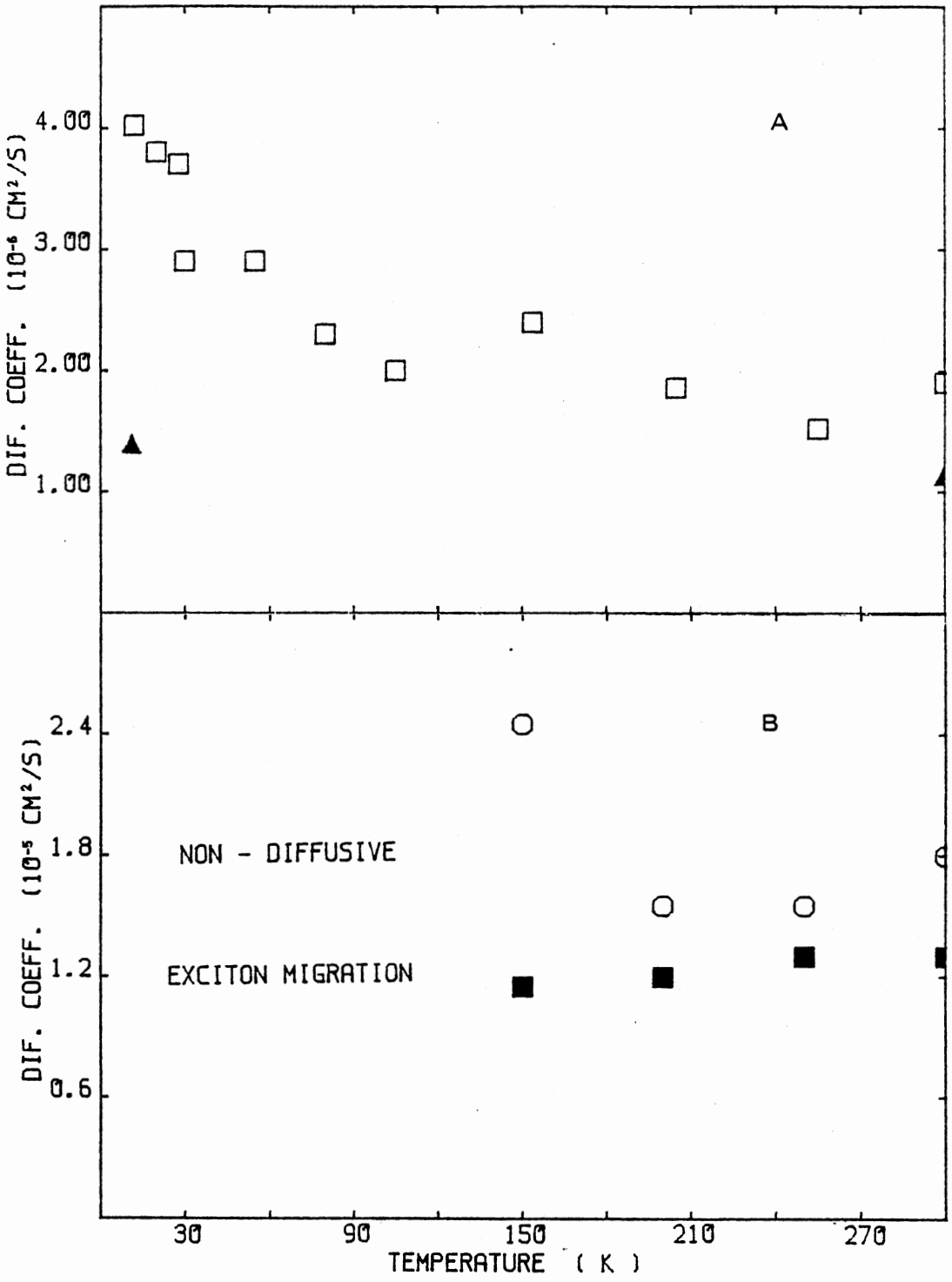

Figure 25. Temperature dependence of the exciton diffusion coefficient in $Nd_xLa_{1-x}P_5O_{14}$ for: x = 0.2, λ_{exc} = 5749 Å, P_{pump} = 0.18 W (A, squares); x = 0.2, λ_{exc} = 5449 Å, x = 0.03 W (A solid trianguls); x = 1, λ_{exc} = 5746 Å, P_{pump} = 0.19 W (B, circles); x = 1, λ_{exc} = 5746 Å, P_{pump} = 0.03 W (solid squares).

TABLE 8

TEMPERATURE DEPENDENCE OF THE DIFFUSION COEFFICIENT
IN $Nd_xLa_{1-x}P_5O_{14}$

X = 0.2, λ_{exc} = 5749				x = 1.0, λ = 5749			
P = 0.18W		P = 0.03W		P = 0.18W		P = 0.03W	
Pump Temperature [T]	Diffusion Coefficient [$10^{-6}cm^2s^{-1}$]	Pump Temperature [T]	Diffusion Coefficient [$10^{-6}cm^25^{-1}$]	Pump Temperature [T]	Diffusion Coefficient [$10^{-6}cm^2s^{-1}$]	Pump Temperature [T]	Diffusion Coefficient [$10^{-6}cm^25^{-1}$]
12					Non-diffusive		Non-diffusive
20	4.0	12.5	1.4		Exciton		Exciton
28	3.8			12.5-100	Migration	12.5-100	Migration
30	3.7			150	10.6	150	5.0
55	2.9			200	6.7	200	5.3
154	3.0			250	6.8	250	5.8
205	2.4			300	7.8	300	5.8
255	1.9						
300	1.9						
	1.9	300	1.1				

obtained for the pump power of 0.18 W. The two solid triangles in Figure 25 A mark the data obtained for the pump power of 0.03 W. Figure 25 B shows the data of x=1.0 obtained at the wavelength of 5746 Å. The circle in Figure 25 B mark the data obtained for the pump power of 0.19 W, while the squares mark the data obtained for, the power of 0.03 W. The data showing the temperature dependence of the diffusion coefficient is summarized in Table 8.

Figure 26 shows the pump power dependence of the diffusion coefficient in the case of x=0.2 sample. Figure 26 A shows the data obtained at the temperature of 12.5 K and the wavelength of 5756 Å. Figure 26 B shows the data obtained at room temperature. The squares mark the data of the excitation wavelength of 5718.5 Å. The solid points mark the data for the excitation wavelength of 5749 Å. The data of the power dependence of the diffusion coefficient of th x=0.2 sample is summarized in Table 9.

Figure 27 shows the pump power dependence of the diffusion coefficient for the x=1.0 sample. The data of Figures 27 A and B were obtained at room temperature. Figure 27 A shows the data obtained for the excitation wavelength of 5743 Å. Figure 27 B shows the data obtained for the excitation wavelengt of 5688.5 Å. The power dependence of the diffusion coefficient data of the x=1.0 sample is summarized in Table 10.

F. Discussion and Conclusions

The shape of the emission spectra from $^4F_{3/2}$ state to $^4I_{9/2}$ state is determined by the free ion transition probabilities, reabsorption process and the ion-crystal field interaction. In the

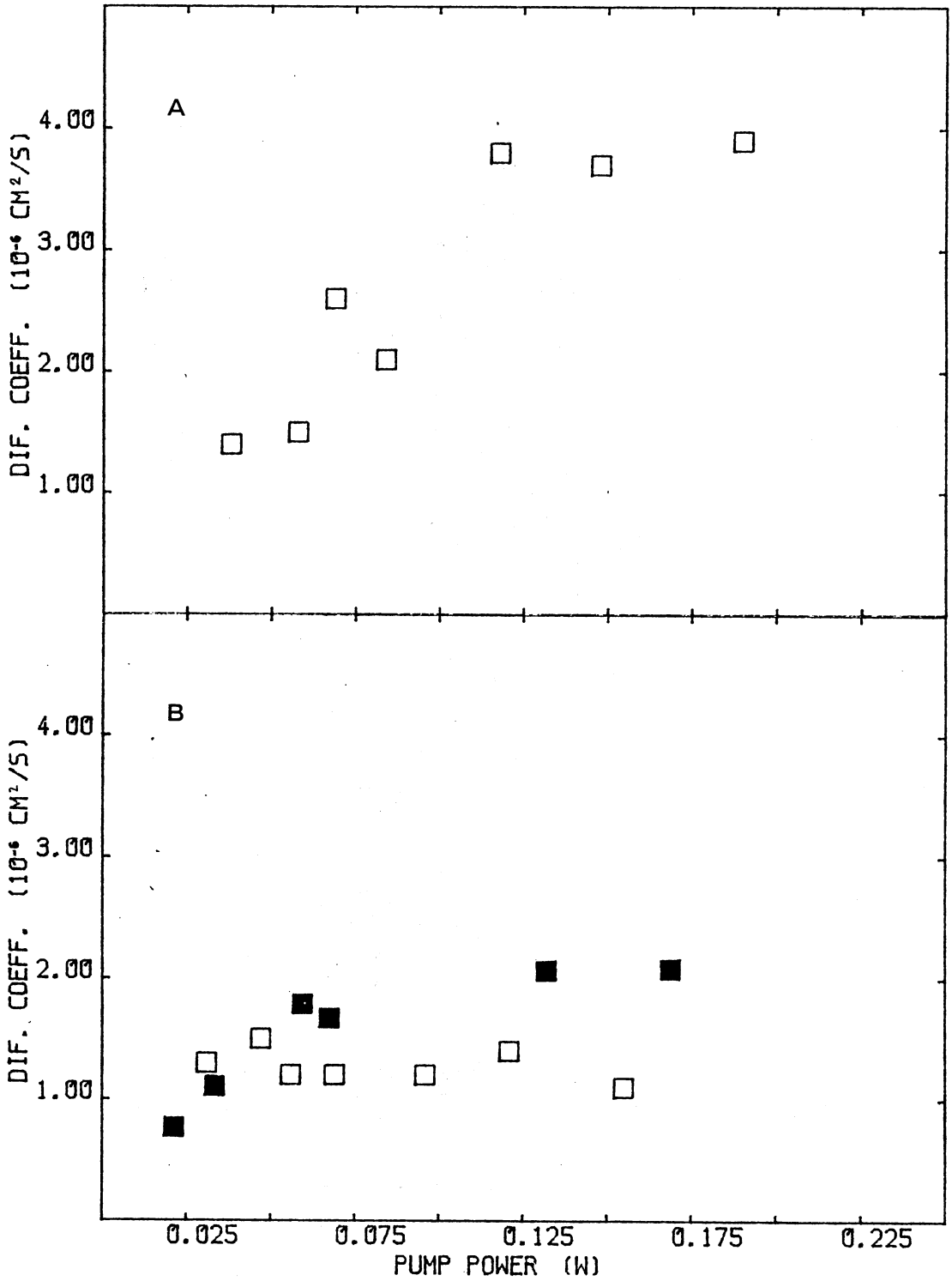

Figure 26. Grating pump power dependence of the exciton diffusion coefficient in $Nd_{0.2}La_{0.8}P_5O_{14}$ for: T = 12.5 K λ_{exc} = 5756 Å (A) T = 300 K λ_{exc} = 5718.5 Å (B squares); T = 300 K, λ_{exc} = 5749 Å (B, solid squares).

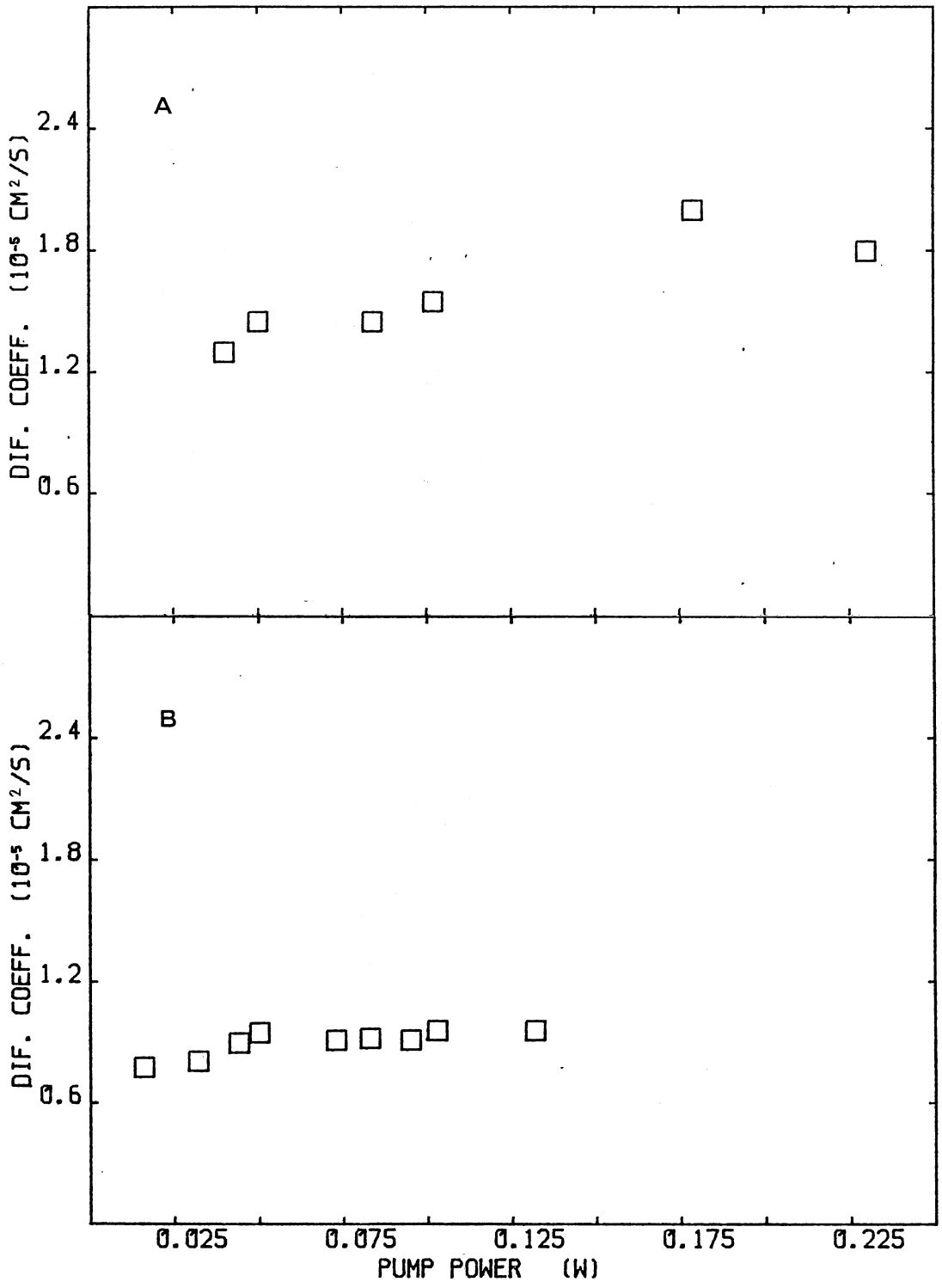

Figure 27. Grating pump power dependence of the exciton diffusion coefficient in NdP_5O_{14} for: T = 300K λ_{exc} = 5743 Å (A), T = 300 K; λ_{exc} = 5688.5 Å (B).

TABLE 9

THE GRATING PUMP POWER DEPENDENCE OF THE DIFFUSION COEFFICIENT IN $Nd_{0.2}La_{0.8}P_5O_{14}$

T=12.5K, λ_{exc} = 5756Å		Room Temperature, λ_{exc} = 5756Å		Room Temperature, λ_{exc} = 5718.5Å	
Pump Power [W]	Diffusion Coefficient [$10^{-6}cm^2s^{-1}$]	Pump Power [W]	Diffusion Coefficient [$10^{-6}cm^2s^{-1}$]	Pump Power [W]	Diffusiong Coefficient [$10^{-6}cm^2s^{-1}$]
0.190	3.9	0.96	0.195	2.23	1.00
0.148	3.7	0.91	0.188	2.15	0.92
0.118	3.8	0.84	0.179	1.99	0.83
0.084	2.1	0.76	0.161	1.84	0.71
0.069	2.6	0.70	0.152	1.74	0.60
0.058	1.5	0.62	0.142	1.63	0.52
0.038	1.4	0.56	0.136	1.56	0.44

TABLE 10

THE GRATING PUMP POWER DEPENDENCE OF THE DIFFUSION COEFFICIENT IN NdP_5O_{14}

Room Temperature, λ_{exc} = 5743Å		Room Temperature, λ_{exc} = 57488	
Pump Power [W]	Diffusion Coefficient [$10^{-6}cm^2s^{-1}$]	Pump Power [W]	Diffusion Coefficient [$10^{-6}cm^2s^{-1}$]
0.230	17	0.132	9.6
0.179	19	0.103	9.6
0.102	14	0.095	9.1
0.084	13	0.083	9.2
0.050	13	0.073	9.1
		0.050	9.5
		0.044	9.0
		0.032	8.1
		0.016	7.8

case of the strong ion-crystal field coupling, the symmetry of the crystal field modified by the geometry of the phonon states can alter the transition probabilities of the excited states. The process of reabsorption, to which the lower Stark components of the angular momentum manifold are more sensitive, influences this part of the luminescence which originates in the bulk of the crystal.

The luminescence spectra of the Nd^{3+} ion in the $Nd_xLa_{1-x}P_5O_{14}$ crystals show a weak power sensitivity of the a_1, line while the second stark component a_2 of the $^4F_{3/2} \longrightarrow {}^4I_{9/2}$ transition changes drastically with the power.

The change of the absorption coefficient is less than 2% in the range between approximately 5720 and 5770 Å. In this range there are dramatic changes in the emission spectrum of the Nd^{3+} ion. Therefore, it should be concluded that power-wavelength change of the emission spectrum takes place through the altering of the transition probabilities in the $^4F_{3/2} \longrightarrow {}^4I_{9/2}$ manifold. This alteration can be caused by the metastable state absorption or the site selective excitation (49). These two processes influence the population of excitons through the generation of different types of excited states. The third process that can influence the power-wavelength dependence transition probabilities can be caused by the strong ion-crystal field coupling (50,51). In this case the distinction between different excitons is made through the properties of the phonon baths with which excitons interact.

The $^4F_{3/2}$ metastable state of Nd^{3+} ion in $Nd_xLa_{1-x}P_5O_{14}$ has the property of maintaining its distinct characteristic under CW

excitation. This is consistent with the reported lack of the spectral energy migration in $Nd_xLa_{1-x}P_5O_{14}$ crystals (53).

As it was shown in the previous paragraph, the scattering efficiency in the three level system reflects the spectroscopic properties of the excited, metastable and the ground state as well as on the kinetic parameters governing the distribution of the ions between the states. The power dependencies of the scattering efficiencies measured in the case of the x=1.0 and x=0.2 confirms these theoretical results.

The measurement of the time dependence of the intensity of the scattered beam showed the possibility of exponential, double exponential and/or oscillatory behavior of $I_s(t)$. The external conditions which control the shape of $I_s(t)$ are the Nd^{3+} ion concentration, excitation wavelength, grating pump power and/or the sample temperature. The temperature of the sample and the pump power of the transient grating as well as the excitation wavelength control the spectrum of the phonon bath interacting with the exciton. In terms of the theory developed by Wong and Kenkre (45,46,47), the sample dopant concentration, temperature, grating pump power and/or excitation wavelength do alter the value of α the randomized parameter of ion-phonon bath interaction. As a result of this the degree of coherence influencing the migration of the $^4F_{3/2}$ state can change while altering the sample dopant concentration, temperature, grating pump power and/or the excitation wavelength. Consequently, the shape of the $I_s(t)$ time dependence can change from a single exponential to an oscillatory type.

The type of the grating decay rate dependence on the pump beams crossing angle indicates that the x=0.2 sample within the entire pump power-temperature-wavelength experimental range, and the x=1.0 outside the 12.5-100 K temperature range and the 5738-5746.6 Å excitation wavelength range show the diffusive type of exciton migration.

The diffusion coefficient can be expressed in terms of the exciton velocity and either the mean free path or the scattering time

$$D = 1/3 \left\langle L_m \upsilon \right\rangle = 1/3 \left\langle t_s \upsilon^2 \right\rangle \tag{189}$$

where L_m is the mean free path of the diffusing exciton, t_s is the excitation lifetime, and υ is the mean exciton velocity.

One special case which is generally true for light doped sample rare earth systems, is the nearest neighbor hopping model in which the free path is just the distance between rare earth ions and the velocity can be expressed in terms of ion-ion energy transfer rate. The temperature dependence of D is contained in this latter factor which leads to

$$D = 1/3 \ (a^2 t_h^{-1}) = 1/3 \ (a^2 w(T)) \tag{190}$$

$$t_h^{-1} = w(T) \sim f_a f_s \Omega \tag{191}$$

where f_s is the activator oscillator strength, f_s is the sensitizer oscillator strength, and Ω is an integral of the overlap of the emission spectrum of the sensitizer and the absorption spectrum of the activator.

The spectral overlap Ω increases as the temperature increases which is not consistent with the data in this case. Thus, one can rule

out the nearest neighbor hopping model as a way of interpreting data for these highly concentrated systems.

Phonon assisted energy migration was investigated by Trilifaj (54,56). The type of obtained temperature dependence rules out this model.

In the general case, the scattering time or mean-free-path of migration of excitons can be limited by several different types of scattering events which can limit the process of exiton migration. Agronovitch and co-workers have derived the temperature dependences associated with each of these mechanisms (56).

Table 11 summarizes the theoretically obtained temperature dependencies of the exciton diffusion coefficient. Obviously, a variety of temperature dependences are possible depending on the type of phonons or defects which dominate the scattering process. Both because of the various assumptions which had to be made about the electron-phonon coupling in deriving these equations and because several machanisms may be active simultaneously, it is difficult to do any quantitive fitting between theory and experiment.

However, one can assume, that the excitons couple mainly to the optical phonons. This is reasonable since in these highly concentrated materials energy will move between ions within the wavelength of acoustic phonons and thus the energy levels of both ions will be modulated simultaneously by these phonons. In contrast, optical phonons will modulate the position and energy of one ions with respect to its nearest neighbor and thus be effective in exciton scattering. Thermal diffusivity measurements (57) indicate that the Debye

TABLE 11

THE TEMPERUTURE DEPENDENCE OF THE EXCITON DIFFUSION COEFFICIENT

Migration Limiting Mechanism	Conditions	D = D(T)
Phonon Assisted Migration (54,55)		$\exp(-E/kT)$
Scattering by the Acustic Phonons (56)	$k_o = 0$; $T < 4K(m^*/m)$	constant
	$k_o = 0$; $T > 4K(m^*/m)$	$1/\sqrt{T}$
	$k_o \neq 0$; $kT \ll E(0) - E(\bar{k}_o)$	$1/T$
	$k_o \neq 0$; $kT \gg E(0) - E(\bar{k}_o)$	$1/\sqrt{T}$
Scattering by the Optical Phonons (56)	$kT \gg \hbar\omega_{op}$	the same as in the case of the acustic phonons
	$kT \ll \hbar\omega_{op}$	constant
Scattering by the Lattice Defects (56)	$T \rightarrow 0$	$\sqrt{T}$
	$T > 0$	constant

In the above table the symbols have the following meaning: k is the Boltzman's constant, T is the temperature, $E(\bar{k})$ is the energy of the phonon with the wave vector $\bar{k}$, $\bar{k}_o$ is the wave vector from the bottom of the phonon band, m* is the phonon effective mass, m is the electron mass, ω_{op} is the optical phonon frequency, $\hbar$ is the Planck's constant.

temperature is around room temperature in these crystals and thus lattice phonons should not contribute to a temperature dependence of the diffusion coefficient.

In the region of excitation wavelengths higher than 5740 Å and at the temperature lower than 150 K, the x=0.2 sample shows a very large increase of the diffusion coefficient while the x=1.0 sample shows departure from the diffusive exciton migration. In this region drastic change in α occurs.

The excitation wavelength dependence of the diffusion coefficient shows a mobility peak between about 5740 and 5770 Å in the x=0.2 sample. In the same region x=1.0 shows a coherent, nondiffusive motion. This region corresponds with the small band contributing to the $^4I_{9/2} \longrightarrow {}^4G_{7/2}$ absorption of $Nd_xLa_{1-x}P_5O_{14}$. The decrease of the $\frac{\alpha}{j}$ ratio in this region cannot be caused only by the increase of j due to the higher concentration of the interacting ions. In this region, absorption of the Nd^{3+} ions changes only by approximately 6%. It is possible, that the change of j is due to the change of the average concentration of the Nd^{3+} ions in resonance is a minor factor influencing $\frac{\alpha}{j}$ ratio. Possibly, the spectrum of generated phonons in this region influences the smaller value of ion-phonon interocition parameter.

The sample x=1.01 shows another decrease in the $\frac{\alpha}{j}$ ratio around 5725-5759 Å region. In this region the diffusion coefficient of the x=0.2 sample stays flat. At the same time, the absorption of the x=1.0 shows in this spectral region a small structure, while x=0.2 shows the region of monotonical behavior. A 2% change of the absorption coefficient of the x=1.0 in this region may cause negligible change of the j value due to the change in the number of the interacting ions.

It was shown that in the inhomogeneously broaden systems, scanning across the absorption band can expose a mobility edge of the excitons (58). The change of concentration of ions in resonance in the inhomogenously broadened systems results in the presence of the mobility edge. However, in the case of $Nd_xLa_{1-x}P_5O_{14}$ the change of the exciton migration process occurs still on the wing of the absorption band. This implies that the plateau of the absorption ranging between 5500 and 5750 Å has a complex (in terms of the ion-ion and ion-phonon interaction) structure allowing for big changes of $\frac{\alpha}{j}$ ratio.

Finally, the power dependence of the diffusion coefficient of the excitons in $Nd_xLa_{1-x}P_5O_{14}$ in the regions of the high exciton mobility, and negligible power dependence of the diffusion coefficient in the region of the low exciton mobility indicates the possibility of the excited state absorption. The excitons in the metastable state can be excited into the higher mobility state. In the regions of the low mobility this effect is possibly masked by the experimental error.

In conclusion it can be emphasized that exciton migration processes in $Nd_xLa_{1-x}P_5O_{14}$ is critically dependent on the conditions of excitation. Motion of the excitons is partially coherent. The degree of coherence can be influenced through the altering $\frac{\alpha}{j}$ ratio of the ion-phonon to ion-ion interaction. The external parameters influencing $\frac{\alpha}{j}$ ratio are dopant concentration, excitation wavelength, the sample temperature, and the grating pump power.

CHAPTER V

SUMMARY AND CONCLUSIONS

A. Summary of the Results

In Chapter II a review of the theoretical efforts to describe the energy migration process in the discrete media was made.

Starting from the discussion of the Generalized Master Equation and the Pauli Master Equation the adequacy to describe the energy dynamics in the discrete medium was reviewed. The theory of the Generalized Diffusion Coefficient was discussed. The limitations of this theory due to two body approximation were also pointed out.

Subsequently, the efforts to develop the survival function formalism were reviewed. The Förster-Dexter model, the Shell Model, the Sphere Model as well as the ATA model were discussed.

Finally, the need to establish the correspondence between the GDC theory and the survival function approach was pointed out.

In Chapter III a technique of Time-resolved site-selection was discussed. The results of experiments on $Eu_xY_{1-x}P_5O_{14}$ were presented and analyzed. The two level system in connection different survival functions was used to discuss the experimental data. In the case of x=1.0 dipole-dipole interaction was found to be responsible for the energy migration. The time dependence of the sinsitizer-activator transfer rate indicates uniform E^{3+} ion distribution. In the case of x=0.01

constant parameter with a possibility of the back transfer energy migration model provided adequate description of the spectra evolution. This implies the possibility of Eu^{3+} ion agregation.

Chapter IV presented the theory of Four Wave mixing in three level systems. The time dependence of the scattered beam intensity in the transient grating experiment was discussed. Application of the FWM technique to investigate the mechanism of the scattered beam generation was demonstrated. The result of the transient grating experiment to investigate the energy migration process in $Nd_xLa_{1-x}P_5O_{14}$ were demonstrated. The energy migration process in $Nd_xLa_{1-x}P_5O_{14}$ was found to be partially coherent. The process of the exciton-phonon interaction was found to be limiting the degree of coherence in the exciton motion.

B. Suggestion for Future Work

The possible directions of the theoretical efforts to sophisticate the knowledge of the energy migration were discussed in Chapter II D of this work.

As far as the experimental efforts goes, transient grating technique will continue to produce new data about the energy migration processes. One important experimental problem to be solved is to find the way of using this technique in the regions of the strong absorption. This will allow us to study even the subtle processes in the inhomogeneously broaden systems.

Quantitative analysis of the FWM process in the three level system still waits to be finalized. One should expect, however, that the information about the three level system dynamics obtained from this analysis will have quite a limited validity. This is due to the

complexity of the procedure required to extract the picture of the exciton dynamics from the scattering efficiency. Such a procedure may produce some degree of the result uncertainty.

Quantitative analysis of the $I_s(t)$ time dependence will allow one to estimate $\frac{\alpha}{j}$ ratio and will give an insight nito the exciton-phonon interaction processes. This could answer the question about the spectroscopic properties of the metastable state of Nd^{3+} ions and possible exciton-phonon scattering process. Such data, complemented by the information about the spectral energy migration will result in consistent and a thorough picture of energy migration processes.

REFERENCES

1. Kenkre, V.M., in "Statistical Mechanics and Statistical Methods in Theory and Application," ed. V. Landman, Plenum Press, 1977.

2. Kenre, V.M., R.S. Knox, Phys. Rev. B 5, 5279, (1974).

3. Klafter, J., R. Silbey, Phys. Rev. Lett., 44, 55, (1980).

4. Huber, D.L. laser Spectroscopy of Solids, eds. Yen, W.M., Selzer, P.M., Springer, 1981.

5. Grover, M., R. Silbey, J. Chem., Phys. 54, 4843, (1971).

6. Haken, J., P. Reiniker, Z. Phys. 249, 253, (1972).

7. Haan, S.W., R. Zwanzing, J. Chem. Phys. 68(4), 1879, (1978).

8. Gochanour, C.R., H.C. Andersen, Fayer, M.D., J. J. Chem. Phys. 70(9), 4254, (1979).

9. Blumen, A., J. Klafter, R. Silbey, J. Chem. Phys. 72(10), 5320, (1980).

10. Forster, Th., Ann. der Phys. ser. 6, vol 2, 55, (1948).

11. Forster, Th., Z. Naturforsch AG, 321, (1949).

12. Dexter, D.L. J. Chem. Phys., 21, 836, (1953).

13. Siebold, H., J. Heber, J. Lum. 22, 297, (1981).

14. Dornauf, H., J. Heber, J. Lum. 22, 1, (1980).

15. Tyminski, J.K., Ch. M. Lawson, R.C. Powell, J. Chem. Phys., 77, 4318, (1982).

16. Stevels, A.L.N., J.A.W. von der, Does De Bye., J. Lum. 18/19, 809, (1979).

17. Jones, W., N.H. March, "Theoretical Solid State Physics," Vol. 2, Wiley-Interscience, 1979.

18. Huber, D.L., 20, 2307 (1979).

19. Burshtein, A.I., Zh. Eksp. Theor. Fiz. 62, 1695, (1972).

20. Ghosh, K.K., J. Hegarty, D.L. Huber, Phys. Rev. B 22, 2831, (1980).

21. Ghosh, K.K., D.L. Huber., Lum. 21, 225, (1971).

21. Ghosh, K.K., D.L. Huber., Lum. 21, 225, (1971).

22. Yokota, K.K., O. Tamimoto, J. Phys. Soc. Jpn. 22, 779, (1967).

23. Huber, D.L., Phys. Rev. B 20, 5333 (1979).

24. Elliot, R.J., J.A., Krumhansl, Leath, Rev. Mod. Phys. 46, 465, (1974).

25. Gosh, K.K., D.L. Huber, Phys. Rev. B 23, 441, (1981).

26. Huber, D.L., to be published.

27. Blumen, A., J. Klafter, R. Silbey, J. Chem. Phys. 72(10), 5320, (1980).

28. Venikouas, G.E., R.C. Powell, Phys. Rev. B 17, 3456, (1978).

29. Powell, R.C., E.E. Freed, J. Chem. Phys. 70, 10 (1979).

30. Brecher, C., J. Chem. Phys. 61, 2297, (1974).

31. Heber, J., K.H. Hellwege, V. Kobler, M. Murnan, Z. Phys. 237, 189, (1970); ibid 250, 217, (1972).

32. Mortegi, N., S. Shinoya, J. Lum. 8, 1, (1973); P. Avouris, A. Campion, El Sayed, M.A., Chem. Phys. Lett. 50, 9, (1977).

33. Weber M.J., E.J. Sharp, J.E. Miller, J. Phys. Chem. Solids 32, 2275, (1971).

34. Blanzat, B., L. Boehm, C.K. Jorgensen, R. Reisfeld, J. Spector, Solid State Chem. 32, 185, (2980).

35. Lawson, Ch. M., Doctoral Dissertation, Oklahoma State University Stillwater, (1981).

36. Lawson, M., R.C. Powell, W.K. Zwicker, Phys. Rev. B 26, 4836, (1982).

37. Pletter, R.D., W.W. Knuhler, W.K. Zwicker, T. Kovats, R.S. Chinn, J. Cryst. Growth 49, 274, (1980).

38. Yariv, A., D.M. Pepper, Opt. Lett. 1, 16, (1977).

39. Abrams, R.L., R.C. Lind, Opt. Lett. 2,194, (1978).

40. Liao, P.F., D.M. Bloom, Opt. Lett. 3,4, (1978).

41. Abrams, R.L., R.C. Lind, Opt. Lett. 3, 205, (1978); Yariv, A., Quantum Electronics, Wiley, New York, (1975).

42. Salcedo, J.R., A.E. Siegman, D.D. Dlott, M.D. Fayer, Phys. Rev. Lett. 41, 131, (1978).

43. Siegman, A.E., J. Opt. Soc. Am. 67, 545, (1977); Hill, K.O., App. Opt. 10, 1095, 1971); D.S. Hamilton, D. Heimon, J. Feinberg, R.W. Hellwarth, Opt. Lett. 9, 129, (1979); Eichler, H.J., J. Eichler, J. Knof, Ch. Noack, Phys. Stat. Solidi (a), 62, 681, (1979).

44. Liao, P.F., L.M. Humphrey, D.M. Bloom, S. Geschwind, Phys. Rev. B 20, 4145, (1979).

45. Wong, Y.M., V.M. Kenkure, Phys. Rev. 3 27, 3072, (1980).

46. Kenkure, V.M., Phys. Rev., B 18, 4064, (1978).

47. Azuel, F., IEEE, J. Quantum Elect. 12, 258, (1976).

48. Kenkure, V.M., R.S. Knox, Phys Rev B 9, 5279, (1979).

49. Zokai, M., R.C. Powell, Butt., American Phys. Soc., 23, 202, (1978).

50. Auzel, F., IEEE J. Quantum Elect. 12, 258, (1976).

51. Judd, B.R., Phys Rev. 127, 750, 1962.

52. Flaherty, J.M., R.C. Powell, Phys. Rev. B 19, 32, (1973); R.C. Powell, D.P. Neikirk, J.M. Flaherty, J. PHys. Chem. Solids, 41, 345, (1980).

53. Broer, M.M., D.L. Huber, W.M. Yen, Phys. Rev. Lett. 49, 394, (1982).

54. Trilifaj, M., J. Czech, Phys. 8, 511, (1958).

55. Trilifaj, M., J. Czech, Phys. 6, 533, (1956); ibid, 5, 463, (1955).

56. Agranovich, V.M., Yu. V. Konobeev, Sov. Phys. Solid State 5, 999, (1966); ibid 6, 644, (1964); V.M. Agranovich, Yu. V. Konobeev, Phys. Stat. Sol. 27, 435, (1968); V.M. Agranovich, Konobeev, Opt. Spect. 6, 155, (1959).

57. Chinn, W.R., W.K. Zwicker, J. App. Phys., 49, 5892, (1979).

58. Anderson, P.W. Phys. Rev., 109, 1982. (1958), Lyo, S.U., Phys. Rev., B 3, 3331, (1971); J. Koo, L.R. Walker, Geschwind, S., Phys. Rev. Lett., 35, 1669; (1975).

APPENDIX

The susceptibility of the two level system as derived by Lawson in reference 35 takes the form

$$\chi = \frac{2\alpha_o}{k} \frac{1 + \delta}{(1 + \delta + \left|\frac{E}{E_s}\right|^2)} \tag{A-1}$$

where δ is the normalized detuning between the excitation wavelength and the ground-excited states gap, α_o is the absorption line small signal excitation field attenuation coefficient, and E_s is the line saturation field.

If the susceptibility of the three level system is assumed to take the form of a linear combination of two, two level systems (see Figure 12 and related comments of the Chapter VI A), then the resultant susceptibility takes the form

$$\chi(E) = \frac{R}{R+1} \chi_1 + \frac{1}{R+1} \chi_2 \tag{A-2}$$

The meaning of the symbols in the above formula is identical to those in Chapter VI A.

According to the definition, the polarization of the material $\overline{P}(\overline{E})$ can be expressed as

$$\overline{P}(\overline{E}) = \varepsilon_o [\sum_{1,2} R_i \chi_i(E)] \overline{E} \tag{A-3}$$

where $\overline{E}$ is the electric field interacting with the isotropic medium.

In the Four-wave mixing experiment when the energy migration process is investigated, the configuration of beams is arranged as shown by Figure 13. Given the fact that the Four ave ixing experiment utilizes nonlinear response of the material, it is advantageous to set the beam intensities such that the pump field e is much bigger than the probe-scattered ΔE_o part of the Four-wave ixing configuration (see definitions (146)-(149) of the mixing fields).

Given this, it is possible to expand $\chi(E)$ around E_o in formula (A-3) leads to the form (144) if the nonlinear terms of ΔE are truncated.

After straightforward differentiation and the application of the slow varying envelope of beams assumption (condition (151) and the application of the non-depleting pump beams assumption (condition (152)) equation (150) gives

$$\cos\Theta \exp(-i\bar{k}_1\bar{r})\partial_z A_1(z) + \exp(-\bar{k}_3\bar{r})\partial_z A_3(z) = \sum_{1,2} R_i \alpha_{oi} I_{si}(1 - i\delta_i)\left[\frac{E_o}{I_{si} + |E_o|^2} + \frac{\Delta E}{(I_s + |E_o|)^2} - \frac{E_2 \Delta E^*}{(I_{si} + |E_o|^2)^2} - \frac{|E_o|^2 \Delta E}{(I_{si} + |E_o|^2)^2}\right] \quad \text{(A-4)}$$

where $I_{si} = |E_{si}|^2/(1+\delta_i)$ and $A_i(z)$, $i = 1,2,3,4$ are the envelopes of the beams.

Comparing the synchronious terms on the left and right side of equation (A-4) (see also reference 35 where the above procedure is demonstrated in great detail), a set of equations is obtained

$$\cos\Theta\partial_z A_1(z) \sum_{1,2} R_i \frac{\alpha_{oi}|E_{si}|^2(1 - i\delta_i)}{(I_{si} + |E_o|^2)^2}$$

$$[(I_{si} + \zeta) A_1(z) - A_2^*(z)A_4(z)A_3(z)] \qquad \text{(A-5)}$$

$$\partial_z A_3(z) = \sum_{1,2} R_i \frac{\alpha_{oi}|E_{si}|^2(1 - i\delta_i)}{(I_{si} + |E_o|^2)^2}$$

$$[(I_{si} + \zeta)A_3(z) - A_2(z)A_4^*(z)A_1(z)] \qquad \text{(A-6)}$$

where $\zeta = A_2(z)A_4(z)\exp[ik(1-\cos\Theta)z]$

(The asterisk in the above formula designates the conjugate value).

Given the fact, that in the Four Wave Mixing configuration $|A_1|>|A_3|$ the probe beam intensity is higher than the scattered beam intensity, and as long as the pump beams are weaker than the saturation fields

$$I_s << |A_2(z)A_4^*(z)| \qquad \text{(A-7)}$$

the set of equations (A-5)-(A-6) simplifies to

$$\cos\Theta\partial_z A_1(z) = \sum_{1,2} R_i \frac{\alpha_{oi}|E_{si}|^2(1 - i\delta_i)}{(I_{si} + |E_o|^2)^2} (I_{si} + \zeta)A_1(z) \qquad \text{(A-8)}$$

$$\partial_z A_3 = \sum_{1,2} R_i \frac{\alpha_{oi}|E_{si}|^2(1 - i\delta_i)}{(I_{si} + |E_o|^2)^2}$$

$$[(I_{si} + \zeta)A_3(z) - A_2(z)A_4^*(z)A_1(z)] \qquad \text{(A-9)}$$

Phases Ψ_i can be defined by formula

$$E_i = |E_i|(\cos\Psi_i + i\sin\Psi_i) \qquad \text{(A-10)}$$

and, according to definitions (146)-(149), the following is obtained

$$\Psi_1 - \Psi_2 = -ik(1-\cos\Theta)z + \Delta$$

where

$$\Delta = \operatorname{actg} \frac{\mathrm{Im}(A_2(z))}{\mathrm{Re}(A_2(z))} - \operatorname{arctg} \frac{\mathrm{Im}(A_4(z))}{\mathrm{Re}(A_4(z))} \tag{A-11}$$

The above formula give

$$|E_o|^2 = I_2 + I_4 + 2|A_2A_4|\cos[k(1 - \cos\Theta)z + \Delta] \tag{A-12}$$

After the introduction of the symbols

$$D_{oi} = I_{si} + I_2 + I_4 \tag{A-13}$$

$$a = |A_2(z)A_4(z)| \tag{A-14}$$

the set of equations (A-8)-(A-9) takes the form

$$\partial_z A_1(z) = \sum_{1,2} R_i \frac{\alpha_{oi}|E_{si}|^2(1 - i\delta_i)}{\cos\Theta} \frac{[I_{si} + a\exp[ik(1 - \cos\Theta)z] + \Delta]}{D_o + 2a\cos[k(1-\cos\Theta) + \Delta]} A_1(z) \tag{A-15}$$

$$\partial_z A_3(z) = \sum_{1,2} \{R_i\alpha_{oi}|E_{si}|^2(1 - i\delta_i) \frac{I_{si} + a\exp[ik(1-\cos\Theta)z + \Delta i]}{[D_{oi} + 2a[k(1-\cos\Theta)z + \Delta]]^2} A_3(z)$$
$$- R_i\alpha_{oi}|E_{si}|^2(1 - i\delta_i) \frac{a\exp(i\Delta)}{[D_{oi} + 2a[k(1-\cos\Theta)z + \Delta]]^2} A_1(z) \tag{A-16}$$

Defining the following quantities

$$\beta = k(1 - \cos\Theta) \tag{A-17}$$

$$R(z) = -\sum_{1,2} R_i \frac{\alpha_{oi}|E_{si}|^2(1 - i\delta_i)}{\cos\Theta} \frac{I_{si} + a\exp(\beta + i\Delta)}{[D_{oi} + 2a\cos(\beta z + \Delta)]^2} \tag{A-18}$$

$$P(z) = -\sum_{1,2} R_i \alpha_{oi} |E_{si}|^2 (1 - i\delta_i) \frac{I_{si} + a \exp(-i\beta - i\Delta)}{[D_{oi} + 2a \cos(\beta z + \Delta)]^2} \quad \text{(A-19)}$$

$$Q(z) = -\sum_{1,2} R_i \alpha_{oi} |E_{si}|^2 (1 - i\delta_i) \frac{a \exp(i\Delta) A_1(z)}{[D_{oi} + 2 \cos(\beta z + \Delta)]^2} \quad \text{(A-20)}$$

one can obtain from the set (A-15)-(A-16) the following equations

$$\partial_z A_1(z) - R(z) A_1(z) = 0 \quad \text{(A-21)}$$

$$\partial_z A_3(z) - P(z) A_3(z) = Q(z) \quad \text{(A-22)}$$

which describes the response of the medium in the FWM experiment.

Case I: Θ angle is large

If the angle of the pump beam crossing is wide enough that the probe-scattered part of the mixing field does not change substantially over the length of the pump part oscillation $\lambda_{osc} = \frac{\lambda}{1-\cos\Theta}$ then it is possible to approximate the set of equations (A-21)-(A-22) by their forms "averaged" over the λ_{osc}. This leads to the set of equations

$$\partial_z A_1(z) + \langle R(z) \rangle A_1(z) = 0 \quad \text{(A-23)}$$

$$\partial_z A_3(z) + \langle P(z) \rangle A_3(z) = \langle q(z) \rangle A_1(z) \quad \text{(A-24)}$$

In particular the formula

$$\frac{1}{\lambda_{osc_o}} \int_{\lambda_{osc}} dz \frac{I_{si} + a \cos\beta + ia \sin\beta z}{(D_{oi} + 2a \cos\beta z)^2} = \frac{D_{oi} I_{si} - 2a^2}{(D_{oi}^2 - 4a^2)^{3/2}} \quad \text{(A-25)}$$

which is valid if the assumption of non-depleting pump field holds is used to obtain

$$\langle R(z)\rangle = -\sum_{1,2} R_i \frac{\alpha_{oi}|E_{si}|^2(1 - i\delta_i)}{\cos\Theta} \frac{D_{oi}I_{si} - 2a^2}{(D_{oi}^2 - 4a^2)^{3/2}} \tag{A-26}$$

$$\langle P(z)\rangle = -\sum_{1,2} R_i\alpha_{oi}|E_{si}|^2(1 - i\delta_i) \frac{D_{oi}I_{si} - 2a^2}{(D_{oi}^2 - 4a^2)^{3/2}} \tag{A-27}$$

$$\langle q(z)\rangle = -\sum_{1,2} R_i\alpha_{oi}|E_{si}|^2(1 - i\delta_i) \frac{D_{oi}a\exp(i\Delta)}{(D_{oi}^2 - 4a^2)^{3/2}}$$

Calculated from set (A-23) and (A-24) the envelopes of the fields take the form

$$A_1(z) = A_1(L)\ \exp[-\langle P(z)\rangle\ (z-L)] \tag{A-28}$$

$$A_3(z) = \frac{\langle q(z)\rangle\ A_1(z)}{\langle P(z)\rangle\ (\cos^{-1}\theta - 1)}$$

$$\left\{\exp[-\frac{\langle P(z)\rangle\ (z-L)}{\cos\Theta}] - \exp[-\langle P(z)\rangle\ (z-L)]\right\} \tag{A-29}$$

From the above, it is straightforward to obtain

$$I_3(0) = |A_3(0)|^2 = \left|\frac{\langle q(z)\rangle}{\langle P(z)\rangle}\right|^2 \frac{|A_1(L)|^2}{(\cos^{-1}\theta - 1)^2}$$

$$\{\exp(-2\zeta_R L) + \exp(-\frac{2\zeta_R L}{\cos\theta}) - 2\exp[-\zeta_R(1 + \cos^{-1}\theta)L]$$

$$\cos[\zeta_I(1 - \cos^{-1}\theta)L]\} \tag{A-30}$$

$$I_1(0) = |A_1(0)|^2 = |A_1(L)|^2 \exp(-2\zeta_R L) \tag{A-31}$$

where

$$\zeta_R = \mathrm{Re}[-\langle P(z)\rangle] \tag{A-32}$$

$$\zeta_I = \mathrm{Im}[-\langle P(z)\rangle] \tag{A-33}$$

The scattering efficiency in the Four-wave mixing experiment is defined as

$$\eta = \left.\frac{I_3(0)}{I_1(0)}\right|_{E_o = 0} \tag{A-34}$$

this leads to the formula

$$\eta = \left|\frac{\rho}{\zeta}\right|^2 \frac{\exp(-\Psi_{E_o})}{(\cos^{-1}\Theta - 1)^2}\left\{ \exp(-2\zeta_R L + \exp(-\frac{2\zeta_R L}{\cos\Theta}) - 2\exp[-\zeta_R L(1+\cos^{-1}\Theta)]\cos[\zeta_I L(1-\cos^{-1}\Theta)]\right\} \tag{A-35}$$

where

$$\left|\frac{\rho}{\zeta}\right| = \frac{\sum_{j=1,2}\left\{\sum_{i=1,2} F_{j,i}\frac{R_i\alpha_{oi}}{(1+\delta_i)^2 I_{si}}\frac{\sqrt{I_2 I_4}\,(1+\frac{I_2+I_4}{I_{si}})}{[(1+\frac{I_2+I_4}{I_{si}})^2 - 2\frac{I_2 I_4}{I_{si}^2}]^{3/2}}\right\}^2}{\sum_{j=3,4}\left\{\sum_{i=1,2} F_{j.i}\frac{R_i\alpha_{oi}}{(1+\delta_i)^2}\frac{(1+\frac{I_2+I_4}{I_{si}})^2 - 2\frac{I_2 I_4}{I_{si}^2}}{[(1+\frac{I_2+I_4}{I_{si}})^2 - 4\frac{I_2 I_4}{I_{si}^2}]^{3/2}}\right\}^2} \tag{A-36}$$

$$F_{1,i} = \cos\Delta + \delta_i \sin\Delta \; ; \; F_{3,i} = 1 \tag{A-37}$$

$$F_{2,i} = \sin\Delta - \delta_i \cos\Delta \; ; \; F_{4,i} = \delta_i$$

$$\Psi_{E_o} = \frac{2L}{\cos\Theta}\sum_{1,2}\frac{R_i\,\alpha_{oi}}{(1+\delta_i)^2} \tag{A-38}$$

$$\zeta_R = -\sum_{1,2} \frac{R_i I_{si} \alpha_{oi}}{(1+\delta_i)^2} \frac{D_{oi} I_{si} - 2a^2}{(D_{oi}^2 - 4a^2)^{3/2}} \tag{A-39}$$

$$\zeta_I = \sum_{1,2} \frac{R_i I_{si} \alpha_{oi}}{(1+\delta_i)^2} \frac{D_{oi} I_{si} - 2a^2}{(D_{oi}^2 - 4a^2)^{3/2}} \tag{A-40}$$

The formula (A-34)-(A-40) express the scattering efficiency in the Four Wave Mixing experiment in the case of a large angle.

Case II: The pump field is far from saturation level.

If the pump field is far from saturation level in the Four Wave Mixing experiment, then the following relationships will be satisfied

$$\frac{a}{I_{si}} \ll 1$$

$$\frac{I_2}{I_{si}} \ll 1 \quad ; \quad i = 1,2 \tag{A-41}$$

$$\frac{I_4}{I_{si}} \ll 1$$

Expanding the expressions of the type

$$\frac{I_{si} + a \exp(i\beta_2 - i\Delta)}{[I_{si} + I_2 + I_4 + 2\cos(\beta_2 + \Delta)]^2}$$

into the power series of $\frac{I_2}{I_{si}}$, $\frac{I_4}{I_{si}}$ and $\frac{a}{I_{si}}$ and truncating nonlinear terms obtains the following formula:

$$R(z) \simeq \sum_{1,2} R_i \frac{\alpha_{oi}(1 - i\delta_i)}{(1+\delta_i)^2 \cos\Theta} \left[1 - \frac{3a}{I_{si}} \cos(\beta z + \Delta) + i \frac{a}{I_{si}} \sin(\beta z + \Delta) - 2 \frac{I_2 + I_4}{I_{si}}\right] \tag{A-42}$$

The above formula together with equation (A-21) leads to

$$A_1(z) = A_1(L)\ \exp\{ \sum_{1,2} - \frac{R_i \alpha_{oi} \delta_i}{(1+\delta_i)^2 \cos\Theta} [(z-L)(1 - 2\frac{I_2 + I_4}{I_{si}}) - \frac{6a}{\beta I_{si}} \sin\frac{\beta(z-L)}{2} \cos\frac{\beta(z+L) + 2\Delta}{2} - \frac{i\,2a}{\beta I_{si}} \sin\frac{\beta(z+L) + 2\Delta}{2} \sin\frac{\beta(z-L)}{2}]\} \qquad (A-43)$$

Using the same approximation the following is also obtained

$$Q(z) \simeq - \sum_{1,2} \frac{R_i \alpha_{oi}(1-i\delta_i)}{(1+\delta_i)^2 I_{si}} a \exp(i\Delta) A_1(z) \qquad (A-44)$$

$$P(z) \simeq - \sum_{1,2} \frac{R_i \alpha_{oi}(1-i\delta_i)}{(1+\delta_i)^2 I_{si}} [1 - \frac{3a}{I_{si}} \cos(\beta z+\Delta) - i \frac{a}{I_{si}} \sin(\beta z+\Delta) - 2\frac{I_2+I_4}{I_{si}}] \qquad (A-45)$$

The solution of equation (A-23) together with formulae (A-44), and (A-45) gives

$$A_3(z) = e^{f(z)}(C_1 + \int_o^z Q(z') e^{-f(z')} dz') \qquad (A-46)$$

which allows to evaluate f(z) as

$$f(z) = - \int_o^z P(z')\ dz' + C_2 \qquad (A-47)$$

and leads to

$$f(z) = \sum_{1,2} \frac{R_i \alpha_{oi}(1 - i\delta_i)}{(1 + \delta_i)^2 I_{si}} \left[z\left(1 - 2\frac{I_2 + I_4}{I_{si}}\right)\right.$$

$$\left. - \frac{3a}{\beta I_{si}} \sin(\beta z + \Delta) + i \frac{a}{I_{si}} \cos(\beta z + \Delta)\right] \qquad \text{(A-48)}$$

Introducing a function F(z) such that

$$F(z) = \int_o^z Q(z') e^{-f(z')} dz' \qquad \text{(A-49)}$$

it is possible to express

$$A_3(Z) = e^{f(A)} [F(Z) - F(L)] \qquad \text{(A-50)}$$

what gives intensity of scattered light on the face L=0 as:

$$I_3 = |A_3(0)| = |e^{f(0)}|^2 |F(0) - F(L)|^2 \qquad \text{(A-51)}$$

for $|e^{f(0)}|^2$ expressed as:

$$|e^{f(0)}|^2 = \exp\left[-6 \sin\Delta \frac{\sqrt{I_2 I_4}}{\beta} \sum_{1,2} \frac{R_i \alpha_{oi}}{(1+\delta_i)^2 I_{si}}\right.$$

$$\left. - 2 \cos\Delta \frac{\sqrt{I_2 I_4}}{\beta} \sum_{1,2} \frac{R_i \alpha_{oi} \delta_i}{(1+\delta_i)^2 I_{si}}\right] \qquad \text{(A-52)}$$

$$|F(0) - F(L)|^2 = L^2|A_1(L)|^2 \frac{I_2 I_4}{\cos^2\Theta} \left[\left(\sum_{1,2} \frac{R_i \alpha_{oi} \delta_i}{(1+\delta_i)^2 I_{si}}\right)^2 + \left(\sum_{1,2} \frac{R_i \alpha_{oi}}{(1+\delta_i)^2 I_{si}}\right)^2\right]\left\{\left[LB_R \cos^2\frac{\Theta}{2} - \frac{L^2}{6}(B_R^2 + B_L^2)\cos\Theta - 1\right]^2 + \left(LB_I \cos^2\frac{\Theta}{2} - \frac{L^2}{3} B_R B_I \cos\Theta\right)^2\right\} \quad \text{(A-53)}$$

$$B_R = \sum_{1,2} \frac{R_i \alpha_{oi}}{(1+\delta_i)^2 \cos\Theta} \quad \text{(A-54)}$$

$$B_I = -\sum_{1,2} \frac{R_i \alpha_{oi} \delta_i}{(1+\delta_i)^2 \cos\Theta} \quad \text{(A-55)}$$

The intensity of the probe beam, while the pump field is turned off is

$$I_1 = |A_1(0)|^2 \Big|_{E_o = 0} = |A_1(L)|^2 \exp\left[-\frac{2L}{\cos\Theta} \sum_{1,2} \frac{R_i \alpha_{oi}}{(1+\delta_i)^2}\right] \quad \text{(A-56)}$$

The formula (A-53)-(A-56) allows one to express the scattering efficiency in Four-wave mixing as:

$$\eta = S_1 I_2 I_4 \exp\left(-S_2 \sqrt{I_2 I_4}\right) \quad \text{(A-57)}$$

$$S_1 = \frac{L^2}{\cos^2\Theta}\{[\sum_{1,2}\frac{R_i\alpha_{oi}\delta_i}{(1+\delta_i)^2}]^2 + [\sum_{1,2}\frac{R_i\alpha_{oi}}{(1+\delta_i)^2}]^2\}$$

$$\exp[\frac{2L}{\cos\Theta}\sum_{1,2}\frac{R_i\alpha_{oi}}{(1+\delta_i)^2}]\{[L\cos^2\frac{\Theta}{2}\sum_{1,2}\frac{R_i\alpha_{oi}}{(1+\delta_i)^2\cos\Theta}$$

$$-\frac{L^2}{6}\cos\Theta\,((\sum_{1,2}\frac{R_i\alpha_{oi}}{(1+\delta_i)^2\cos\Theta})^2 +$$

$$+(\sum_{1,2}\frac{R_i\alpha_{oi}\delta_i}{(1+\delta_i)^2\cos\Theta})^2) - 1]^2 + [\frac{L\cos^2\frac{\Theta}{2}}{\cos\Theta}\sum_{1,2}\frac{R_i\alpha_{oi}\delta_i}{(1+\delta_i)^2}$$

$$-\frac{L^2}{3\cos\Theta}(\sum_{1,2}\frac{R_i\alpha_{oi}\delta_i}{(1+\delta_i)^2})(\sum_{1,2}\frac{R_i\alpha_{oi}}{(1+\delta_i)^2})]^2\} \qquad \text{(A-58)}$$

$$S_2 = \frac{2}{\sqrt{\beta}}\cos\Delta\sum_{1,2}\frac{R_i\alpha_{oi}\delta_i}{(1+\delta_i)^2 I_{si}} + 3\sin\Delta\sum_{1,2}\frac{R_i\alpha_{oi}}{(1+\delta_i)^2 I_{si}} \qquad \text{(A-59)}$$

Formulae (A-57)-(A-59) describes the scattering process in the Four-wave mixing experiment while the intensity of the pump field is below its saturation level.

VITA

Jacek Kazimierz Tyminski

Candidate for the Degree of

Doctor of Philosophy

Thesis: ENERGY MIGRATION PROCESSES IN RARE EARTH PENTAPHOSPHATES

Major Field: Physics

Biographical:

Personal Data: Born in Starogard Gdanski, Poland, October 31, 1954, the son of Mieczyslaw and Damuta Tyminski.

Education: Graduate from Copernicus High School in Elblag, Poland, in May 1973; recived Magister Inzynier degree from Politechnika Gdanska in 1978; completed requirements for Doctor of Philosophy degree at Oklahoma State University in July,1983.

Professional Experiences: Teaching and Research Assistant, Institute of Physics, Technical University of Gdansk, Poland, 1977-1979; Teaching Assistant, Department of Physics, Oklahoma State University, 1980-1981; Research Assistant, Department of Physics, Oklahoma State University, 1981-1983.